



# Heterogeneous architectures, Hybrid methods, Hierarchical matrices for Sparse Linear Solvers

Pierre Ramet

## ► To cite this version:

Pierre Ramet. Heterogeneous architectures, Hybrid methods, Hierarchical matrices for Sparse Linear Solvers. Distributed, Parallel, and Cluster Computing [cs.DC]. Université de Bordeaux, 2017. tel-01668740v2

**HAL Id: tel-01668740**

**<https://inria.hal.science/tel-01668740v2>**

Submitted on 6 Jan 2018

**HAL** is a multi-disciplinary open access archive for the deposit and dissemination of scientific research documents, whether they are published or not. The documents may come from teaching and research institutions in France or abroad, or from public or private research centers.

L'archive ouverte pluridisciplinaire **HAL**, est destinée au dépôt et à la diffusion de documents scientifiques de niveau recherche, publiés ou non, émanant des établissements d'enseignement et de recherche français ou étrangers, des laboratoires publics ou privés.

# HABILITATION À DIRIGER DES RECHERCHES

AU TITRE DE L'ÉCOLE DOCTORALE  
DE MATHÉMATIQUES ET D'INFORMATIQUE

Par **Pierre RAMET**

---

*Heterogeneous architectures, Hybrid methods,*  
*Hierarchical matrices for Sparse Linear Solvers*

---

Soutenue et présentée publiquement le : 27 novembre 2017

**Après avis des rapporteurs :**

Frédéric DESPREZ	Deputy Scientific Director, Inria
Iain DUFF ....	Senior Scientist, Rutherford Appleton Lab.
Yousef SAAD ...	Professor, University of Minnesota

**Devant la commission d'examen composée de :**

Iain DUFF ....	Senior Scientist, Rutherford Appleton Lab. ...	Examineur
Raymond NAMYST	Professor, Bordeaux University .....	Examineur
Esmond NG ....	Senior Scientist, Lawrence Berkeley National Lab.	Examineur
Yves ROBERT ..	Professor, ENS-Lyon .....	Examineur
Yousef SAAD ...	Professor, University of Minnesota .....	Examineur
Isabelle TERRASSE	Research Director, Airbus Group .....	Examineur
Sivan TOLEDO ..	Professor, Tel-Aviv University .....	Examineur



# Contents

<b>Introduction</b>	<b>1</b>
<b>1 Static scheduling and data distributions</b>	<b>7</b>
1.1 Context and algorithmic choices . . . . .	7
1.2 Background . . . . .	8
1.3 Static scheduling . . . . .	11
1.3.1 Preprocessing steps . . . . .	11
1.3.2 Parallel scheme of the factorization . . . . .	11
1.3.3 Hybrid MPI+Thread implementation . . . . .	12
1.3.4 Parallel factorization algorithm . . . . .	13
1.3.5 Matrix mapping and task scheduling . . . . .	15
1.4 Reducing the memory footprint using partial agregation techniques . . . . .	16
<b>2 Dynamic scheduling and runtime systems</b>	<b>19</b>
2.1 A dedicated approach . . . . .	19
2.1.1 NUMA architectures . . . . .	19
2.1.2 NUMA-aware allocation . . . . .	21
2.1.3 Communication overlap . . . . .	22
2.1.4 Dynamic scheduling . . . . .	23
2.1.5 Numerical experiments . . . . .	27
2.2 A generic approach . . . . .	28
2.2.1 Related work . . . . .	29
2.2.2 Runtimes . . . . .	30
2.2.3 Supernodal factorization over DAG schedulers . . . . .	33
2.2.4 Heterogeneous experiments . . . . .	39
<b>3 Incomplete factorization and domain decomposition</b>	<b>43</b>
3.1 Amalgamation algorithm for $iLU(k)$ factorization . . . . .	43
3.1.1 Methodology . . . . .	44
3.1.2 Amalgamation algorithm . . . . .	46
3.1.3 Numerical experiments . . . . .	49
3.2 Graph partitioning for well balanced domain decomposition . . . . .	52
3.2.1 Multilevel Framework . . . . .	55
3.2.2 Graph Partitioning Algorithms . . . . .	57
3.2.3 Experimental Results . . . . .	63
<b>4 Towards <math>\mathcal{H}</math>-matrices in sparse direct solvers</b>	<b>67</b>
4.1 Reordering strategy for blocking optimization . . . . .	67
4.1.1 Intra-node reordering . . . . .	67
4.1.2 Related work . . . . .	70
4.1.3 Improving the blocking size . . . . .	70
4.2 On the use of low rank approximations in PASTIX . . . . .	72
4.2.1 Block Low-Rank solver . . . . .	73
4.2.2 Low-rank kernels . . . . .	75
4.2.3 Numerical experiments . . . . .	78

4.2.4 Discussion . . . . .	83
<b>Conclusion</b>	<b>87</b>
<b>A PaSTiX 6.0 updated performance</b>	<b>91</b>
A.1 Experimental conditions . . . . .	91
A.2 Performance on the Kepler architecture . . . . .	92
A.3 Performance on the KNL architecture . . . . .	92
<b>B Bibliography</b>	<b>93</b>

# Introduction

Over the last few decades, there have been innumerable science, engineering and societal breakthroughs enabled by the development of high performance computing (HPC) applications, algorithms and architectures. These powerful tools have provided researchers with the ability to computationally find efficient solutions for some of the most challenging scientific questions and problems in medicine and biology, climatology, nanotechnology, energy and environment; to name a few. It is admitted today that *numerical simulation, including data intensive treatment, is a major pillar for the development of scientific discovery at the same level as theory and experimentation*. Numerous reports and papers also confirmed that extreme scale simulations will open new opportunities not only for research but also for a large spectrum of industrial and societal sectors.

An important force which has continued to drive HPC has been to focus on frontier milestones which consist in technical goals that symbolize the next stage of progress in the field. In the 1990s, the HPC community sought to achieve computing at a teraflop rate and currently we are able to compute on the first leading architectures at more than ten petaflops. General purpose petaflop supercomputers are available and exaflop computers are foreseen in early 2020.

For application codes to sustain petaflops and more in the next few years, hundreds of thousands of processor cores or more are needed, regardless of processor technology. Currently, a few HPC simulation codes easily scale to this regime and major algorithms and codes development efforts are critical to achieve the potential of these new systems. Scaling to a petaflop and more involves improving physical models, mathematical modeling, super scalable algorithms.

In this context, the purpose of my research is to contribute to performing efficiently frontier simulations arising from challenging academic and industrial research. It involves massively parallel computing and the design of highly scalable algorithms and codes to be executed on emerging hierarchical many-core, possibly heterogeneous, platforms. Throughout this approach, I contribute to all steps that go from the design of new high-performance more scalable, robust and more accurate numerical schemes to the optimized implementations of the associated algorithms and codes on very high performance supercomputers. This research is conducted in close collaboration with European and US initiatives.

Thanks to three associated teams, namely PhyLeaS <sup>1</sup>, MORSE <sup>2</sup> and FASTLA <sup>3</sup>, I have contributed with world leading groups to the design of fast numerical solvers and their parallel implementation.

► For the solution of large sparse linear systems, we design numerical schemes and software packages for direct and hybrid parallel solvers. Sparse direct solvers are mandatory when the linear system is very ill-conditioned; such a situation is often encountered in structural mechanics codes, for example. Therefore, to obtain an industrial software tool that must be robust and versatile, high-performance sparse direct solvers are mandatory, and parallelism is then necessary for reasons of memory capability and acceptable solution time. Moreover, in order to solve efficiently 3D problems with more than 50 million unknowns, which is now a reachable challenge with new multicore supercomputers, we must achieve good scalability in time and control memory overhead. Solving a sparse linear system by a direct method is generally a highly irregular problem that provides some challenging algorithmic problems and requires a sophisticated implementation scheme in order to fully exploit the capabilities of modern supercomputers. It would be hard work to provide here a complete survey on direct methods for sparse linear systems and the corresponding software. Jack Dongarra has maintained for many years a list of

---

<sup>1</sup><http://www-sop.inria.fr/nachos/phyleas/>

<sup>2</sup><http://icl.cs.utk.edu/morse/>

<sup>3</sup><https://www.inria.fr/en/associate-team/fastla>

freely available software packages for linear algebra <sup>4</sup>. And a recent survey by Tim Davis et al. has been published [44] with a list of available software in the last section.

New supercomputers incorporate many microprocessors which are composed of one or many computational cores. These new architectures induce strongly hierarchical topologies. These are called NUMA architectures. In the context of distributed NUMA architectures, we study optimization strategies to improve the scheduling of communications, threads and I/O. In the 2000s, our first attempts to use available generic runtime systems, such as PM2 [15] or ATHAPASCAN [25], failed to reach acceptable performance. We then developed dedicated dynamic scheduling algorithms designed for NUMA architectures in the PASTIX solver. The data structures of the solver, as well as the patterns of communication have been modified to meet the needs of these architectures and dynamic scheduling. We are also interested in the dynamic adaptation of the computational granularity to use efficiently multi-core architectures and shared memory. Several numerical test cases have been used to prove the efficiency of the approach on different architectures.

The pressure to maintain reasonable levels of performance and portability forces application developers to leave the traditional programming paradigms and explore alternative solutions. We have studied the benefits and limits of replacing the highly specialized internal scheduler of the PASTIX solver with generic runtime systems. The task graph of the factorization step is made available to the runtimes systems, allowing them to process and optimize its traversal in order to maximize the algorithm efficiency for the targeted hardware platform. The aim was to design algorithms and parallel programming models for implementing direct methods for the solution of sparse linear systems on emerging computers equipped with GPU accelerators. More generally, this work was performed in the context of the associated team MORSE and the ANR SOLHAR project which aims at designing high performance sparse direct solvers for modern heterogeneous systems. The main competitors in this research area are the QR-MUMPS and SUITESPARSE packages, mainly the CHOLMOD (for sparse Cholesky factorizations) and SPQR (for sparse QR factorizations) solvers that achieve a rather good speedup using several GPU accelerators but only using one node (shared memory). In collaboration with the ICL team from the University of Tennessee, a comparative study of the performance of the PASTIX solver on top of its native internal scheduler, PARSEC, and STARPU frameworks, on different execution environments, has been performed. The analysis highlights that these generic task-based runtimes achieve comparable results to the application-optimized embedded scheduler on homogeneous platforms. Furthermore, they are able to significantly speed up the solver on heterogeneous environments by taking advantage of the accelerators while hiding the complexity of their efficient manipulation from the programmer.

More recently, many works have addressed heterogeneous architectures to exploit accelerators such as GPUs or Intel Xeon Phi with interesting speedup. Despite research towards generic solutions to efficiently exploit those accelerators, their hardware evolution requires continual adaptation of the kernels running on those architectures. The recent Nvidia architectures, such as Kepler, present a larger number of parallel units thus requiring more data to feed every computational unit. A solution considered for supplying enough computation has been studied on problems with a large number of small computations. The batched BLAS libraries proposed by Intel, Nvidia, or the University of Tennessee are examples of this solution. We have investigated the use of the variable size batched matrix-matrix multiply to improve the performance of the PASTIX sparse direct solver. Indeed, this kernel suits the supernodal method of the solver, and the multiple updates of variable sizes that occur during the numerical factorization.

► In addition to the main activities on direct solvers, we also studied some robust preconditioning algorithms for iterative methods. The goal of these studies is to overcome the huge memory consumption inherent to the direct solvers in order to solve 3D problems of huge size. Our study was focused on the building of generic parallel preconditioners based on incomplete LU factorizations. The classical incomplete LU preconditioners use scalar algorithms that do not exploit well CPU power and are difficult to parallelize. Our work was aimed at finding some new orderings and partitionings that lead to a dense block structure of the incomplete factors. Then, based on the block pattern, some efficient parallel blockwise algorithms can be devised to build robust preconditioners that are also able to fully exploit the capabilities of modern high-performance computers.

The first approach was to define an adaptive blockwise incomplete factorization that is much more accurate (and numerically more robust) than the scalar incomplete factorizations commonly used to precondition iterative solvers. Such incomplete factorization can take advantage of the latest breakthroughs

---

<sup>4</sup><http://www.netlib.org/utk/people/JackDongarra/la-sw.html>

in sparse direct methods and particularly should be very competitive in CPU time (effective power used from processors and good scalability) while avoiding the memory limitation encountered by direct methods. In this way, we expected to be able to solve systems in the order of a hundred million unknowns and even one billion unknowns. Another goal was to analyze and justify the chosen parameters that can be used to define the block sparse pattern in our incomplete factorization. The driving rationale for this study is that it is easier to incorporate incomplete factorization methods into direct solution software than it is to develop new incomplete factorizations. Our main goal at this point was to achieve a significant reduction in the memory needed to store the incomplete factors (with respect to the complete factors) while keeping enough fill-in to make the use of BLAS3 (in the factorization) and BLAS2 (in the triangular solves) primitives profitable. In this approach, we focused on the critical problem of finding approximate supernodes of ILU(k) factorizations. The problem was to find a coarser block structure of the incomplete factors. The “exact” supernodes that are exhibited from the incomplete factor nonzero pattern are usually very small and thus the resulting dense blocks are not large enough for efficient use of the BLAS3 routines. A remedy to this problem was to merge supernodes that have nearly the same structure. These algorithms have been implemented in the PASTIX library.

A second approach is the use of hybrid methods that hierarchically combine direct and iterative methods. These techniques inherit the advantages of each approach, namely the limited amount of memory and natural parallelization for the iterative component and the numerical robustness of the direct part. The general underlying ideas are not new since they have been intensively used to design domain decomposition techniques; these approaches cover a fairly large range of computing techniques for the numerical solution of partial differential equations (PDEs) in time and space. Generally speaking, it refers to the splitting of the computational domain into subdomains with or without overlap. The splitting strategy is generally governed by various constraints/objectives but the main one is to express parallelism. The numerical properties of the PDEs to be solved are usually intensively exploited at the continuous or discrete levels to design the numerical algorithms so that the resulting specialized technique will only work for the class of linear systems associated with the targeted PDE. Under this framework, Pascal Hénon and Jérémie Gaidamour [50] have developed in collaboration with Yousef Saad, from University of Minnesota, algorithms that generalize the notion of “faces” and “edges” of the “wire-basket” decomposition. The interface decomposition algorithm is based on defining a “hierarchical interface structure” (HID). This decomposition consists in partitioning the set of unknowns of the interface into components called connectors that are grouped in “classes” of independent connectors [78]. This has led to software developments on the design of algebraic non-overlapping domain decomposition techniques that rely on the solution of a Schur complement system defined on the interface introduced by the partitioning of the adjacency graph of the sparse matrix associated with the linear system. Different hierarchical preconditioners can be considered, possibly multilevel, to improve the numerical behavior of the approaches implemented in HIPS [51] and MAPHYS [2]. For both software libraries the principle is to build a decomposition of the adjacency matrix of the system into a set of small subdomains. This decomposition is built from the nested dissection separator tree obtained using the sparse matrix reordering software SCOTCH. Thus, at a certain level of the separator tree, the subtrees are considered as the interior of the subdomains and the union of the separators in the upper part of the elimination tree constitutes the interface between the subdomains. The interior of these subdomains are treated by a direct method, such as PASTIX or MUMPS. Solving the whole system is then equivalent to solving the Schur complement system on the interface between the subdomains which has a much smaller dimension. The PDSLIN package is another parallel software for algebraic methods based on Schur complement techniques that is developed at Lawrence Berkeley National Laboratory. Other related approaches based on overlapping domain decomposition (Schwarz type) ideas are more widely developed and implemented in software packages at Argonne National Laboratory (software contribution to PETSC where Restrictive Additive Schwarz is the default preconditioner) and at Sandia National Laboratories (SHYLU in the TRILINOS package).

► Nested dissection is a well-known heuristic for sparse matrix ordering to both reduce the fill-in during numerical factorization and to maximize the number of independent computational tasks. By using the block data structure induced by the partition of separators of the original graph, very efficient parallel block solvers have been designed and implemented according to supernodal or multifrontal approaches. Considering hybrid methods mixing both direct and iterative solvers such as HIPS or MAPHYS, obtaining a domain decomposition leading to a good balancing of both the size of domain interiors and the



size of interfaces is a key point for load balancing and efficiency in a parallel context. We have revisited some well-known graph partitioning techniques in the light of the hybrid solvers and have designed new algorithms to be tested in the SCOTCH package. These algorithms have been integrated in SCOTCH as a prototype.

On the other hand, the preprocessing steps of sparse direct solvers, ordering and block-symbolic factorization, are two major steps that lead to a reduced amount of computation and memory and to a better task granularity to reach a good level of performance when using BLAS kernels. With the advent of GPUs, the granularity of the block computations became more important than ever. In this work, we present a reordering strategy that increases this block granularity. This strategy relies on the block-symbolic factorization to refine the ordering produced by tools such as METIS or SCOTCH, but it has no impact on the number of operations required to solve the problem. We integrate this algorithm in the PASTIX solver and show an important reduction in the number of off-diagonal blocks on a large spectrum of matrices. Furthermore, we propose a parallel implementation of our reordering strategy, leading to a computational cost that is really low with respect to the numerical factorization and that is counterbalanced by the improvement to the factorization time. In addition, if multiple factorizations are applied on the same structure, this benefits the additional factorization and solve steps at no extra cost. We proved that such a preprocessing stage is cheap in the context of 3D graphs of bounded degree, and showed that it works well for a large set of matrices. We compared this with the HSL reordering [134, 80], which targets the same objective of reducing the overall number of off-diagonal blocks. While our TSP (Travelling Salesman Problem) heuristic is often more expensive, the quality is always improved, leading to better performance. In the context of multiple factorizations, or when using GPUs, the TSP overhead is recovered by performance improvement, while it may be better to use HSL for the other cases.

► The use of low-rank approximations in sparse direct methods is ongoing work. When applying Gaussian elimination, the Schur complement induced appears to exhibit this low-rank property in several physical applications, especially those arising from elliptic partial differential equations. This property on the low rank of submatrices may then be exploited. Each supernode or front may then be expressed in a low-rank approximation representation. Finally, solvers that exploit this low-rank property may be used either as accurate direct solvers or as powerful preconditioners for iterative methods, depending on how much information is kept.

In the context of the FASTLA associated team, in collaboration with E. Darve from Stanford University, we have been working on applying fast direct solvers for dense matrices to the solution of sparse direct systems with a supernodal approach. We observed that the extend-add operation (during the sparse factorization) is the most time-consuming step. We have therefore developed a series of algorithms to reduce this computational cost. We have presented two approaches using a Block Low-Rank (BLR) compression technique to reduce the memory footprint and/or the time-to-solution of the sparse supernodal solver PASTIX. This flat, non-hierarchical, compression method allows us to take advantage of the low-rank property of the blocks appearing during the factorization of sparse linear systems, which come from the discretization of partial differential equations. The first approach, called *Minimal Memory*, illustrates the maximum memory gain that can be obtained with the BLR compression method, while the second approach, called *Just-In-Time*, mainly focuses on reducing the computational complexity and thus the time-to-solution. We compare Singular Value Decomposition (SVD) and Rank-Revealing QR (RRQR), as compression kernels, in terms of factorization time, memory consumption, as well as numerical properties.

To improve the efficiency of our sparse update kernel for both BLR (block low-rank) and HODLR (hierarchically off-diagonal low-rank), we are now investigating a BDLR (boundary distance low-rank) approximation scheme to preselect rows and columns in the low-rank approximation algorithm. We also have to improve our ordering strategies to enhance data locality and compressibility. The implementation is based on runtime systems to exploit parallelism.

Regarding our activities around the use of hierarchical matrices for sparse direct solvers, this topic is also widely investigated by our competitors. Some related work is described in the last section of this report, but we mention here the following codes :

- STRUMPACK uses Hierarchically Semi-Separable (HSS) matrices for low-rank structured factorization with randomized sampling.
- MUMPS uses Block Low-Rank (BLR) approximations to improve a multifrontal sparse solver.

► This report mainly concerns my work on the PASTIX sparse linear solvers, developed thanks to a long-term collaboration with CEA/CESTA. But I also contributed to external applications through joint research efforts with academic partners enabling efficient and effective technological transfer towards industrial R&D. Outside the scope of this document, I would like to summarize here some of these contributions.

- **Plasma physic simulation:** scientific simulation for ITER tokamak modeling provides a natural bridge between theory and experiment and is also an essential tool for understanding and predicting plasma behavior. Recent progress in numerical simulation of fine-scale turbulence and in large-scale dynamics of magnetically confined plasma has been enabled by access to petascale supercomputers. This progress would have been unreachable without new computational methods and adapted reduced models. In particular, the plasma science community has developed codes for which computer runtime scales quite well with the number of processors up to thousands cores. Other numerical simulation tools designed for the ITER challenge aim at making significant progress in understanding active control methods of plasma edge MHD instability Edge Localized Modes (ELMs) which represent a particular danger with respect to heat and particle loads for Plasma Facing Components (PFC) in the tokamak. The goal is to improve the understanding of the related physics and to propose possible new strategies to improve effectiveness of ELM control techniques. The simulation tool used (JOEKE code) is related to non linear MHD modeling and is based on a fully implicit time evolution scheme that leads to 3D large very badly conditioned sparse linear systems to be solved at every time step. In this context, the use of the PASTIX library to solve efficiently these large sparse problems by a direct method was a challenging issue [81].

Please look at [http://www.labri.fr/perso/ramet/restricted/HDR\\_PPCF09.pdf](http://www.labri.fr/perso/ramet/restricted/HDR_PPCF09.pdf) for a full version of this work with some experiments made during the PhD thesis of Xavier Lacoste [95].

- **Nuclear core simulation:** EDF R&D is developing a nuclear core simulation code named COCAGNE that relies on a Simplified PN (SPN) method for eigenvalue calculations to compute the neutron flux inside the core. In order to assess the accuracy of SPN results, a 3D Cartesian model of PWR nuclear cores has been designed and a reference neutron flux inside this core has been computed with a Monte Carlo transport code from Oak Ridge National Lab. This kind of 3D whole core probabilistic evaluation of the flux is computationally very expensive. An efficient deterministic approach is therefore required to reduce the computation cost dedicated to reference simulations. First, we have completed a study to parallelize an SPN simulation code by using a domain decomposition method, applied for the solution of the neutron transport equations (Boltzmann equations), based on the Schur dual technique and implemented in the COCAGNE code from EDF. This approach was very reliable and efficient on computations coming from the IAEA benchmark and from industrial cases [22]. Secondly, we worked on the parallelization of the DOMINO code, a parallel 3D Cartesian SN solver specialized for PWR core reactivity computations. We have developed a two-level (multi-core + SIMD) parallel implementation of the sweep algorithm on top of runtime systems [112].

Please look at [http://www.labri.fr/perso/ramet/restricted/HDR\\_JCP10.pdf](http://www.labri.fr/perso/ramet/restricted/HDR_JCP10.pdf) and also at [http://www.labri.fr/perso/ramet/restricted/HDR\\_JCP17.pdf](http://www.labri.fr/perso/ramet/restricted/HDR_JCP17.pdf) (submitted to JCP) for a full version of this work with some experiments made during the PhD thesis of Bruno Lathuiliere [97] and Salli Moustafa [111].

- **Electromagnetism simulation:** in collaboration with CEA/CESTA, during his PhD thesis [35], Mathieu Chanaud developed a new parallel platform based on a combination of a multigrid solver and a direct solver (PASTIX) to solve huge linear systems arising from Maxwell's equations discretized with first-order Nédelec elements [36]. In the context of the HPC-PME initiative, we also started a collaboration with AlgoTech and we have organized one of the first PhD-consultant actions at Inria implemented by Xavier Lacoste and led by myself. AlgoTech is one of the most innovative SMEs (small and medium-sized enterprises) in the field of cabling embedded systems, and more broadly, automatic devices. The main target of the project was to validate our sparse linear solvers in the area of electromagnetic simulation tools developed by AlgoTech.

► This report is organized as follows. In Chapter 1, we recall the original implementation of the PASTIX solver based on static scheduling that was well suited for homogeneous architectures. Thanks to the expertise of Pascal Hénon, we developed our basic kernels for the analysis steps that are still relevant for our prediction models. Chapter 2 presents the two approaches we have investigated to address the need for dynamic scheduling when architectures becomes too difficult to model. The second approach is probably the most promising because it allows us to deal with GPU accelerators and Intel Xeon Phi while obtaining rather good efficiency and scalability. In Chapter 3, we first recall our contribution on parallel implementation of an  $ILU(k)$  algorithm within the PASTIX framework. This solution allows us to reduce the memory needed by the numerical factorization. Compared to the other incomplete factorization methods and hybrid solvers based on domain decomposition, we do not need to consider numerical information from the linear system. But the gain in terms of flops and memory is not enough in many cases to compete with multigrid solvers for instance. The second part of this chapter describes some preliminary work regarding using graph partitioning techniques to build a domain decomposition leading to a good balancing of both the interface and the internal nodes of each subdomain, which is a relevant criteria to optimize parallel implementation of hybrid solvers. Finally, we introduce a reordering strategy to improve the blocking arising during the symbolic factorization in Chapter 4. Our attempt to apply fast direct solvers for dense matrices to the solution of sparse direct systems is presented in the second part of this chapter and benefits from both our graph partitioning and reordering heuristics.

# Chapter 1

## Static scheduling and data distributions

This chapter presents some unpublished technical elements that have been introduced in the PASTIX solver to enable MPI+Threads paradigm. This joint work with Pascal Hénon extends the contributions that have been published in [74, 75].

Please look at [http://www.labri.fr/perso/ramet/restricted/HDR\\_PC02.pdf](http://www.labri.fr/perso/ramet/restricted/HDR_PC02.pdf) for a full version of this work with some experiments.

### 1.1 Context and algorithmic choices

Solving large sparse symmetric positive definite systems  $Ax = b$  of linear equations is a crucial and time-consuming step, arising in many scientific and engineering applications. For a complete survey on direct methods, one can refer to [46, 53, 54]. Due to their robustness, direct solvers are often used in industrial codes despite their memory consumption. In addition, the factorization today's used in direct solvers are able to take advantage of the superscalar capabilities of the processors by using blockwise algorithms and BLAS primitives. Consequently, many parallel techniques for sparse matrix factorization have been studied and implemented. The goal of our work was to design efficient algorithms that were able to take advantage of the architectures of the modern parallel computers. In our work, we did not consider the factorization with dynamic pivoting and we only considered matrices with a symmetric sparsity pattern ( $A + A^t$  can be used for unsymmetric cases). In this context, the block structure of the factors and the numerical operations are known in advance and consequently allow the use of static (i.e. before the effective numerical factorization) regulation algorithms for the distribution and the computational task scheduling. Therefore, we developed some high performing algorithms for the direct factorization that were able to exploit very strongly the specificities of the networks and processors of the targeted architectures. In this work, we present some static assignments heuristics and an associated factorization algorithm that achieve very performant results for both runtime and memory overhead reduction.

There are two main approaches for numerical factorization algorithms: the *multifrontal* approach [6, 47], and the *supernodal* one [67, 127].

Both can be described by a computational tree whose nodes represent computations and whose edges represent transfer of data. In the case of the multifrontal method, at each node, some steps of Gaussian elimination are performed on a dense frontal matrix and the remaining Schur complement, or contribution block, is passed to the parent node for assembly. In the case of the supernodal method, the distributed memory version uses a right-looking formulation which, having computed the factorization of a column-block corresponding to a node of the tree, then immediately sends the data to update the column-blocks corresponding to ancestors in the tree. In a parallel context, we can locally aggregate contributions to the same block before sending the contributions. This can significantly reduce the number of messages.

Independently of these different methods, a static or dynamic scheduling of block computations can be used. For homogeneous parallel architectures, it is useful to find an efficient static scheduling [121]. In this context, this scheduling can be induced by a fine cost computation/communication model.

The PSPASES solver [85] is based on a multifrontal approach without pivoting for symmetric positive definite systems. It uses METIS [87] for computing a fill-reducing ordering which is based on a multilevel nested dissection algorithm; when the graph is separated into  $p$  parts, a multiple minimum degree (MMD [102]) is then used. A “subtree to subcube”-like algorithm is applied to build a static mapping before the numerical factorization. In [7] the performance of MUMPS [4] and SUPERLU [99] are compared for nonsymmetric problems. MUMPS uses a multifrontal approach with dynamic pivoting for stability while SUPERLU is based on a supernodal technique with static pivoting.

In previous work [74, 75], we have proposed some high performing algorithms for high performance sparse supernodal factorization without pivoting. These techniques yield a static mapping and scheduling algorithm based on a combination of 1D and 2D block distributions. Thus, we achieved very good performance by taking into account all the constraints of the problem as well as the specificities (communication and computation) of the parallel architecture. In addition, we have studied a way to control the memory overhead due to the buffering needed to reduce the communication volume. In the case of our supernodal factorization, this buffering corresponds to the local aggregation approach in which all local contributions for the same non-local block are summed in a temporary block buffer before being sent (see section 1.3). Consequently, we have improved the mechanism of local aggregation that may lead to great overheads of memory consumption for 3D problems in an all-distributed memory context. In [76] we presented the mechanism to control this memory overhead that preserves relatively good runtime performance.

We have implemented our algorithms in a library called PASTiX that manages  $L.L^t$ ,  $L.D.L^t$  factorizations and more generally  $L.U$  factorization when the symmetrized pattern  $A + A^t$  is considered. We have both real and complex version for the  $L.D.L^t$  and  $L.U$  factorization. The PASTiX library has been successfully used in industrial simulation codes to solve systems of several million unknowns [59, 60]. Until now, our study was suitable for homogeneous parallel/distributed architectures in the context of a message passing paradigm.

In the context of Symmetric Multi-Processing (SMP) node architectures, to fully exploit shared memory advantages, a relevant approach is to use a hybrid MPI+Thread implementation. This approach in the framework of direct solvers aims to solve problems with more than 10 million unknowns, which is now a reachable challenge with new SMP supercomputers. The rationale that motivated this hybrid implementation was that the communications within an SMP node can be advantageously substituted by direct accesses to shared memory between the processors in the SMP node using threads. In addition, the MPI-communication between processes are grouped by SMP nodes. Consequently, whereas in the pure MPI implementation the static mapping and scheduling were computed by MPI process, in the new MPI+Thread implementation, the mapping is still computed by MPI process but the task scheduling is computed by thread.

## 1.2 Background

This section provides a brief background on sparse Gaussian elimination techniques, including their graph models. Details can be found in [40, 46, 54] among others. Consider the linear system

$$Ax = b \tag{1.1}$$

where  $A$  is a symmetric definite positive matrix of size  $n \times n$  or a unsymmetric matrix with a symmetric nonzero pattern. In this context, sparse matrix techniques often utilize the non-oriented adjacency graph  $G = (V, E)$  of the matrix  $A$ , a graph whose  $n$  vertices represent the  $n$  unknowns, and whose edges  $(i, j)$  represent the couplings between unknowns  $i$  and  $j$ . The Gaussian Elimination ( $L.L^t$  Cholesky factorization or  $L.U$  factorization) process introduces “fill-in”s, i.e., new edges in the graph. The quality of the direct solver depends critically on the ordering of the unknowns as this has a major impact on the number of fill-ins generated.

Sparse direct solvers often utilize what is known as the “filled graph” of  $A$ , which is the graph of the (complete) Cholesky factor  $L$ , or rather of  $L + U$ . This is the original graph augmented with all the fill-in generated during the elimination process. We will denote by  $G^* = (V, E^*)$  this graph.

Two well-known and useful concepts will be needed in later sections. The first is that of *fill paths*. This is a path between two nodes  $i$  and  $j$  (with  $i \neq j$ ) in the original graph  $G = (V, E)$ , whose intermediate

nodes are all numbered lower than both  $i$  and  $j$ . A theorem by Rose and Tarjan [100] states that there is a fill path between  $i$  and  $j$  if and only if  $(i, j)$  is in  $E^*$ , i.e., there will be a fill-in in position  $(i, j)$ .

The second important concept is that of an *elimination tree* [103], which is useful among other things, for scheduling the tasks of the solver in a parallel environment [8, 75]. The elimination tree captures the dependency between columns in the factorization. It is defined from the filled graph using the parent relationship:

$$\text{parent}(j) = \min\{i \mid i > j \text{ and } (i, j) \in E^*\}.$$

Two broad classes of reorderings for sparse Gaussian elimination have been widely utilized. The first, which tends to be excellent at reducing fill-in is the *minimal degree* ordering. This method, which has many variants, is a local heuristic based on a greedy algorithm [5]. The class of *nested dissection* algorithms [54], considered in this work, is common in the “static” variants of Gaussian elimination which preorder the matrix and define the tasks to be executed in parallel at the outset. The nested dissection ordering utilizes recursively a sequence of separators. A separator  $C$  is a set of nodes which splits the graph into two subgraphs  $G_1$  and  $G_2$  such that there is no edge linking a vertex of  $G_1$  to a vertex of  $G_2$ . This is then done recursively on the subgraphs  $G_1$  and  $G_2$ . The left side of Figure 1.1 shows an example of a physical domain (e.g., a finite element mesh) partitioned recursively in this manner into a total of 8 subgraphs. The labeling used by Nested Dissection can be defined recursively as follows: label the nodes of the separator last after (recursively) labeling the nodes of the children. This defines naturally a tree structure as shown in the right side of Figure 1.1. The remaining subgraphs are then ordered by a minimum degree algorithm under constraints [117].

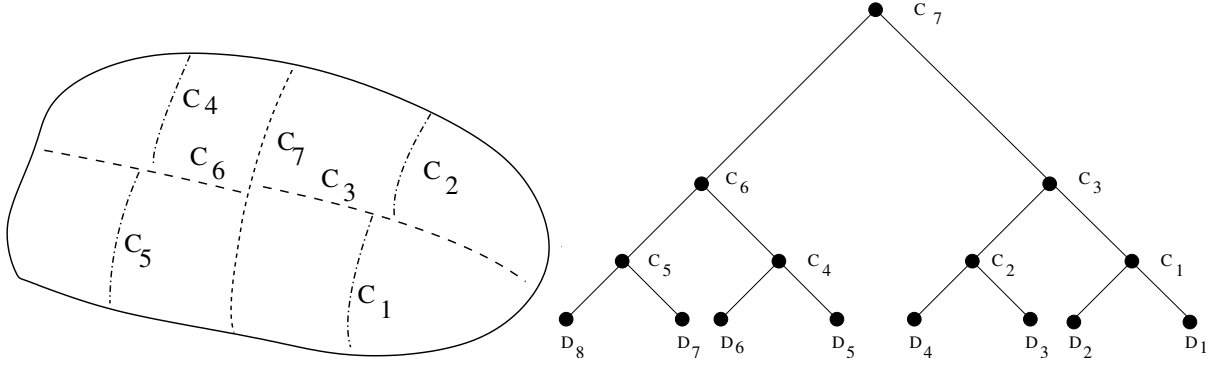


Figure 1.1: The nested dissection of a physical mesh and corresponding tree

An ideal separator is such that  $G_1$  and  $G_2$  are of about the same size while the set  $C$  is small. A number of efficient graph partitioners have been developed in recent years which attempt to reach a compromise between these two requirements, see, e.g., [87, 116, 71] among others.

After a good ordering is found a typical solver performs a *symbolic factorization* which essentially determines the pattern of the factors. This phase can be elegantly expressed in terms of the elimination tree. We will denote by  $[i]$  the sparse pattern of a column  $i$  which is the list of rows indices in increasing order corresponding to nonzeros terms.

---

**Algorithm 1:** Sequential symbolic factorization algorithm

---

Build  $[i]$  for each column  $i$  in the original graph;  
**for**  $i = 1 \dots n - 1$  **do**  
   $[\text{parent}(i)] = \text{merge}([i], [\text{parent}(i)])$  ;

---

where  $\text{merge}([i], [j])$  is a function which merges the patterns of column  $i$  and  $j$  in the lower triangular factor. In a parallel implementation, this is better done with the help of a post-order traversal of the tree: the pattern of a given node only depends on the patterns of the children and can be obtained once these are computed. The symbolic factorization is a fairly inexpensive process since it utilizes two nested loops instead of the three loops normally required by Gaussian elimination. Note that all computations are symbolic, the main kernel being the **merge** of two column patterns.

Most sparse direct solvers take advantage of dense computations by exhibiting a *dense block structure in the matrix  $L$* . This dense block structure is directly linked to the ordering techniques based on the

nested dissection algorithm (ex: METIS [87] or SCOTCH [118]). Indeed the columns of  $L$  can be grouped in sets such that all columns of a same set have a similar non zero pattern. Those sets of columns, called *supernodes*, are then used to prune the block structure of  $L$ . The supernodes obtained with such orderings mostly correspond to the separators found in the nested dissection process of the adjacency graph  $G$  of matrix  $A$ .

An important result used in direct factorization is that the partition  $\mathcal{P}$  of the unknowns induced by the supernodes can be found without knowing the non zero pattern of  $L$  [104]. The partition  $\mathcal{P}$  of the unknowns is then used to compute the block structure of the factorized matrix  $L$  during the so-called *block symbolic factorization*. The block symbolic factorization exploits the fact that, when  $\mathcal{P}$  is the partition of separators obtained by nested dissection then we have:

$$Q(G, \mathcal{P})^* = Q(G^*, \mathcal{P})$$

where  $Q(G, \mathcal{P})$  is the quotient graph of  $G$  with regards to partition  $\mathcal{P}$ . Then, we can deduce the *block elimination tree* which is the elimination tree associated with  $Q(G, \mathcal{P})^*$  and which is well suited for parallelism [75]. It is important to keep in mind that this property can be used to prune the block structure of the factor  $L$  because one can find the supernode partition from  $G(A)$  [104].

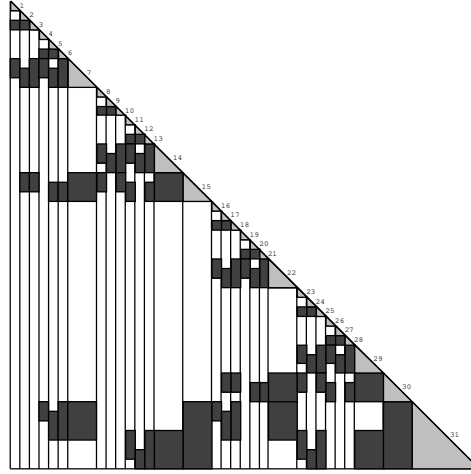


Figure 1.2: Block data structure of a factorized matrix.  $N = 31$  column-blocks. Diagonal blocks are drawn in light grey and off-diagonal blocks in dark grey.

Figure 1.2 shows the block structure obtained for a 7x7 grid ordered by nested dissection.

The block symbolic structure (see Figure 1.2) consists of  $N$  column-blocks, each of them containing a dense symmetric diagonal block and a set of dense rectangular off-diagonal blocks. In this block data structure, an off-diagonal block is represented by a pair of integers  $(\alpha, \beta)$  corresponding to the first and the last rows of this block in the column block. We will denote by  $[i]$  the block sparse pattern of a supernode  $i$  which is the list in increasing order of such intervals.

As a result the block symbolic factorization will now need to merge two sets of intervals.

---

**Algorithm 2:** Block symbolic factorization

---

Build  $[i]$  for each supernode  $i$  in the original graph ;

**for**  $i = 1 \dots N - 1$  **do**

$[ \text{parent}(i) ] = \mathbf{Bmerge} ([i], [ \text{parent}(i) ] ) ;$

---

where now **Bmerge** will merge two sorted lists of intervals and where **parent()** defines the father relationship in the block elimination tree.

It was shown by Charrier and Roman [38] that the cost of computing the block symbolic factorization when a nested dissection algorithm is used, is  $O(N)$  for most graphs. In other words, the total number of blocks to be handled is  $O(N)$  which means that a total of  $O(N)$  pointers and operations are required to perform the block symbolic factorization.

A sparse block factorization algorithm can be obtained by restricting the standard dense block algorithm to the sparsity pattern which has been computed by the symbolic factorization phase.

---

**Algorithm 3:** Sparse block  $LDL^t$  Factorization

---

```

for  $k = 1, \dots, N$  do
  Factor  $A_{k,k}$  into  $A_{k,k} = L_k D_k L_k^T$  ;
  for  $j \in [k]$  do
    Compute  $A_{jk}^T = D_k^{-1} L_k^{-1} A_{jk}^T$  ;
  for  $j \in [k]$  do
    for  $i \in [k], i > j$  do
       $A_{ij} := A_{ij} - A_{ik} D_k A_{jk}^T$  ;

```

---

These algorithms are parallelized and implemented in our supernodal direct solver PASTIX [75, 76]. Since PASTIX deals with matrices that have a symmetric pattern, the algorithms presented in the remain of this work are based on the assumption that the adjacency graph is symmetric.

## 1.3 Static scheduling

### 1.3.1 Preprocessing steps

In order to achieve efficient parallel sparse factorization, we perform the three sequential preprocessing phases:

- The *ordering* phase, which computes a symmetric permutation of the initial matrix  $A$  such that the factorization process will exhibit as much concurrency as possible while incurring low fill-in. In the software chain, we use the package SCOTCH [116] that uses a tight coupling of the Nested Dissection and Approximate Minimum Degree algorithms [5, 117]. The partition of the original graph into supernodes is achieved by merging the partition of separators computed by the Nested Dissection algorithm and the supernodes amalgamated for each subgraph ordered by Halo Approximate Minimum Degree.
- The *block symbolic factorization* phase, which determines the block data structure of the factorized matrix  $L$  associated with the partition resulting from the ordering phase. This structure consists of  $N$  column-blocks, each containing a dense symmetric diagonal block and a set of dense rectangular off-diagonal blocks (see Figure 1.2). One can efficiently perform such a block symbolic factorization in quasi-linear space and time complexities [38]. From the block structure of  $L$ , one can deduce the weighted elimination quotient graph that describes all dependencies between column-blocks, as well as the supernodal elimination tree.
- The *block repartitioning and scheduling* phase, which refines the previous partition by splitting large supernodes in order to exploit concurrency within dense block computations in addition to the parallelism provided by the block elimination tree, both induced by the block computations in the supernodal solver (we use a version with a local aggregation of the outgoing contributions for the blocks mapped on other processors). Once the initial supernodal partition is refined, the scheduling phase consists in mapping onto the processors the resulting blocks according to a 1D scheme (i.e. by column blocks) for the lower part of the tree, and according to a 2D scheme (i.e. by blocks) for the upper part of the tree. In this phase, we also compute a static optimized scheduling of the computational and communication tasks according to BLAS and communication time models calibrated on the target machine. This static scheduling will drive the parallel factorization and the backward and forward substitutions [72, 76]. The *block repartitioning and scheduling* phase will be detailed in the section 1.3.5.

### 1.3.2 Parallel scheme of the factorization

In this section, we describe how the factorization algorithm is parallelized. For the ease of understanding, we will firstly describe the parallelization in a classical all distributed way: each processor is assigned to a part of the matrix and all communications are made using MPI. Then the section 1.3.3 will describe



how the parallelization is modified to benefit from SMP nodes architecture through the MPI+Thread implementation and the section 1.3.4 will give details of the parallel algorithm.

Using the block structure induced by the symbolic factorization, the sequential blockwise supernodal factorization algorithm can be written as in Algorithm 3.

The parallelization of the algorithm can be made in two different ways that come along with two block distribution schemes. The first one is to parallelize the main loop over the column blocks (first line of the Algorithm 3). This kind of parallelization leads to a column-block distribution; each processor computes the main loop iterations for a column-block subset of the global matrix. This type of distribution is called “one dimensional” (1D) distribution because it only involves a partition of the matrix along the column-block indices. The only communications needed are then the updates of blocks  $A_{ij}$  in the inner loop. Generally, within the local column-block factorization, a processor has to update several times a block  $A_{ij}$  on another processor. It would be costly to send each contribution for a same non-local block in separated messages. The so-called “local aggregation” variant of the supernodal parallel factorization consists in adding locally any contribution for a non-local block  $A_{ij}$  in a local temporary block and sending it once all the contributions for this block have been added. We will denote such a temporary block by  $AUB_{ij}$  in the following sections.

The second way is to parallelize the inner loop over the blocks. This kind of parallelization leads to a block distribution; the blocks of a column-block can be mapped on different processors. This kind of distribution is called “two dimensional” (2D) distribution. In this version, the communications are of two types:

- the first type is the updates of non-local blocks; these communications are made in the same manner as in the 1D distribution;
- the second type is the communications needed to perform the block operations when the processor in charge of these operations does not own all the blocks involved in the same column-block.

The 1D and 2D parallelization are appealing in different ways:

- the 1D distribution allows us to use BLAS with the maximum efficiency allowed by the blockwise algorithmic. Indeed, the ‘solve’ steps in the same column-block of the Algorithm 3 can be grouped in a single *TRSM* (BLAS3 subroutine). In addition, for an iteration  $j$ , the ‘update’ steps can be grouped in a single *GEMM*. This compacting optimizes the pipeline effect in the BLAS subroutine and consequently the runtime performance.
- the 2D distribution has a finer grain parallelism. It exhibits more parallelism in the factorization than the 1D distribution but loses some BLAS efficiency in comparison.

We use a parallelization that takes advantage of both 1D and 2D parallelizations. Considering the block elimination tree, the nodes on the lower part usually involve one or a few processors in their elimination during the factorization whereas the upper part involved many of the processors and the root potentially involve all the processors. As a consequence, the factorization of the column-blocks corresponding to the lower nodes of the block elimination tree takes more benefit from a 1D distribution in which the BLAS efficiency is privileged over the parallelism grain. For the opposite reasons, the column-blocks corresponding to the highest nodes of the block elimination tree use a parallel elimination based on a 2D distribution scheme. The criterion to switch between a 1D and 2D distribution depends on the machine network capabilities, the number of processors and the amount of work in the factorization. Such a criterion seems difficult to obtain from a theoretical analysis. Then we use an empirical criterion that is calibrated on the targeted machine [74].

### 1.3.3 Hybrid MPI+Thread implementation

Until now, we have discussed the parallelization in a full distributed memory environment. Each processor was assumed to manage a part of the matrix in its own memory space and any communication needed to update non local blocks of the matrix was considered under the message passing paradigm. Nowadays the massively parallel high performance computers are generally designed as a network of

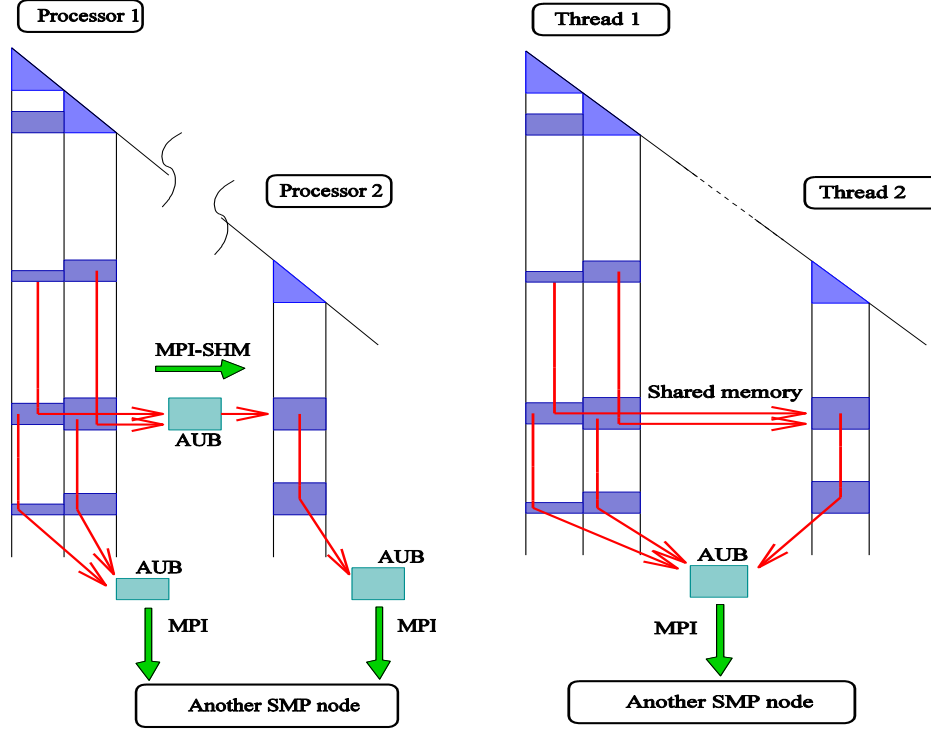


Figure 1.3: MPI+Thread implementation for multicore architectures.

SMP nodes. Each SMP nodes consists in a set of processors that share the same physical memory. On most of these machines, though the MPI interface is not changed, the communication layer of the library takes advantage of the share memory capabilities for the messages between processors in the same SMP node.

Nevertheless, a major memory bottleneck for the parallel supernodal factorization is caused by the local aggregation mechanism we discussed in the previous section. Indeed, an aggregate update block ( $AUB$ ) resides in memory from the first time a contribution is added until the last contribution is added. For matrices coming from 3D problems, the peak memory consumption due to the storage of  $AUB$ s during the factorization is several times greater than for the local part of the matrix.

The local aggregation mechanism is inherent to the message passing model used in the parallel factorization algorithm. So, in an SMP context, the simplest way to reduce the use of aggregate update blocks is to avoid the message passing communications between processors on a same node. In order to avoid these intra-node communications, we use threads that share the same memory space. Inside a node, a unique MPI process spawns a thread on each processor. These threads are then able to address the whole memory space of the node. Each thread is therefore able to access the part of the matrix mapped on the MPI process. In this way, though the computational tasks are distributed between the threads, any update on the matrix part of the MPI process is directly added in the local matrix. The communication between MPI processes still use the local aggregation scheme we described before. This hybrid MPI+Thread strategy is pictured in the figure 1.3.

#### 1.3.4 Parallel factorization algorithm

Let us consider the block data structure of the factorized matrix  $L$  computed by the block symbolic factorization. Recall that each of the  $N$  column-blocks holds one dense diagonal block and some dense

off-diagonal blocks. Then we define the two sets:  $BStruct(L_{k*})$  is the set of column-blocks that update column-block  $k$ , and  $BStruct(L_{*k})$  is the set of column-blocks updated by column-block  $k$  (see [72, 73, 74, 75] for details).

Let us now consider a parallel supernodal version of sparse factorization with total local aggregation: all non-local block contributions are aggregated locally in block structures. This scheme is close to the Fan-In algorithm [19] as processors communicate using only aggregated update blocks. These aggregated update blocks, denoted in what follows by AUB, can be built from the block symbolic factorization. These contributions are locally aggregated before being sent. The proposed algorithm can yield 1D (column-block) or 2D (block) distributions [72, 74].

The pseudo-code of  $LL^T$  factorization can be expressed in terms of dense block computations or *tasks*; these computations are performed, as much as possible, on compacted sets of blocks for BLAS efficiency.

Let us introduce the notation:

- $\tau$  : local thread number;
- $\pi$  : local process number;
- $N_\tau$  : total number of tasks mapped on thread  $\tau$ ;
- $K_\tau[i]$  :  $i^{th}$  task of thread  $\tau$ ;
- for the column-block  $k$ , symbol  $\star$  means  $\forall j \in BStruct(L_{*k})$ ;
- let  $j \geq k$ ; sequence  $[j]$  means  $\forall i \in BStruct(L_{*k}) \cup \{k\}$  with  $i \geq j$ .
- $map2process(,)$  operator is the 2D block mapping function by process.

Block computations can be classified in four types, and the associated tasks are defined as follows:

- **COMP1D(k)** : *factorize the column-block  $k$  and compute all the contributions for the column-blocks in  $BStruct(L_{*k})$* 
  - . Factorize  $A_{kk}$  into  $L_{kk}L_{kk}^t$
  - . Solve  $L_{kk}A_{*k}^t = A_{*k}^t$
  - . **For**  $j \in BStruct(L_{*k})$  **Do**
  - .     Compute  $C_{[j]} = L_{[j]k}A_{*k}^t$
  - .     **If**  $map2process([j], j) == \pi$  **Then**  $A_{[j]j} = A_{[j]j} - C_{[j]}$
  - .     **Else**  $AUB_{[j]j} = AUB_{[j]j} + C_{[j]}$
- **FACTOR(k)** : *factorize the diagonal block  $k$* 
  - . Factorize  $A_{kk}$  into  $L_{kk}L_{kk}^t$
- **BDIV(j,k)** : *update the off-diagonal block  $j$  in column-block  $k$* 
  - . Solve  $L_{kk}A_{jk}^t = A_{jk}^t$
- **BMOD(i,j,k)** : *compute the contribution of the block  $i$  in column-block  $k$  for block  $i$  in column-block  $j$* 
  - . Compute  $C_i = L_{ik}A_{jk}^t$
  - . **If**  $map2process(i, j) == \pi$  **Then**  $A_{ij} = A_{ij} - C_i$
  - . **Else**  $AUB_{ij} = AUB_{ij} + C_i$

On each thread  $\tau$ ,  $K_\tau$  is the vector of tasks for computations (lines 2 on Figure 1.4), ordered by priority. Each task should have received all its contributions and should have updated associated local data before any new contribution is computed. When the last contribution is aggregated in the corresponding AUB, this aggregated update block is said to be “completely aggregated” and is ready to be sent. To achieve a good efficiency, the sending of AUB has to match the static scheduling of tasks on the destination processor.

```

1. For  $n = 1$  to  $N_\tau$  Do
2.   Switch (  $\text{Type}(K_\tau[n])$  ) Do
3.     COMP1D: Receive all  $\text{AUB}_{[k]k}$  for  $A_{[k]k}$ 
4.     COMP1D( $k$ )
5.     If  $\text{AUB}_{[j],j}$  is completed then send it to  $\text{map2process}(i,j)$ 
6.     FACTOR: Receive all  $\text{AUB}_{kk}$  for  $A_{kk}$ 
7.     FACTOR( $k$ )
8.     send  $L_{kk}D_k$  to  $\text{map2process}([k], k)$ 
9.     BDIV: Receive  $L_{kk}$  and all  $\text{AUB}_{jk}$  for  $A_{jk}$ 
10.    BDIV( $j, k$ )
11.    send  $A_{jk}^t$  to  $\text{map2process}([j], k)$ 
12.    BMOD: Receive  $A_{jk}^t$ 
13.    BMOD( $i, j, k$ )
14.    If  $\text{AUB}_{i,j}$  is completed then send it to  $\text{map2process}(i,j)$ 

```

Figure 1.4: Outline of the parallel factorization algorithm.

### 1.3.5 Matrix mapping and task scheduling

Before running the general parallel algorithm presented above, we must perform a step consisting of partitioning and mapping the blocks of the symbolic matrix onto the set of SMP nodes. The partitioning and mapping phase aims at computing a static assignment that balances workload and enforces the precedence constraints imposed by the factorization algorithm; the block elimination tree structure must be used there.

Our main algorithm is based on a static regulation led by a time simulation during the mapping phase. Thus, the partitioning and mapping step generates a fully ordered schedule used in the parallel factorization. This schedule aims at statically regulating all of the issues that are classically managed at runtime. To make our scheme very reliable, we estimate the workload and message passing latency by using a BLAS and communication network time model, which is automatically calibrated on the target architecture.

Unlike usual algorithms, our partitioning and distribution strategy is divided in two distinct phases. The partition phase splits column-blocks associated with large supernodes, builds, for each column-block, a set of candidate threads for its mapping, and determines if it will be mapped using a 1D or 2D distribution. Once the partitioning step is over, the task graph is built. In this graph, each task is associated with the set of candidate threads of its column-block. The mapping and scheduling phase then optimally maps each task onto one of these threads. An important constraint is that once a task has been mapped on a thread then all the data accessed by this thread are also mapped on the process associated with the thread. This means that an unmapped task that accesses a block already mapped will be necessarily mapped on the same process (i.e. SMP node).

The partitioning algorithm is based on a recursive top-down strategy over the block elimination tree provided by block symbolic factorization. Pothen and Sun presented such a strategy in [121]. It starts by splitting the root and assigning it to a set of candidate threads  $Q$  that is the set of all threads. Given the number of candidate threads and the size of the supernodes, it chooses the strategy (1D or 2D) that the mapping and scheduling phase will use to distribute this supernode. Then each subtree is recursively assigned to a subset of  $Q$  proportionally to its workload.

Once the partitioning phase has built a new partition and the set of candidate threads for each task, the election of an owner thread for each task falls to the mapping and scheduling phase. The idea behind this phase is to simulate parallel factorization as each mapping comes along. Thus, for each thread, we define a timer that will hold the current elapsed computation time, and a ready task heap. At a given time, this task heap will contain all tasks that are not yet mapped, that have received all of their contributions, and for which the thread is a candidate. The algorithm starts by mapping the leaves of the elimination tree (those which have only one candidate thread). After a task has been mapped, the next task to be mapped is selected as follows: we take the first task of each ready task heap and choose the one that comes from the lowest node in the elimination tree. The communication pattern of all the contributions for a task depends on the already mapped tasks and on the candidate thread for the ownership of this task. The task is mapped onto the candidate thread that will be able to compute it the soonest.

As a conclusion about the partitioning and mapping phase, we can say that we obtain a strategy that allows us to take into account, in the mapping of task computations, all the phenomena that occur during the parallel factorization. Thus we achieve a block computation and communication scheme that drives the parallel solver efficiently.

## 1.4 Reducing the memory footprint using partial agregation techniques

In the previous section, we have presented a mapping and scheduling algorithm for clusters of SMP nodes and we have shown the benefits on performance of such strategies. In addition to the problem of runtime performance, another important aspect in the direct resolution of very large sparse systems is the large memory requirement usually needed to factorize the matrix in parallel. A critical point in industrial large-scaled application can be the memory overhead caused by the structures related to the distributed data managment and the communications. These memory requirements can be caused by either the structures needed for communication (the AUB structures in our case) or by the matrix coefficients themselves.

To deal with those problems of memory management, our statically scheduled factorization algorithm can take advantage of the deterministic access (and allocation) pattern to all data stored in memory. Indeed the data access pattern is determined by the computational task ordering that drives the access to the matrix coefficient blocks, and by the communication priorities that drive the access to the AUB structures. We can consider two ways of using this predictable data access pattern:

- the first one consists in reducing the memory used to store the AUB by allowing some AUB still uncompleted to be sent in order to temporarily free some memory. In this case, according to a memory limit fixed by the user, the AUB access pattern is used to determine which partially updated AUB should be sent in advance to minimize the impact on the runtime performance;
- the second one is applied to an “out-of-core” version of the parallel factorization algorithm. In this case, according to a memory limit fixed by the user, we use the coefficient block access pattern to reduce the I/O volume and anticipate I/O calls.

In the case of the supernodal factorization with total aggregation of the contributions, this overhead is mainly due to the memory needed to store the AUB until they are entirely updated and sent. Indeed, an aggregated update block AUB is an overlapping block of all the contributions from a processor to a block mapped on another processor. Hence an AUB structure is present in memory since the first contribution is added within and is released when it has been updated by its last contribution and actually sent. In some cases, particularly for matrices coming from 3D problems, the amount of memory needed for the AUB still in memory can become important compared to the memory needed to store the matrix coefficients.

A solution to address this problem is to reduce the number of AUBs simultaneously present in memory. Then, the technique consists in sending some AUBs partially updated before their actual completion and then temporarily save some memory until the next contribution to be added in such AUB. This method is called *partial agregation* [20].

The *partial agregation* induces a time penalty compared to the *total agregation* due to more dynamic memory reallocations and an increased volume of communications. Nevertheless, using the knowledge of the AUB access pattern and the priority set on the messages, one can minimize this overhead.

Indeed by using the static scheduling, we are able to know, by following the ordered task vector and the communication priorities, when an allocation or a deallocation will occur in the numerical factorization. That is to say that we are able to trace the memory consumption along the factorization tasks without actually running it. Then, given a memory limit set by the user, the technique to minimize the number of partially updated AUBs needed to enforce this limitation is to choose some partially updated AUBs among the AUBs in “memory” that will be updated again the later in the task vector. This is done whenever this limit is overtaken in the logical traversal of the task vector.

Name	Columns	NNZ <sub>A</sub>	NNZ <sub>L</sub>	OPC	$\frac{NNZ_L}{OPC}$	Description
<b>BMWCR1</b>	148770	5247616	6.597301e+07	5.701988e+10	1.16e-3	PARASOL
<b>SHIP003</b>	121728	3982153	5.872912e+07	8.008089e+10	0.73e-3	PARASOL
<b>CUBE47</b>	103823	1290898	4.828456e+07	6.963850e+10	0.69e-3	3D Mesh
<b>THREAD</b>	29736	2220156	2.404333e+07	3.884020e+10	0.62e-3	PARASOL

Table 1.1: Description of some test problems. NNZ<sub>A</sub> is the number of off-diagonal terms in the triangular part of matrix  $A$ , NNZ<sub>L</sub> is the number of off-diagonal terms in the factorized matrix  $L$  and  $OPC$  is the number of operations required for the factorization. Matrices are sorted in decreasing order of  $\frac{NNZ_L}{OPC}$  which is a measure of the potential data reuse.

Our experiments are performed on some sparse matrices coming from the PARASOL Project. The almost part of theses matrices are structural mechanics and CFD matrices. The values of the associated measurements in Table 1.1 come from scalar column symbolic factorization.

Figure 1.5 shows the time penalty observed for 4 test problems with different levels of AUB memory constraints. That stresses the interest of the partial aggregation technique, there is a fine trade-off between the runtime performance provided by the total aggregation strategy and the low memory overhead provided by an aggregation-free algorithm. These results show that the memory reduction is acceptable in terms of time penalty up to 50% extra-memory reduction. As we can see, an extra-memory reduction about 50% induces a factorization time overhead between 2.7% and 28.4% compared to the time obtained with total aggregation technique. In that context, our extra-memory management leads to a good memory scalability.

Furthermore, this technique allows us to factorize the AUDI matrix (3D problem from PARASOL collection with more than 5 Tflop which is a difficult problem for direct methods in terms of memory overhead) in 188s on 64 Power3 processors with a reduction of 50% of memory overhead (about 28 Gflops).

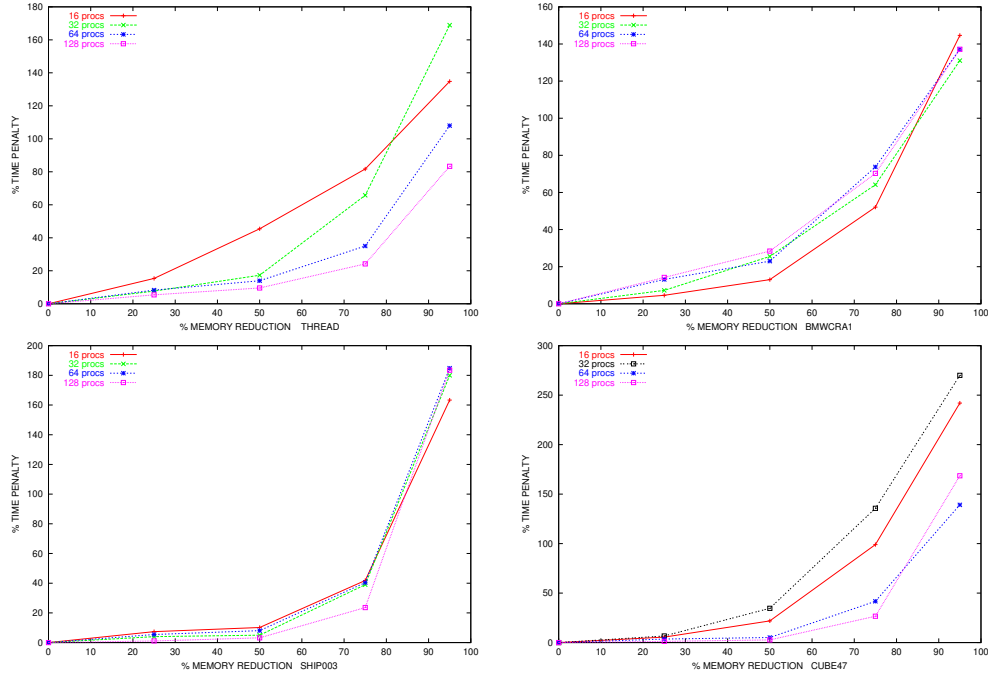


Figure 1.5: Percentage of time penalty / percentage of memory overhead reduction.



## Chapter 2

# Dynamic scheduling and runtime systems

The first part of this chapter presents the work that has been developed in the PhD thesis of Mathieu Faverge [48] (in french) that I have co-advised. Some contributions have been submitted to [49] (*according to the organizers, the proceedings have suffered many unfortunate delays due to extenuating circumstances, but will finally be published in two volumes, LNCS 6126 and 6127 in 2012*).

The second part of this chapter presents the work that has been developed in the PhD thesis of Xavier Lacoste [95] (in english) that I have co-advised. Some contributions have been published in [96].

Please look at [http://www.labri.fr/perso/ramet/restricted/HDR\\_HCW14.pdf](http://www.labri.fr/perso/ramet/restricted/HDR_HCW14.pdf) for a full version of this work with some experiments.

## 2.1 A dedicated approach

NUMA (Non Uniform Memory Access) architectures have an important effect on memory access costs, and introduce contention problems which do not exist on SMP (Symmetric Multi-Processor) nodes. Thus, the main data structure of the sparse direct solver PASTIX has been modified to be more suitable for NUMA architectures. A second modification, relying on overlapping opportunities, allows us to split computational or communication tasks and to anticipate as much as possible the data receptions. We also introduce a simple way to dynamically schedule an application based on a dependency tree while taking into account NUMA effects. Results obtained with these modifications are illustrated by showing the performance of the PASTIX solver on different platforms and matrices.

After a short description of architectures and matrices used for numerical experiments in Section 2.1.1, we study data allocation and mapping taking into account NUMA effects (see Section 2.1.2). Section 2.1.3 focuses on the improvement of the communication overlap as preliminary work for a dynamic scheduler. Finally, a dynamic scheduler is described and evaluated on the PASTIX solver for various test cases in Sections 2.1.4 and 2.1.5.

### 2.1.1 NUMA architectures

Two NUMA and one SMP platforms have been used in this work :

- The first NUMA platform, see Figure 2.1a, denoted as “NUMA8”, is a cluster of ten nodes interconnected by an Infiniband network. Each node is made of four Dual-Core AMD Opteron(tm) processors interconnected by HyperTransport. The system memory amounts to 4GB per core giving a total of 32GB.
- The second NUMA platform, see Figure 2.1b, called “NUMA16”, is a single node of eight Dual-Core AMD Opteron(tm) processors with 64GB of memory.



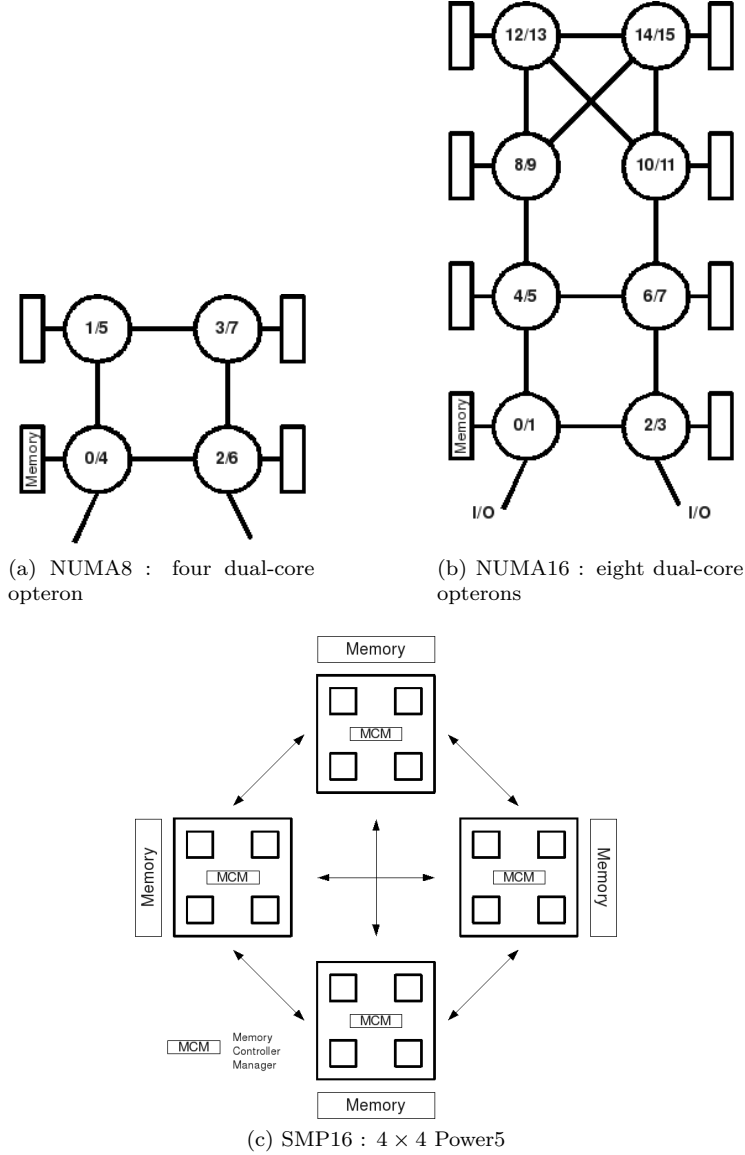


Figure 2.1: Architectures used for benchmarks

- The SMP platform is a cluster of six IBM p575 nodes, see Figure 2.1c, called “SMP16”. These nodes are interconnected by an IBM Federation network. Four blocks of four Power5 with 8GB are installed in each node. However, the memory available is limited to 28GB by the system.

Tests on NUMA effects have been performed on the three platforms and tests on communications have been performed on the IBM Federation network and on the Infiniband network with respectively the IBM MPI implementation and Mvapich2 that support the `MPI_THREAD_MULTIPLE` threading model.

Our research targeted the parallel sparse direct solver PASTIX which uses a hybrid MPI+Threads implementation. Improvements made on the solver have been tested on a set of eight matrices described in Table 2.1. All matrices are double precision real matrices with the exception of the last one (*HALTERE*) which is a double precision complex matrix. *MATR5* is an unsymmetric matrix (with a symmetric pattern).

Name	Columns	$NNZ_A$	$NNZ_L$	OPC
MATR5	485 597	24 233 141	1 361 345 320	9.84422e+12
AUDI	943 695	39 297 771	1 144 414 764	5.25815e+12
NICE20	715 923	28 066 527	1 050 576 453	5.19123e+12
INLINE	503 712	18 660 027	158 830 261	1.41273e+11
NICE25	140 662	2 914 634	51 133 109	5.26701e+10
MCHLNF	49 800	4 136 484	45 708 190	4.79105e+10
THREAD	29 736	2 249 892	25 370 568	4.45729e+10
HALTERE	1 288 825	10 476 775	405 822 545	7.62074e+11

$NNZ_A$  is the number of off-diagonal terms in the triangular part of the matrix  $A$ ,  $NNZ_L$  is the number of off-diagonal terms in the factorized matrix  $L$  and  $OPC$  is the number of operations required for the factorization.

Table 2.1: Matrices used for experiments

### 2.1.2 NUMA-aware allocation

Modern multi-processing architectures are commonly based on shared memory systems with a NUMA behavior. These computers are composed of several chipsets including one or several cores associated with a memory bank. The chipsets are linked together with a cache-coherent interconnection system. Such an architecture implies hierarchical memory access times from a given core to the different memory banks. This architecture also possibly incurs different bandwidths following the respective location of a given core and the location of the data sets that this core is using [16, 92]. It is thus important on such platforms to take these processor/memory locality effects into account when allocating resources. Modern operating systems commonly provide some API dedicated to NUMA architectures which allow programmers to control where threads are executed and memory is allocated. These interfaces have been used in the following part to exhibit NUMA effects on our three architectures.

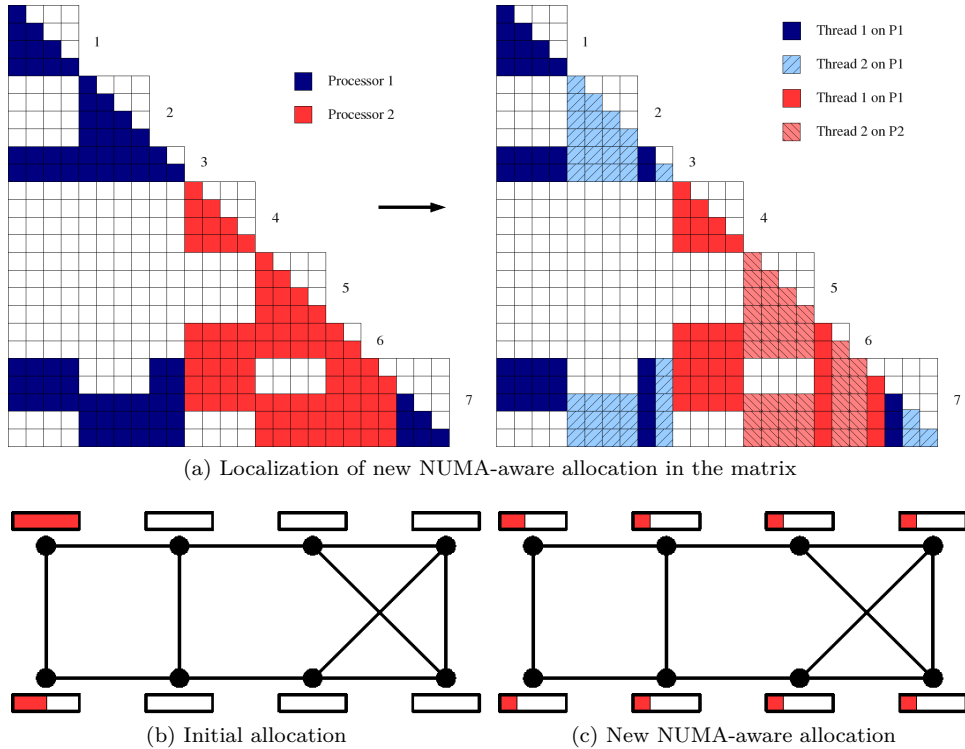


Figure 2.2: NUMA-aware allocation

The hybrid MPI/thread version of the PASTIX solver already uses a function to bind threads on cores for different systems (LINUX, AIX, MacOS, ...). However, in its initial version, PASTIX does not take

into account NUMA effects in memory allocation. The initialization step allocates all structures needed by computations and especially the part of the matrix computed on the node, and fills it with local coefficients provided by the user. After this step, as many threads as cores are created to compute the numerical factorization (eight threads for NUMA8 platform and sixteen threads for NUMA16 and SMP16 clusters). The problem is therefore that all data are allocated close to the core where the initialization steps have occurred. Memory allocation is not evenly spread on the node and access times are thus not optimal (see Figure 2.2b).

In the new version of PASTIX, data structures have been modified to allow each thread to allocate and to fill its part of the matrix as shown in Figure 2.2a. This example shows the allocation repartition on each process and on each thread of each process. The memory is better spread over the nodes as shown in Figure 2.2c and thus allows us to obtain the best memory access as seen previously. Moreover, thanks to the method used to predict the static scheduling [74, 75], access to remote data is restrained, as well as in the results presented in [106].

Matrix	NUMA8		NUMA16		SMP16	
	Global	Local	Global	Local	Global	Local
MATR5	437	<b>410</b>	527	<b>341</b>	162	<b>161</b>
AUDI	256	<b>217</b>	243	<b>185</b>	101	<b>100</b>
NICE20	227	<b>204</b>	204	<b>168</b>	91.40	<b>91</b>
INLINE	9.70	<b>7.31</b>	20.90	<b>15.80</b>	5.80	<b>5.63</b>
NICE25	3.28	<b>2.62</b>	6.28	<b>4.99</b>	2.07	<b>1.97</b>
MCHLNF	3.13	<b>2.41</b>	5.31	<b>3.27</b>	1.96	<b>1.88</b>
THREAD	2.48	<b>2.16</b>	4.38	<b>2.17</b>	1.18	<b>1.15</b>
HALTERE	<b>134</b>	136	103	<b>93</b>	48.40	<b>47.90</b>

Table 2.2: Influence of NUMA-aware allocation on numerical factorization of PASTIX solver (in seconds)

Table 2.2 highlights the influence of NUMA-aware allocation on the factorization time on the different platforms. The **Global** columns are the times for the numerical factorization in the initial version of PASTIX with a global allocation performed during the initialization step. The **Local** columns are the factorization times with the new NUMA-aware allocation: the columns-blocks are allocated locally by the thread which factorizes them. A gain of 5% to 15% is observed on the NUMA8 architecture on all the matrices (except for the complex test case where there is no improvement). The gains on the NUMA16 platform are of 10% to 35% even with the complex test case. And, as expected, the SMP16 architecture shows no meaningful improvement.

Finally, results on a high performance application confirm the outcome of the benchmarks realized previously about the importance of taking into account the locality of memory on NUMA architectures. This could indeed significantly improve the execution time of algorithms with potentially huge memory requirements. And as shown by the last results, these effects increase with the size of the platforms used.

### 2.1.3 Communication overlap

In large distributed applications, communications are often a critical limit to the scalability and programmers try to overlap them by computations. Often, this consists in using asynchronous communications to give the MPI implementation the opportunity to transfer data on the network while the application performs computations. Unfortunately, not all implementations make the asynchronous communications progress efficiently. It is especially true when messages reach the *rendezvous* threshold. A non-overlapped *rendezvous* forces a computing thread to delay the data exchange until a call to *MPI\_Wait* or *MPI\_Test*.

To avoid this problem, we try to let communications progress thanks to one dedicated thread, following the *tasklet* mechanism used for instance in the PIOMAN library implementation [138]. Moreover, in the perspective of dynamic scheduling, it is important to receive data as soon as possible to release new tasks and provide more possibilities to choose the next task to compute.

The Gantt diagrams, presented at the end of the section, highlight these results (see Figures 2.5b and 2.5a). In the initial version, each thread manages its own communications using asynchronous mode. The time for a communication (white arrow) is significantly decreased thanks to a dedicated thread compared to the diagram of the initial version. A substantial overlap, obtained with the dedicated communication

thread method, allows us to reach better a performance on factorization time as we can see in Table 2.5 (between the versions V0 and V1).

Nb. Node	Nb. Thread	AUDI			MATR5		
		Initial	1 ThCcom	2 ThCom	Initial	1 ThCom	2 ThCom
2	1	684	<b>670</b>	672	1120	<b>1090</b>	1100
	2	388	<b>352</b>	354	594	<b>556</b>	558
	4	195	<b>179</b>	180	299	<b>279</b>	280
	8	100	<b>91.9</b>	92.4	158	<b>147</b>	<b>147</b>
	16	60.4	<b>56.1</b>	<b>56.1</b>	113	88.3	<b>87.4</b>
4	1	381	<b>353</b>	<b>353</b>	596	<b>559</b>	568
	2	191	<b>179</b>	180	304	<b>283</b>	284
	4	102	<b>91.2</b>	94.2	161	<b>148</b>	150
	8	55.5	<b>48.3</b>	54.9	98.2	<b>81.2</b>	87.3
	16	33.7	<b>32.2</b>	32.5	59.3	56.6	<b>56</b>
8	1	195	<b>179</b>	183	316	<b>290</b>	300
	2	102	<b>90.7</b>	94	187	<b>153</b>	164
	4	56.4	<b>47.1</b>	50.7	93.7	<b>78.8</b>	101
	8	31.6	<b>27.6</b>	32.4	58.4	<b>50</b>	58.7
	16	21.7	<b>20.4</b>	32.3	49.3	<b>41.6</b>	43.5

Table 2.3: Impact of dedicated threads for communications on numerical factorization (in seconds) on SMP16

Another interesting question is to find how many threads should be dedicated to communication when several network cards are available in the platform nodes. For instance, two network cards per node are available in the SMP16 clusters. We study the impact of adding one more thread dedicated to communications on the PASTIX solver (see Table 2.3).

The results show that even with a small number of computation threads, having two threads dedicated to communication is not useful. The performance is quite similar for small numbers of MPI process but decreases significantly for 8 MPI process. We can conclude that this MPI implementation already makes good use of the two network cards. Adding one more thread to stress MPI is not a good solution. This result is not surprising since the article [137] highlights the bad performance of the IBM MPI implementation in multi-threaded mode compared to the single thread mode.

In the remainder of this section, we choose to dedicate a single thread to manage communications.

#### 2.1.4 Dynamic scheduling

We now present our work on the conception and on the implementation of a dynamic scheduler for applications which have a tree shaped dependency graph, such as sparse direct solvers, which are based on an elimination tree (see Figure 2.3a). In the following of this section, Tnode will denote a node of the elimination tree, and we will call Cnode a node of the cluster architecture used for computations. Each Tnode corresponds to a column block to factorize and needs the updates from its descendants. In the case of a right-looking version of the standard Cholesky algorithm, it is possible to compute a dynamic scheduling on such a structure. When a Tnode of the tree is computed, it sends its contributions to different Tnodes higher in the tree and is able to know if a Tnode is ready to be computed or not. Hence, a simple list of ready tasks is the only data structure we need to design a dynamic algorithm.

However, Section 2.1.2 highlighted the problem of NUMA effects on memory allocation. The main problem here is to find a way to preserve memory affinity between the threads that look for a task and the location of the associated data during the dynamic scheduling. The advantage of such an elimination tree is that contributions stay close in the path to the root. Thus, to preserve memory affinity, we need to assign to each thread a contiguous part of the tree and include a work stealing algorithm which could take into account NUMA effects.

Finally, there are two steps in our proposed solution. The first one distributes data efficiently among

all the Cnodes of the cluster. The second one builds a NUMA-aware dynamic scheduling on the local tasks mapped on each Cnode. We will now focus on the sparse direct linear solver PASTIX, which is our target application for this work.

### Sparse direct solver and static scheduling

In order to achieve efficient parallel sparse factorization, three preprocessing phases are commonly required in direct sparse solvers (see Section 1.3).

In this work, we focus on the last preprocessing phase of the PASTIX solver, detailed in [74], that computes a scheduling used during the numerical factorization phase. To build a static scheduling, first a proportional mapping algorithm is applied on the processors of the target architecture. A BLAS2 and/or BLAS3 time model gives weights for each column block in the elimination tree. Then, a recursive top-down algorithm over the tree assigns a set of candidate processors to each Tnode (see Figure 2.3a). Processors chosen to compute a column block are assigned to its sons proportionally to the cost of each son and to the computations already affected to each candidate. It is possible to map the same processor on two different branches to balance the computations on all available resources. The last step corresponds to the data distribution over the Cnodes. A simulation of the numerical factorization is performed thanks to an additional time model for communications. Thus, all tasks are mapped on one of its candidates processors. Beforehand, tasks are sorted by priority based on the cost of the critical path in the elimination tree. Then a greedy algorithm distributes tasks onto the candidates able to compute it the soonest. We obtain a vector of local tasks fully ordered by priority for each processor.

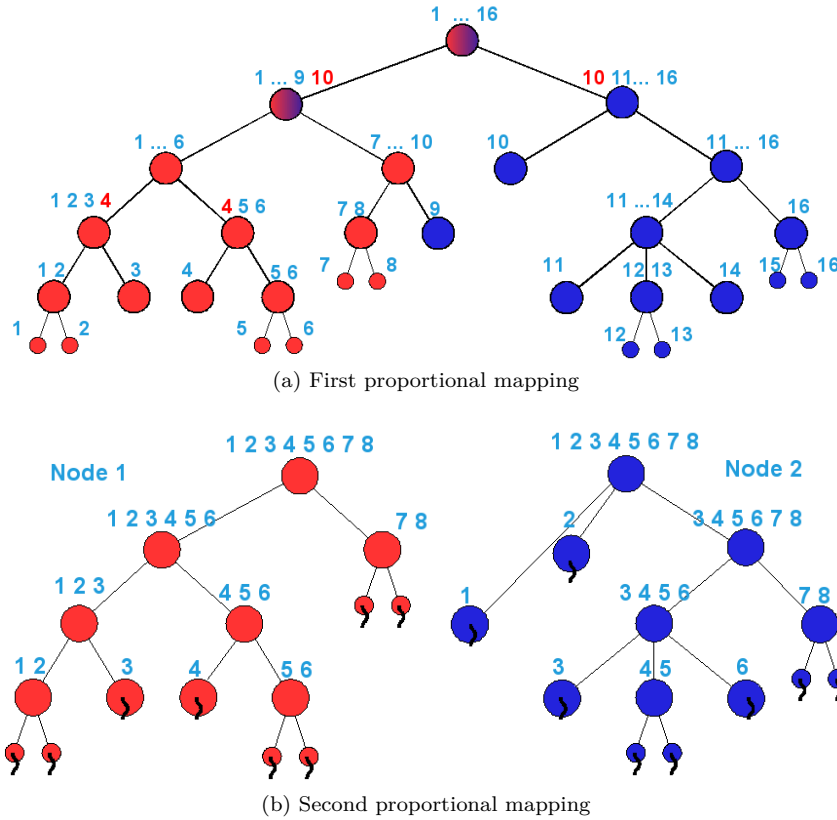


Figure 2.3: Proportional mapping in elimination tree for static and dynamic scheduler.

This static scheduling gives very good results on most platforms. However we want to implement a dynamic scheduler at least as efficient as the static one, more suitable for NUMA or heterogeneous architectures. The objective is to reduce some observed idle times due to approximations in our time cost models, especially when communications have to be estimated. This is highlighted in Figure 2.5a. The other main objective is to preserve the memory affinity and locality particularly on architectures with a large number of cores. Our static scheduling can be naturally adapted since all threads are bound

on a processor and data associated with the distributed tasks are allocated close to it.

### Dynamic scheduling over an elimination tree

The dynamic scheduling algorithm has to dispatch tasks over the available threads on the same Cnode but does not have to re-assign tasks between them. The first step of our new algorithm is thus the same as in the static one: apply a proportional mapping of the elimination tree over the Cnodes and simulate the numerical factorization to distribute data. The simulation is based on the same cost model with all the processors or cores available in the system.

Once we have applied the first proportional mapping, each Cnode owns a set of subtrees of the initial elimination tree as in Figure 2.3b. These subtrees are refined with a smaller block size to obtain fine grain parallelism. Then, a second proportional mapping is done on them based on the local number of available processors. In that case, we do not allow a thread to be a candidate for two different subtrees to ensure memory affinity between tasks affected by each one. This provides a tree with a list of fully ordered tasks where a set of candidate threads is mapped onto each node as shown in Figure 2.4.

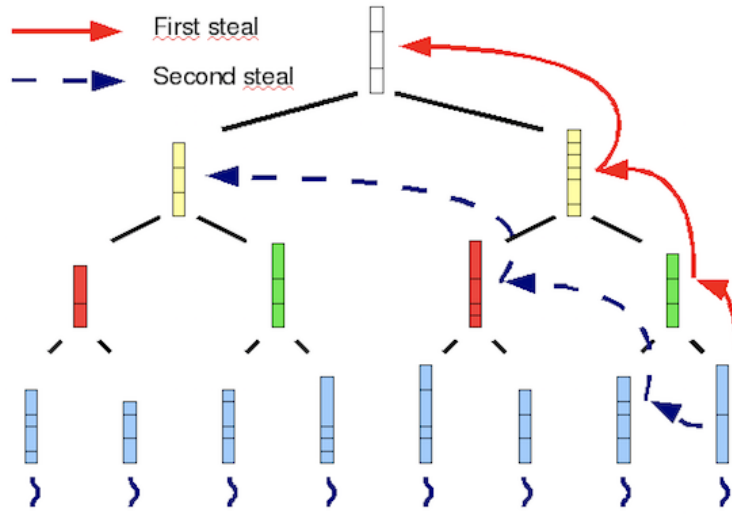
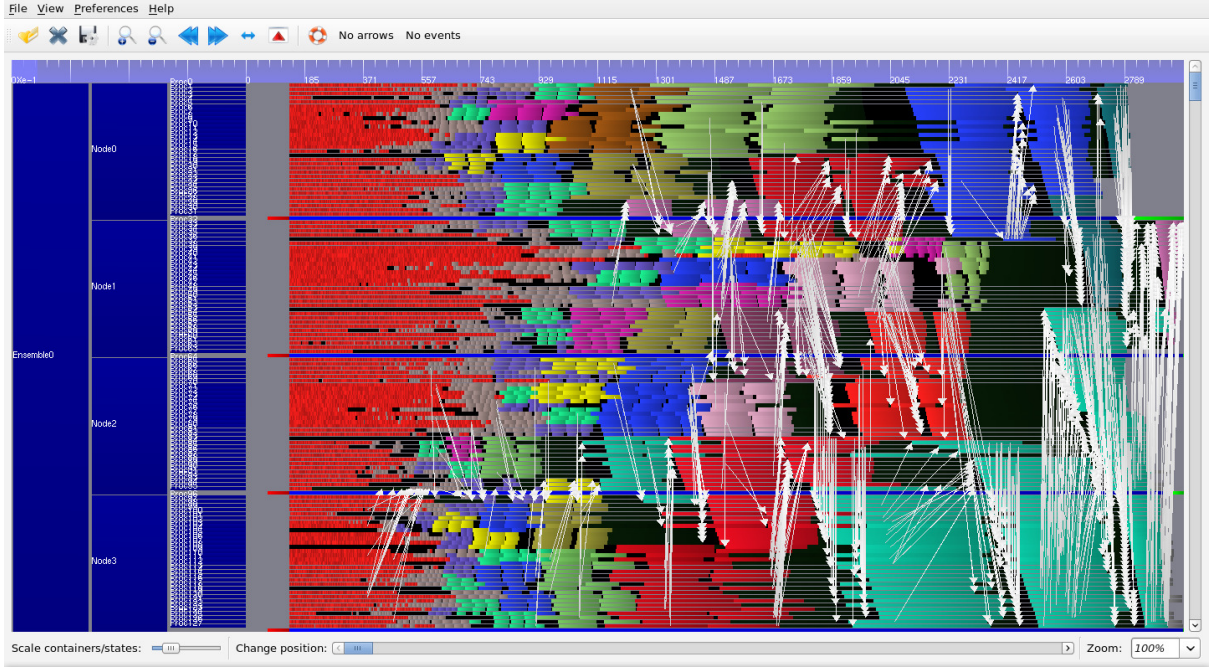


Figure 2.4: Work stealing algorithm

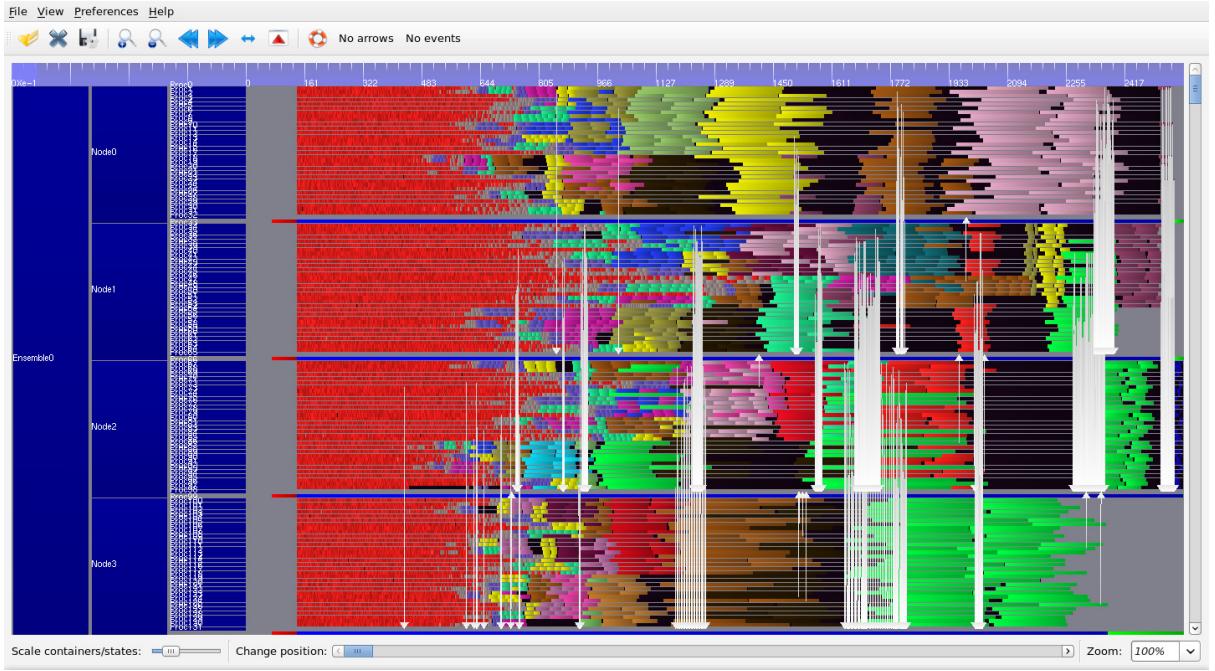
In the following, the nodes of the tree used for the work stealing algorithm will be called Snodes. A set of candidate threads assigned to each Snode is a subset of the candidate threads assigned to the father of this Snode.

This tree, denoted by  $T$ , of task queues  $q_n$  (where  $n$  is a Snode) has as many leaves as threads required to factorize the matrix. At runtime, as well as in the static version, threads are bound on one dedicated core in the order of a breadth-first search to ensure that closer threads will be in the same sets. During the numerical factorization, the threads will have to compute mainly the tasks which belong to Snodes from their critical path on  $T$ . Thus, tasks in the queues  $q_n$  associated with the leaves of  $T$  are allocated by the only thread that is allowed to compute them. Memory affinity is then preserved for the main part of the column blocks. However, we also have to allocate data associated with remaining tasks in Snodes which are not leaves. A set of threads are able to compute them. We choose, in the current implementation, to use a round-robin algorithm on the set of candidates to allocate those column blocks. Data allocation is then not optimal, but, if the cores are numbered correctly, this allocation reflects the physical mapping of cores inside a Cnode. It is important to notice that two cores with two successive ids are not always close in the architecture.

Once a thread  $t$  has no more jobs in its set of ready tasks  $q_t$ , it steals jobs in the queues of its critical path as described by the filled red arrows in Figure 2.4. Thus, we ensure that each thread works only on a subtree of the elimination tree and on some column blocks of its critical path. This ensures good



(a) Static scheduling



(b) Dynamic scheduling using two ways of work stealing

Figure 2.5: Gantt diagrams with 4 MPI process with 32 threads for a matrix with 10 million unknowns coming from CEA. Idle time is represented by black blocks and communications by white arrows. Elapse time is reduced by 15%.

memory affinity and improves the performance in the higher levels of the tree  $T$  especially when several threads are available.

However, there still remain idle times during the execution of the lower part of the tree  $T$  (mainly due to approximations of our cost models). Performance is improved by using two ways of work stealing (see Figure 2.5b). Once a thread has no more ready tasks from its critical path, it tries to steal a task in the



sons of the Snodes that belong to its critical path as described by the dotted blue arrows in Figure 2.4.

### 2.1.5 Numerical experiments

This section summarizes the results obtained with the improved algorithms implemented in the PASTIX solver and especially the dynamic scheduler. Table 2.4 highlights the improvements to the solver for a single Cnode. All test cases are run using eight threads for the NUMA8 platform and sixteen threads for the NUMA16 and SMP16 clusters. Column V0 (respectively V1) presents the factorization time obtained with the initial version without the NUMA-aware allocation (respectively with the NUMA-aware allocation). The third column gives the results with the NUMA-aware allocation and with the dynamic scheduler using two ways of work stealing.

Firstly, we observe that results are globally improved for all the test cases and for all the architectures when the dynamic scheduler is enabled. However, in few cases, the factorization time obtained with dynamic scheduling can be less efficient than with a static one. This is mainly due to the round-robin algorithm used to allocate data in the upper levels of the elimination tree. Secondly, the results presented on the SMP16 platforms show that the dynamic scheduler can improve the performance and thus, confirm that problems on NUMA architecture are mainly due to weakness in memory location.

Matrix	NUMA8			NUMA16			SMP16		
	V0	V1	V2	V0	V1	V2	V0	V1	V2
MATR5	437	410	<b>389</b>	527	341	<b>321</b>	162	161	<b>150</b>
AUDI	256	217	<b>210</b>	243	185	<b>176</b>	101	100	<b>100</b>
NICE20	227	<b>204</b>	227	204	168	<b>162</b>	91.40	91	<b>90.30</b>
INLINE	9.70	<b>7.31</b>	7.32	20.90	15.80	<b>14.20</b>	5.80	<b>5.63</b>	5.87
NICE25	3.28	<b>2.62</b>	2.82	6.28	<b>4.99</b>	5.25	2.07	1.97	<b>1.90</b>
MCHLNF	3.13	<b>2.41</b>	2.42	5.31	3.27	<b>2.90</b>	1.96	1.88	<b>1.75</b>
THREAD	2.48	2.16	<b>2.05</b>	4.38	2.17	<b>2.03</b>	1.18	1.15	<b>1.06</b>
HALTERE	134	136	<b>129</b>	103	<b>93</b>	94.80	48.40	47.90	<b>47.40</b>

Table 2.4: Comparaison of numerical factorization time in seconds on three versions of PASTIX solver. V0 is the initial version with static scheduling and without NUMA-aware allocation. V1 is the version with NUMA-aware allocation and static scheduling. V2 is the version with NUMA-aware allocation and dynamic scheduling.

Table 2.5 presents results of the dynamic scheduler with multiple MPI processes on NUMA8 and SMP16 platforms. All versions have enabled the NUMA-aware allocation. Once again, all test cases are run using, for each MPI process, eight threads for NUMA8 platform and sixteen threads for SMP16 clusters. The first version V0 does not use a dedicated thread for communications contrary to the two other versions, and the third version V2 uses the dynamic scheduler.

Nb. Node	NUMA8						SMP16					
	AUDI			MATR5			AUDI			MATR5		
	V0	V1	V2	V0	V1	V2	V0	V1	V2	V0	V1	V2
1	217	-	<b>210</b>	410	-	<b>389</b>	100	-	<b>100</b>	161	-	<b>150</b>
2	142	111	<b>111</b>	212	208	<b>200</b>	60.4	<b>56.1</b>	56.8	113	88.3	<b>87</b>
4	69	60.5	<b>57.7</b>	171	121	<b>114</b>	33.7	<b>32.2</b>	32.6	59.3	56.6	<b>54.6</b>
8	45.3	37.2	<b>35.6</b>	117	82.7	<b>78.8</b>						

Table 2.5: Comparaison of numerical factorization time in seconds of PASTIX solver with several MPI processes. The three versions (V0, V1 and V2) have the NUMA-aware allocation enabled. V0 uses the initial communication model with static scheduling. V1 uses one thread dedicated to communications with static scheduling. V2 uses one thread dedicated to communications with dynamic scheduling.

As seen in section 2.1.3, using a thread dedicated to communications improves performance and using the dynamic scheduler further reduces the factorization time. The first improvement allows a better communications/computations overlap and the second improvement allows better reactivity to exploit incoming contributions from other MPI process. Results are more significant with the unsymmetric



matrix *MATR5*, that generates more communications, than with symmetric matrices.

The improvements are mainly due to communications overlap and the gain obtained with the dynamic scheduler is about 5% on the factorization time. Even if our dynamic scheduler is not perfect, it already improves the hybrid MPI+Thread version of the PASTIX solver for all the platforms.

The NUMA-aware allocation implemented in the PASTIX solver gives very good results and can be easily adapted to many applications. This points out that it is important to take care of memory allocation during the initialization steps when using threads on NUMA architectures. Splitting communication and computational tasks also achieves some improvements in connection with the communication/computation overlap in the PASTIX solver. The work stealing algorithm can still be improved, but the dynamic scheduler already improved the execution time for different test cases on platforms with or without a NUMA factor.

## 2.2 A generic approach

Emerging processor technologies put an emphasis on increasing the number of computing units instead of increasing their working frequencies. As a direct outcome of the physical multiplexing of hardware resources, complex memory hierarchies have to be installed to reduce the memory bottleneck and ensure a decent rate of memory bandwidth for each resource. The memory becomes divided into several independent areas, capable of delivering data simultaneously through a complex and hierarchical topology, leading to the mainstream Non Uniform Memory Accesses (NUMA) machines we know today. Together with the availability of hardware accelerators, this trend profoundly altered the execution model of current and future platforms, progressing them towards a scale and a complexity unattained before. Furthermore, with the established integration of accelerators into modern architectures, such as GPUs or Intel Xeon Phis, high-end multi-core CPUs are consistently outperformed by these novel, more integrated, architectures both in terms of data processing rate and memory bandwidth. As a consequence, the working environment of today's application developers has evolved towards a multi-level massively parallel environment, where computation becomes cheap but data movements expensive, driving up the energy cost and algorithmic overheads and complexities.

With the advent of APIs for GPU programming, such as CUDA or OpenCL, programming accelerators has been rapidly evolving in the past years, permanently bringing accelerators into the mainstream. Hence, GPUs are becoming a more and more attractive alternative to traditional CPUs, particularly for their more interesting cost-per-flop and watts-per-flop ratios. However, the availability of a particular programming API only partially addresses the development of hybrid algorithms capable of taking advantage of all computational resources available, including accelerators and CPUs. Extracting a satisfactory level of performance, out of such entangled architectures, remains a real challenge due to the lack of consistent programming models and tools to assess their performance. In order to efficiently exploit current and future architectures, algorithm developers are required to expose a large amount of parallelism, adapt their code to new architectures with different programming models, and finally, map it efficiently on the heterogeneous resources. This is a gargantuan task for most developers as they do not possess the architectural knowledge necessary to mold their algorithms on the hardware capabilities in order to achieve good efficiency, and/or do not want to spend new efforts with every new generation of hardware.

A significant amount of research has been done on dense linear algebra, but sparse linear algebra on heterogeneous system is work in progress. Multiple reasons warrant this divergence, including the intrinsic algorithmic complexity and the highly irregular nature of the resulting problem, both in terms of memory accesses and computational intensities. Combined with the heterogeneous features of current and future parallel architectures, this depicts an extremely complex software development field.

In this work, we advance the state-of-the-art in supernodal solvers by migrating PASTIX towards a new programming paradigm, one with a promise of efficiently handling hybrid execution environments while abstracting the application from the hardware constraints. Many challenges have to be overcome, going from exposing the PASTIX algorithms using a task-based programming paradigm, to delivering a level of task parallelism, granularity, and implementation allowing the runtime to efficiently schedule the resulting, highly irregular tasks, in a way that minimizes the execution span. We exposed the original algorithm using the concept of tasks, a self-contained computational entity, linked to the other

tasks by data dependencies. Specialized task-graph description formats were used in accordance with the underlying runtime system (PARSEC or STARPU). We provided specialized GPU-aware versions for some of the most compute intensive tasks, providing the runtimes with the opportunity to unroll the graph of tasks on all available computing resources. The resulting software is, to the best of our knowledge, the first implementation of a sparse direct solver with a supernodal method supporting hybrid execution environments composed of multi-cores and multi-GPUs. Based on these elements, we pursue the evaluation of the usability and the appeal of using a task-based runtime as a substrate for executing this particular type of algorithm, an extremely computationally challenging sparse direct solver. Furthermore, we take advantage of the integration of accelerators (GPUs in this context) with our supporting runtimes, to evaluate and understand the impact of this drastically novel portable way of writing efficient and perennial algorithms. Since the runtime system offers a uniform programming interface, disassociate from a specific set of hardware or low-level software entities, applications can take advantage of these uniform programming interfaces for ensuring their portability. Moreover, the exposed graph of tasks allows the runtime system to apply specialized optimization techniques and minimize the application’s time to solution by strategically mapping the tasks onto computing resources by using state-of-the-art scheduling strategies.

The rest of the section is organized as follows. We first introduce some related work in Section 2.2.1, followed by a description of the runtimes used in Section 2.2.2. Section 2.2.3 explains the implementation over the DAG schedulers with a preliminary study over multi-core architectures, followed by details on the extension to heterogeneous architectures. All choices are supported and validated by a set of experiments on a set of matrices with a wide range of characteristics in Section 2.2.4.

### 2.2.1 Related work

The dense linear algebra community has spent a great deal of effort to tackle the challenges raised by the sharp increase in the number of computational resources. Due to their heavy computational cost, most of their algorithms are relatively simple to handle. Avoiding common pitfalls such as the “fork-join” parallelism, and expertly selecting the blocking factor, provide an almost straightforward way to increase the parallelism and thus achieve better performance. Moreover, due to their natural load-balance, most of the algorithms can be approached hierarchically, first at the node level, and then at the computational resource level. In a shared memory context, one of the seminal papers [28] replaced the commonly used LAPACK layout with one based on tiles/blocks. Using basic operations on these tiles exposes the algorithms as a graph of tasks augmented with dependencies between them. In shared memory, this approach quickly generates a large number of ready tasks, while, in distributed memory, the dependencies allow the removal of hard synchronizations. This idea leads to the design of new algorithms for various algebraic operations [29], now at the base of well-known software packages like PLASMA [1].

This idea is recurrent in almost all novel approaches surrounding the many-core revolution, spreading outside the boundaries of dense linear algebra. Looking at sparse linear algebra, the efforts were directed towards improving the behavior of the existing solvers by taking into account both task and data affinity and relying on a two-level hybrid parallelization approach, mixing multithreading and message passing. Numerous solvers are now able to efficiently exploit the capabilities of these new platforms [49, 130]. New solvers have also been designed and implemented to address these new platforms. For them the chosen approach follows the one for dense linear algebra, fine-grained parallelism, thread-based parallelization, and advanced data management to deal with complex memory hierarchies. Examples of this kind of solver are HSL [80] and SuperLU-MT [98] for sparse LU or Cholesky factorizations and SPQR [42] and `qr_mumps` [27] for sparse QR factorizations.

One commonly employed approach consists in reducing the granularity of computations and avoiding “fork-join” parallelism, as the scalability of this scheme suffers from an excessive amount of synchronization. Most of the related work focuses on intra-node parallelization with a shared memory parallel programming paradigm. To be more precise, thread based parallelization is widely used to tackle the performance issues within a computing node. These concepts have been first introduced in the field of dense linear algebra computations [28] where the main idea was to replace the commonly used data layout for dense matrices with one based on tiles/blocks and to write novel algorithms suited to this new data organization; by defining a task as the execution of an elementary operation on a tile and by expressing data dependencies among these tasks in a Directed Acyclic Graph (DAG), the number of synchronizations is drastically reduced in comparison with classical approaches (such as the LAPACK or

ScaLAPACK libraries) thanks to a dynamic data-flow parallel execution model. This idea leads to the design of new algorithms for various algebra operations [29, 123] now at the base of well known software packages like PLASMA [1] and FLAME [139].

Due to their deeply hierarchical architecture, memory accesses of multi-core based platforms are not uniform. Therefore, if the data is not carefully laid out in memory and if access to it is not coherent, multithreaded software may incur heavy performance penalties. The efficiency of the algorithms discussed above can be considerably improved by accurately placing data in memory and by employing tasks scheduling algorithms that aim at maximizing the locality of accesses. This has only been made possible by the availability of tools such as hwloc [26] that allow the application to discover the hardware architecture of the underlying system and take advantage of it in a portable way.

With the advent of accelerator-based platforms, a lot of attention has shifted towards extending the multi-core aware algorithms to fully exploit the huge potential of accelerators (mostly GPUs). The main challenges raised by these heterogeneous platforms are mostly related to task granularity and data management: although regular cores require fine granularity of data as well as computations, accelerators such as GPUs need coarse-grain tasks. This inevitably introduces the need for identifying the parts of the algorithm which are more suitable to be processed by accelerators. As for the multi-core case described above, the exploitation of this kind of platform was first considered in the context of dense linear algebra algorithms.

Moreover, one constant becomes clear: a need for a portable layer that will insulate the algorithms and their developers from the rapid hardware changes. Recently, this portability layer appeared under the denomination of a task-based runtime. The algorithms are described as tasks with data dependencies in-between, and the runtime systems are used to manage the tasks dynamically and schedule them on all available resources. These runtimes can be generic, like the two runtimes used in the context of this study (STARPU [21] or PARSEC [24]), or more specialized like QUARK [147]. These efforts resulted in the design of the DPLASMA library [23] on top of PARSEC and the adaptation of the existing FLAME library [83]. On the sparse direct methods front, preliminary work has resulted in mono-GPU implementations based on offloading parts of the computations to the GPU [56, 105, 148]. Due to its very good data locality, the multifrontal method is the main target of these approaches. The main idea is to treat some parts of the task dependency graph entirely on the GPU. Therefore, the main originality of these efforts is in the methods and algorithms used to decide whether or not a task can be processed on a GPU. In most cases, this was achieved through a threshold based criterion on the size of the computational tasks.

Concerning accelerator-based platforms for sparse direct solvers, a lot of attention has been recently paid to design new algorithms that can exploit the huge potential of GPUs. For a multifrontal sparse direct solver, some preliminary work has been proposed in the community [56, 148], resulting in single-GPU implementations based on off-loading parts of the computations to the GPU. The main idea is to treat some parts of the task dependency graph entirely on the GPU. Therefore, the main originality of these efforts was in the methods and algorithms used to decide whether or not a task can be processed on a GPU. In most cases this was achieved through a threshold based criterion on the size of the computational tasks. From the software point of view, most of these studies have only produced software prototypes and few sparse direct solvers exploiting GPUs have been made available to the users, most of them being developed by private software companies such as MatrixPro<sup>1</sup>, Acceleware<sup>2</sup> and BCSLib-GPU<sup>3</sup>. As far as we know, there are no publications nor reports where the algorithmic choices are depicted. Recent progress towards a multifrontal sparse QR factorization on GPUs have been presented in [41].

## 2.2.2 Runtimes

In our exploratory approach towards moving to a generic scheduler for PASTIX, we considered two different runtimes: STARPU and PARSEC. Both runtimes have been proven mature enough in the context of dense linear algebra, while providing two orthogonal approaches to task-based systems.

The PARSEC [24] distributed runtime system is a generic data-flow engine supporting a task-based implementation targeting hybrid systems. Domain specific languages are available to expose a user-friendly interface to developers and allow them to describe their algorithm using high-level concepts.

---

<sup>1</sup><http://www.matrixprosoftware.com/>

<sup>2</sup><http://www.acceleware.com/matrix-solvers>

<sup>3</sup><http://www.boeing.com/phantom/bcslib/>

This programming paradigm constructs an abridged representation of the tasks and their dependencies as a graph of tasks – a structure agnostic to algorithmic subtleties, where all intrinsic knowledge about the complexity of the underlying algorithm is extricated, and the only constraints remaining are annotated dependencies between tasks [39]. This symbolic representation, augmented with a specific data distribution, is then mapped on a particular execution environment. This runtime system supports the use of different types of accelerators, GPUs and Intel Xeon Phi, in addition to distributed multi-core processors. Data are transferred between computational resources based on coherence protocols and computational needs, with emphasis on minimizing the unnecessary transfers. The resulting tasks are dynamically scheduled on the available resources following a data reuse policy mixed with different criteria for adaptive scheduling. The entire runtime system targets very fine grain tasks (order of magnitude under ten microseconds), with a flexible scheduling and adaptive policies to mitigate the effect of system noise and to take advantage of the algorithmic-inherent parallelism to minimize the execution span.

The experiment presented in this work takes advantage of a specialized domain specific language of PARSEC, designed for affine loops-based programming [23]. This specialized interface allows for a drastic reduction in the memory used by the runtime, as tasks do not exist until they are ready to be executed, and the concise representation of the task-graph allows for an easy and stateless exploration of the graph. In exchange for the memory saving, generating a task requires some extra computation, and lies in the critical path of the algorithm. The need for a window of visible tasks is then pointless, the runtime can explore the graph dynamically based on the ongoing state of the execution.

STARPU [21] is a runtime system aiming to allow programmers to exploit the computing power of clusters of hybrid systems composed of CPUs and various accelerators (GPUs, Intel Xeon Phi, etc) while relieving them from the need to specially adapt their programs to the target machine and processing units. The STARPU runtime supports a *task-based programming model*, where applications submit computational tasks, with CPU and/or accelerator implementations, and STARPU schedules these tasks and associated data transfers on available CPUs and accelerators. The data that a task manipulates is automatically transferred among accelerators and the main memory in an optimized way (minimized data transfers, data prefetch, communication overlapped with computations, etc.), so that programmers are relieved of scheduling issues and technical details associated with these transfers. STARPU takes particular care of scheduling tasks efficiently, by establishing performance models of the tasks through on-line measurements, and then using well-known scheduling algorithms from the literature. In addition, it allows scheduling experts, such as compilers or computational library developers, to implement custom scheduling policies in a portable fashion.

The differences between the two runtimes can be classified into two groups: conceptual and practical differences. At the conceptual level the main differences between PARSEC and STARPU are the task submission process, the centralized scheduling, and the data movement strategy. PARSEC uses its own parameterized language to describe the DAG in comparison with the simple sequential submission loops typically used with STARPU. Therefore, STARPU relies on a centralized strategy that analyzes, at runtime, the dependencies between tasks and schedules these tasks on the available resources. On the contrary, through compile-time information, each computational unit of PARSEC immediately releases the dependencies of the completed task solely using the local knowledge of the DAG. Finally, while PARSEC uses an opportunistic approach, the STARPU scheduling strategy exploits cost models of the computation and data movements to schedule tasks to the right resource (CPU or GPU) in order to minimize overall execution time. However, it does not have a data-reuse policy on CPU-shared memory systems, resulting in lower efficiency when no GPUs are used, compared to the data-reuse heuristic of PARSEC. At the practical level, PARSEC supports multiple streams to manage the CUDA devices, allowing partial overlap between computing tasks, maximizing the occupancy of the GPU. On the other hand, STARPU allows data transfers directly between GPUs without going through central memory, potentially increasing the bandwidth of data transfers when data is needed by multiple GPUs.

## JDF representation of a DAG

In PARSEC, the data distribution and dependencies are specified using the Job Data Flow (JDF) format. Fig. 2.6 shows our JDF representation of the sparse Cholesky factorization using the tasks **panel** and **gemm**. The task **gemm** is based only on the block id parameter and computes internally the supernode (**fcblk**) in which to apply the update. On Line 2 of **panel(j)**, **cblknbr** is the number of block columns in the Cholesky factor. Once the *j*-th panel is factorized, the trailing submatrix can be updated using

1. panel(j) [high_priority = on]	1. gemm(k)
2. j = 0 .. cblknbr-1	2. k = 0 .. blocknbr-1
3. ... set up parameters for the j-th task ...	3. ... set up parameters for the k-th task ...
4. :A(j)	4. :A(fcblk)
5. RW A ← ( leaf ) ? A(j) : C gemm( lastbrow )	5. READ A ← diag ? A(fcblk) : A panel(cblk)
6.     → A gemm(firstblock+1..lastblock)	6. RW C ← first ? A(fcblk) : C gemm( prev )
7.     → A(j)	7.     → diag ? A(fcblk)
	8.     → ((!diag) && (next == 0)) ? A panel( fcblk )
	9.     → ((!diag) && (next != 0)) ? C gemm( next )

(a) Panel factorization

(b) Trailing submatrix update

Figure 2.6: JDF representation of Cholesky.

the  $j$ -th panel. This data dependency of the submatrix update on the panel factorization is specified on Line 6, where **firstblock** is the block index of the  $j$ -th diagonal block, and **lastblock** is the block index of the last block in the  $j$ -th block column. The output dependency on Line 7 indicates that the  $j$ -th panel is written to memory at the completion of the panel factorization. The input dependency of the  $j$ -th panel factorization is specified on Lines 4 and 5, where **leaf** is *true* if the  $j$ -th panel is a leaf in the elimination-tree, and **lastbrow** is the index of the last block updating the  $j$ -th panel. Hence, if the  $j$ -th panel is a leaf, the panel is read from memory. Otherwise, the panel is passed in as the output of the last update on the panel.

Similarly, **gemm(k)** updates the **fcblk**-th block column using the  $k$ -th block, where **fcblk** is the index of the block row that the  $k$ -th block belongs to, and **blocknbr** on Line 2 is the number of blocks in the Cholesky factor. The input dependencies of **gemm** are specified on Lines 4 through 6, where the **cblk**-th panel **A** is being used to update the **fcblk**-th column **C**. Specifically, on these lines, **diag** is *true* if the  $k$ -th block is a diagonal block, and it is *false* otherwise, and **prev** is *false* if the  $k$ -th block is the first block in the **fcblk**-th block row, and it is the index of the block in the block row just before the  $k$ -th block otherwise. Hence, the **prev**-th block updated the **fcblk**-th column just before the  $k$ -th block does. Hence, the data dependency of **gemm(k)** is resolved once the **cblk**-th panel is factorized, and the **fcblk**-th column is updated using the **prev**-th block. Notice that the diagonal blocks are not used to update the trailing submatrix, but it is included in the code to have a continuous space of execution for the task required by PARSEC. Finally, Lines 7 through 9 specify the output dependencies of **gemm(k)**, where **next** is *false* if the  $k$ -th block is a diagonal block, and it is the index of the next block after the  $k$ -th block in the **fcblk**-th row otherwise. Hence, the completion of **gemm(k)** resolves the data dependency of the **fcblk**-th panel factorization if this is the last update on the panel, or it resolves the dependency of updating the **fcblk**-th block column using the **next**-th block otherwise.

### STARPU tasks submission

STARPU builds its DAG following the task ordering provided by the user and by using data dependencies. The pseudocode presented in Algorithm 4 shows the STARPU tasks submission loop for the Cholesky decomposition. The submissions of the tasks follows the sequential algorithm and STARPU uses the task insertion ordering to discover the dependencies among the tasks using the same data.

---

#### Algorithm 4: Starpu tasks insertion algorithm

---

```

forall Supernode  $S_1$  do
    submit_panel( $S_1$ ) ;                               /* update of the panel */
    forall extra diagonal block  $b_i$  of  $S_1$  do
         $S_2 \leftarrow \text{supernode\_in\_front\_of}(B_i)$  ;
        submit_gemm( $S_1, S_2$ ) ;                       /*  $S_2 = S_2 - B_{k,k \geq i} \times B_i^T$  */

```

---

Whereas PARSEC requires the tasks to be chained (2.7a) more parallelism can be exposed (2.7b) using the **STARPU\_COMMUTE** option provided by STARPU to allow two tasks targeting the same data to be executed in an undefined order.

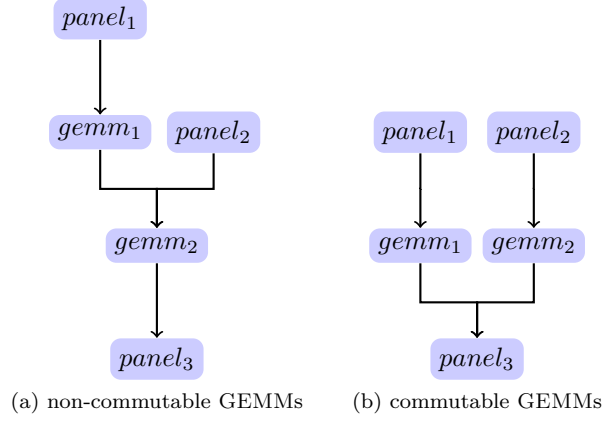


Figure 2.7: Task graph

### 2.2.3 Supernodal factorization over DAG schedulers

Similarly to dense linear algebra, sparse direct factorization relies on three types of operations: the factorization of the diagonal block (POTRF), the solve on off-diagonal blocks belonging to the same panel (TRSM), and the trailing panels updates (GEMM). Whereas the task dependency graph from a dense Cholesky factorization [29] is extremely regular, the DAG describing the supernodal method contains rather small tasks with variable granularity and less uniform ranges of execution space. This lack of uniformity makes the DAG resulting from a sparse supernodal factorization complex – cf Fig 2.9 – , making it difficult to efficiently schedule the resulting tasks on homogeneous and heterogeneous computing resources.

The current scheduling scheme of PASTIX exploits a 1D-block distribution, where a task assembles a set of operations together, including the tasks factorizing one panel (POTRF and TRSM) and all updates generated by this factorization. However, increasing the granularity of a task in such a way limits the potential parallelism, and has a growing potential for bounding the efficiency of the algorithm when using many-core architectures. To improve the efficiency of the sparse factorization on a multi-core implementation, we introduced a way of controlling the granularity of the BLAS operations. This functionality dynamically splits update tasks, so that the critical path of the algorithm can be reduced. In this work, for both the PARSEC and STARPU runtimes, we split PASTIX tasks into two subsets of tasks:

- the diagonal block factorization and off-diagonal blocks updates, performed on one panel;
- the updates from off-diagonal blocks of the panel to one other panel of the trailing submatrix.

Hence, the number of tasks is bounded by the number of blocks in the symbolic structure of the factorized matrix.

Moreover, when taking into account heterogeneous architectures in the experiments, a finer control of the granularity of the computational tasks is needed. Some references for benchmarking dense linear algebra kernels are described in [140] and show that efficiency could be obtained on GPU devices only on relatively large blocks – a limited number of such blocks can be found in a supernodal factorization only on top of the elimination tree. Similarly, the amalgamation algorithm [77], reused from the implementation of an incomplete factorization, is a crucial step to obtain larger supernodes and efficiency on GPU devices. The default parameter for amalgamation has been slightly increased to allow up to 12% more fill-in to build larger blocks while maintaining a decent level of parallelism.

In the remainder of this section, we present the extensions to the solver to support heterogeneous many-core architectures. These extensions were validated through experiments conducted on *Mirage* nodes from the PLAFRIM cluster at INRIA Bordeaux. A *Mirage* node is equipped with two hexa-core Westmere Xeon X5650 (2.67 GHz), 32 GB of memory and 3 Tesla M2070 GPUs. PASTIX was built without MPI support using GCC 4.6.3, CUDA 4.2, Intel MKL 10.2.7.041, and SCOTCH 5.1.12b. Experiments were performed on a set of nine matrices, all part of the University of Florida sparse matrix collection [43], that are described in Table 2.6. These matrices represent different research fields and

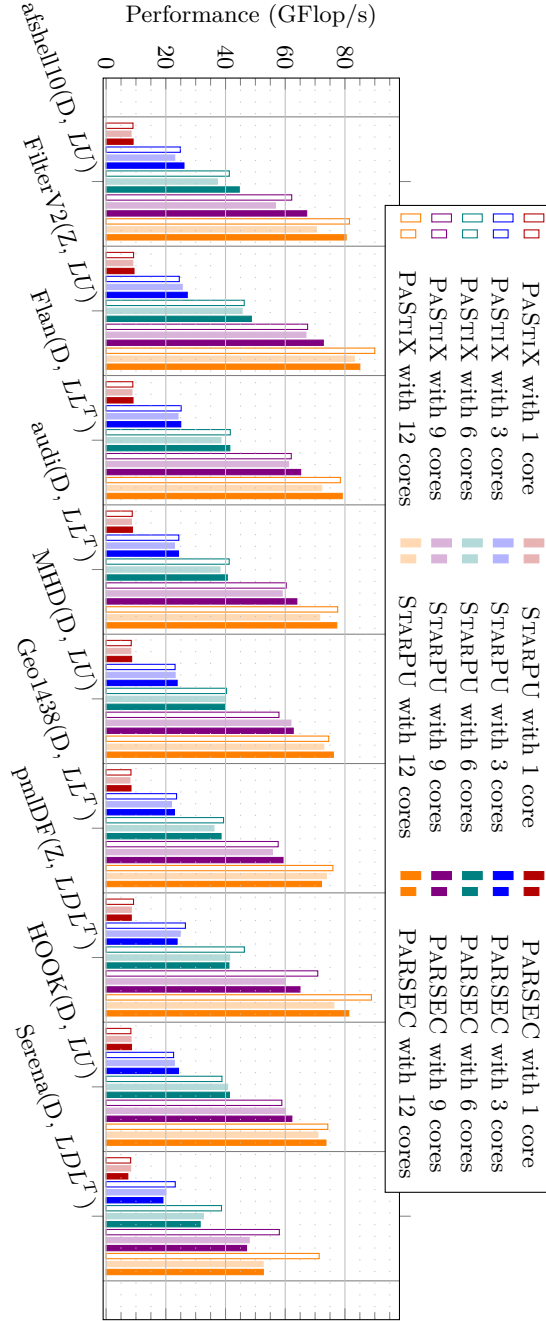


Figure 2.8: CPU scaling study: GFlop/s performance of the factorization step on a set of nine matrices with the three schedulers.





exhibit a wide range of properties (size, arithmetic, symmetry, definite problem, etc). The last column reports the number of floating-point operations (Flop) required to factorize those matrices and used to compute the performance results shown in this section.

Matrix	Prec	Method	Size	nnz <sub>A</sub>	nnz <sub>L</sub>	TFlop
Afshell10	D	$LU$	1.5e+6	27e+6	610e+6	0.12
FilterV2	Z	$LU$	0.6e+6	12e+6	536e+6	3.6
Flan	D	$LL^T$	1.6e+6	59e+6	1712e+6	5.3
Audi	D	$LL^T$	0.9e+6	39e+6	1325e+6	6.5
MHD	D	$LU$	0.5e+6	24e+6	1133e+6	6.6
Geo1438	D	$LL^T$	1.4e+6	32e+6	2768e+6	23
PmlDF	Z	$LDL^T$	1.0e+6	8e+6	1105e+6	28
Hook	D	$LU$	1.5e+6	31e+6	4168e+6	35
Serena	D	$LDL^T$	1.4e+6	32e+6	3365e+6	47

Table 2.6: Matrix description (Z: double complex, D: double).

## Multi-core architectures

As mentioned earlier, the PASTIX solver has already been optimized for distributed clusters of NUMA nodes. We use the current state-of-the-art PASTIX scheduler as a basis, and compare the results obtained using the STARPU and PARSEC runtimes from there. In this section, before studying the solver on heterogeneous platforms, we study the impact of using generic runtimes on multi-core architectures compare to internal PASTIX schedulers. Thus, we first compared PASTIX original light-weight and finely tuned static scheduler against STARPU and PARSEC.

Figure 2.8 reports the results from a strong scaling experiment, where the number of computing resources varies from 1 to 12 cores, and where each group represents a particular matrix. Empty bars correspond to the PASTIX original scheduler, shaded bars correspond to STARPU, and filled bars correspond to PARSEC. The figure is in Flop/s, and a higher value on the Y-axis represents a more efficient implementation. Overall, this experiment shows that on a shared memory architecture the performance obtained with any of the above-mentioned approaches are comparable, the differences remaining minimal on the target architecture.

We can also see that, in most cases, the PARSEC implementation is more efficient than STARPU, especially when the number of cores increases. STARPU shows an overhead on multi-core experiments attributed to its lack of cache reuse policy compared to PARSEC and the PASTIX internal scheduler. A careful observation highlights the fact that both runtimes obtain lower performance compared with PASTIX for  $LDL^T$  on both **PmlDF** and **Serena** matrices. Due to its single task per node scheme, PASTIX stores the  $DL^T$  matrix in a temporary buffer which allows the update kernels to call a simple GEMM operation. On the contrary, both STARPU and PARSEC implementations are using a less efficient kernel that performs the full  $LDL^T$  operation at each update. Indeed, due to the extended set of tasks, the life span of the temporary buffer could cause large memory overhead. In conclusion, using these generic runtimes shows similar performance and scalability to the PASTIX internal solution on the majority of test cases, while providing a suitable level of performance and a desirable portability, allowing for a smooth transition towards more complex heterogeneous architectures.

As PASTIX was already using a task based algorithm, the implementations of a sparse Cholesky decomposition on top on the two generic runtimes barely took a month. However, an iteration processus between the linear solver development team and the runtimes one were required to reach good scalability both in multi-core and heterogeneous context. Indeed, the study of the sparse linear algebra solver on top of runtimes highlighted few defects of the runtime systems. As the improvements resulting from this feedback were not specific to sparse linear algebra, other applications developed on top of the two runtime systems will benefit from them.

## Heterogeneous architectures implementation

While obtaining an efficient implementation was one of the goals of this experiment, it was not the major one. The ultimate goal was to develop a portable software environment allowing for an easy transition to accelerators, a software platform where the code is factorized as much as possible, and where the human cost of adapting the sparse solver to current and future hierarchical complex heterogeneous architectures remains consistently low. Building upon the efficient supernodal implementation on top of DAG based runtimes, we can more easily exploit heterogeneous architectures. The GEMM updates are the most compute-intensive part of the matrix factorization, and it is important that these tasks are offloaded to the GPU. We decide not to offload the tasks that factorize and update the panel to the GPU due to the limited computational load, in direct relationship with the small width of the panels. It is common in dense linear algebra to use the accelerators for the update part of a factorization while the CPUs factorize the panel; so from this perspective our approach is conventional. However, such an approach combined with look-ahead techniques gives really good performance for a low programming effort on the accelerators [145]. The same solution is applied in this study, since the panels are split during the analysis step to fit the classic look-ahead parameters.

It is a known fact that the update is the most compute intensive task during a factorization. Therefore, generally speaking, it is paramount to obtain good efficiency on the update operation in order to ensure a reasonable level of performance for the entire factorization. Due to the embarrassingly parallel architecture of the GPUs and to the extra cost of moving the data back and forth between the main memory and the GPUs, it is of greatest importance to maintain this property on the GPU.

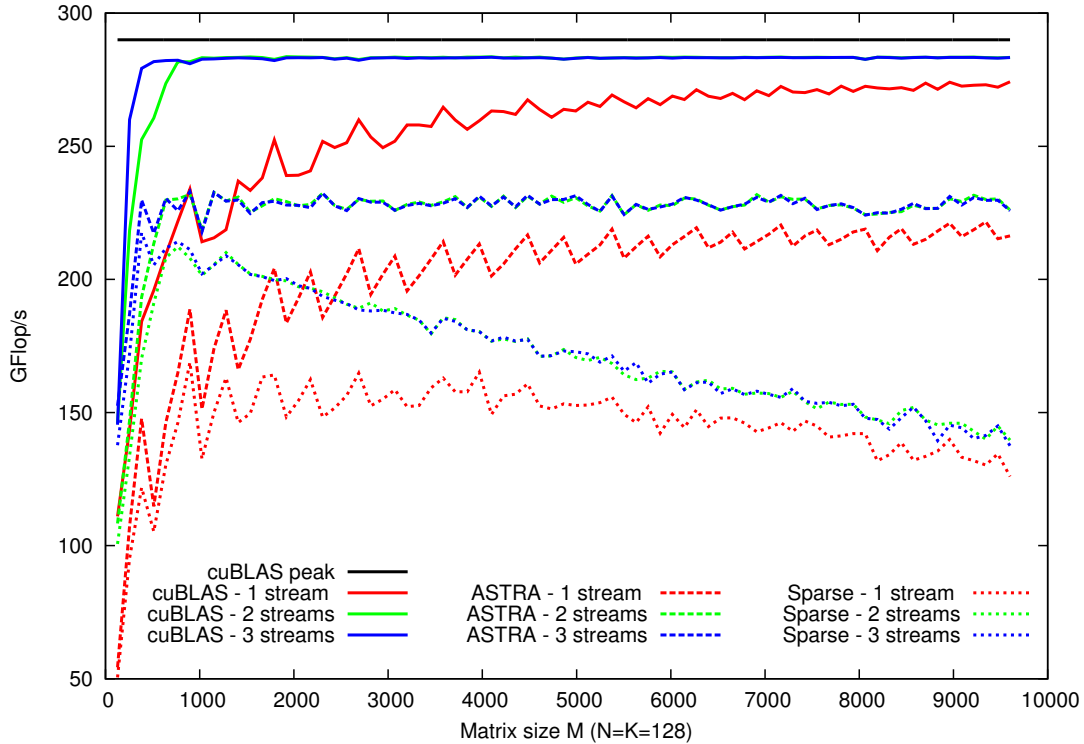


Figure 2.10: Multi-stream performance comparison on the DGEMM kernel for three implementations: cuBLAS library, ASTRA framework, and the sparse adaptation of the ASTRA framework.

The update task used in the PASTIX solver groups together all outer products that are applied to a same panel. On the CPU side, this GEMM operation is split in two steps due to the gaps in the destination panel: the outer product is computed in a contiguous temporary buffer, and upon completion, the result is dispatched on the destination panel. This solution has been chosen to exploit the performance of vendor provided BLAS libraries in exchange for constant memory overhead per working thread.

For the GPU implementation, the requirements for an efficient kernel are different. First, a GPU

has significantly less memory compared with what is available to a traditional processor, usually in the range of 3 to 6 GB. This forces us to carefully restrict the amount of extra memory needed during the update, making the temporary buffer used in the CPU version unsuitable. Second, the uneven nature of sparse irregular matrices might limit the number of active computing units per task. As a result, only a partial number of the available warps on the GPU might be active, leading to a deficient occupancy. Thus, we need the capability to submit multiple concurrent updates in order to provide the GPU driver with the opportunity to overlap warps between different tasks to increase the occupancy, and thus the overall efficiency.

Many CUDA implementations of the dense GEMM kernel are available to the scientific community. The most widespread implementation is provided by Nvidia itself in the cuBLAS library [114]. This implementation is extremely efficient since CUDA 4.2 allows for calls on multiple streams, but is not open source. Volkov developed an implementation for the first generation of CUDA enabled devices [140] in real single precision. In [136], the authors propose an assembly code of the DGEMM kernel that provides a 20% improvement on the cuBLAS 3.2 implementation. The MAGMA library proposed a first implementation of the DGEMM kernel [113] for the Nvidia Fermi GPUs. Later, an auto-tuned framework, called ASTRA, was presented in [94] and included in the MAGMA library. This implementation, similar to the ATLAS library for CPUs, is a highly configurable skeleton with a set of scripts to tune the parameters for each precision.

As our update operation is applied on a sparse representation of the panel and matrices, we cannot exploit an efficient vendor-provided GEMM kernel. We need to develop our own, starting from a dense version and altering the algorithm to fit our needs. Due to the source code availability, the coverage of the four floating-point precisions, and its tuning capabilities, we decided to use the ASTRA-based version for our *sparse* implementation. As explained in [94] the matrix-matrix operation is performed in two steps in this kernel. Each block of threads computes the outer-product  $tmp = AB$  into the GPU shared memory, and then the addition  $C = \beta C + \alpha tmp$  is computed. To be able to compute directly into  $C$ , the result of the update from one panel to another, we extended the kernel to provide the structure of each panel. This allows the kernel to compute the correct position directly into  $C$  during the *sum* step. This introduces a loss in the memory coalescence and deteriorates the update parts, however it prevents the requirement of an extra buffer on the GPU for each offloaded kernel.

One problem in choosing the best parameters used in the MAGMA library for the ASTRA kernel is that it has been determined that using textures gives the best performance for the update kernel. The function `cudaBindTexture` and `cudaUnbindTexture` are not compatible with concurrent kernel calls on different streams. Therefore, the textures have been disabled in the kernel, reducing the performance of the kernel by about 5% on large square matrices.

Figure 2.10 shows the study we made on the GEMM kernel and the impact of the modifications we did on the ASTRA kernel. These experiments are done on a single GPU of the *Mirage* cluster. The experiments consist of computing a representative matrix-matrix multiplication of what is typically encountered during sparse factorization. Each point is the average performance of 100 calls to the kernel that computes:  $C = C - AB^T$ , with  $A$ ,  $B$ , and  $C$ , matrices respectively of dimension  $M$ -by- $N$ ,  $K$ -by- $N$ , and  $M$ -by- $N$ .  $B$  is taken as the first block of  $K$  rows of  $A$  as it is the case in Cholesky factorization. The plain lines are the performance of the cuBLAS library with 1 stream (*red*), 2 streams (*green*), and 3 streams (*red*). The black line represents the peak performance obtained by the cuBLAS library on square matrices. This peak is never reached with the particular configuration case studied here. The dashed lines are the performance of the ASTRA library in the same configuration. We observe that this implementation already loses 50GFlop/s, around 15%, against the cuBLAS library, and that might be caused by the parameters chosen by the auto-tuning framework which has been run only on square matrices. Finally, the dotted lines illustrate the performance of the modified ASTRA kernel to include the gaps into the  $C$  matrix. For the experiments,  $C$  is a panel twice as tall as  $A$  in which blocks are randomly generated with average size of 200 rows. Blocks in  $A$  are also randomly generated with the constraint that the rows interval of a block of  $A$  is included in the rows interval of one block of  $C$ , and no overlap is made between two blocks of  $A$ . We observe a direct relationship between the height of the panel and the performance of the kernel: the taller the panel, the lower the performance of the kernel. The memory loaded to do the outer product is still the same as for the ASTRA curves, but memory loaded for the  $C$  matrix grows twice as fast without increasing the number of Flop to perform. The ratio Flop per memory access is dropping and explains the decreasing performance. However, when the factorization progresses and moves up the elimination trees, nodes get larger and the real number of

blocks encountered is smaller than the one used in this experiment to illustrate worst cases.

Without regard to the kernel choice, it is important to notice how the multiple streams can have a large impact on the average performance of the kernel. For this comparison, the 100 calls made in the experiments are distributed in a round-robin manner over the available streams. One stream always gives the worst performance. Adding a second stream increases the performance of all implementations and especially for small cases when matrices are too small to feed all resources of the GPU. The third one is an improvement for matrices with  $M$  smaller than 1000, and is similar to two streams over 1000.

This kernel is the one we provide to both runtimes to offload computations on GPUs in the case of Cholesky and LU factorizations. An extension to the kernel has been made to handle the  $LDL^T$  factorization that takes as an extra parameter the diagonal matrix  $D$  and computes:  $C = C - LDL^T$ . This modified version decreases the performance by 5%.

## Data mapping over multiple GPUs

We noticed that both runtimes encountered difficulties to compute the GEMM mapping onto the GPUs. Tasks' irregularities – size of the GEMM block, Flop in the operation – complicates the prediction model calibration of STARPU to determine which process unit fits best for a task. Dynamic tasks mapping in PARSEC could also result in a large unbalanced workload. Indeed in PARSEC, the mapping of a panel to a given GPU enforces the mapping of all other tasks applied to the same panel, for the same reason as in STARPU, the irregularities in the task made it difficult for the simple model used in the dense case to correctly detect the actual load of each GPU. In order to help the runtime, panels that will be updated on GPUs are selected at analyze time, such that the amount of data updated on a GPU does not exceed the memory of the GPU. This limit will reduce the data transfer by keeping data on the GPUs. It is necessary to sort the panels according to a criterion to decide in which ones will be mapped on a GPU. Several sorting criteria were tested: *target panel's size*, the larger a panel is the more chance it has to receive uploads; *number of updates performed on the panel*: this corresponds to the number of GEMMs applied to the panel; *Flop produced by these updates*: not only the number of updates is important, but the larger the updates are the more Flops will be performed; and, finally, *the priority statically computed in PASTIX*: higher is the priority, sooner the result is required, such that accelerators can help providing them rapidly. Panels are marked to be updated on a specific GPU thanks to a greedy algorithm that associates at each step of the algorithm the first panel according to the selected criteria to the less loaded GPU. A check is made to guarantee we do not exceed the memory capacity of the GPU to avoid excess use of the runtime LRU.

### 2.2.4 Heterogeneous experiments

Figure 2.11 presents the performance obtained on our set of matrices on the *Mirage* platform by enabling the GPUs in addition to all available cores. The PASTIX run is shown as a reference. STARPU runs are empty bars, PARSEC runs with 1 stream are shaded and PARSEC runs with 3 streams are fully colored. This experiment shows that we can efficiently use the additional computational power provided by the GPUs using the generic runtimes. In its current implementation, STARPU has either GPU or CPU worker threads. A GPU worker will execute only GPU tasks. Hence, when a GPU is used, a CPU worker is removed. With PARSEC, no thread is dedicated to a GPU, and they all might execute CPU tasks as well as GPU tasks. The first computational thread that submits a GPU task takes the management of the GPU until no GPU work remains in the pipeline. Both runtimes manage to get similar performance and satisfying scalability over the 3 GPUs. In only two cases, MHD and pmlDF, STARPU outperforms PARSEC results with 3 streams. This experiment also reveals that, as was expected, the computation takes advantage of the multiple streams that are available through PARSEC. Indeed, the tasks generated by a sparse factorization are rather small and won't use the entire GPU. This PARSEC feature compensates for the prefetch strategy of STARPU that gave it the advantage when compared to the one stream results. One can notice the poor performance obtained on the *afshell* test case: in this case, the amount of Flop produced is too small to efficiently benefit from the GPUs.

Memory is a critical resource for a direct solver. Figure 2.12 compares the memory peaks obtained with the three implementations of the solver, using *eztrace*. The runs were obtained with 12 cores but the results would not be much different with an other setup.

The memory allocated can be separated into five categories :

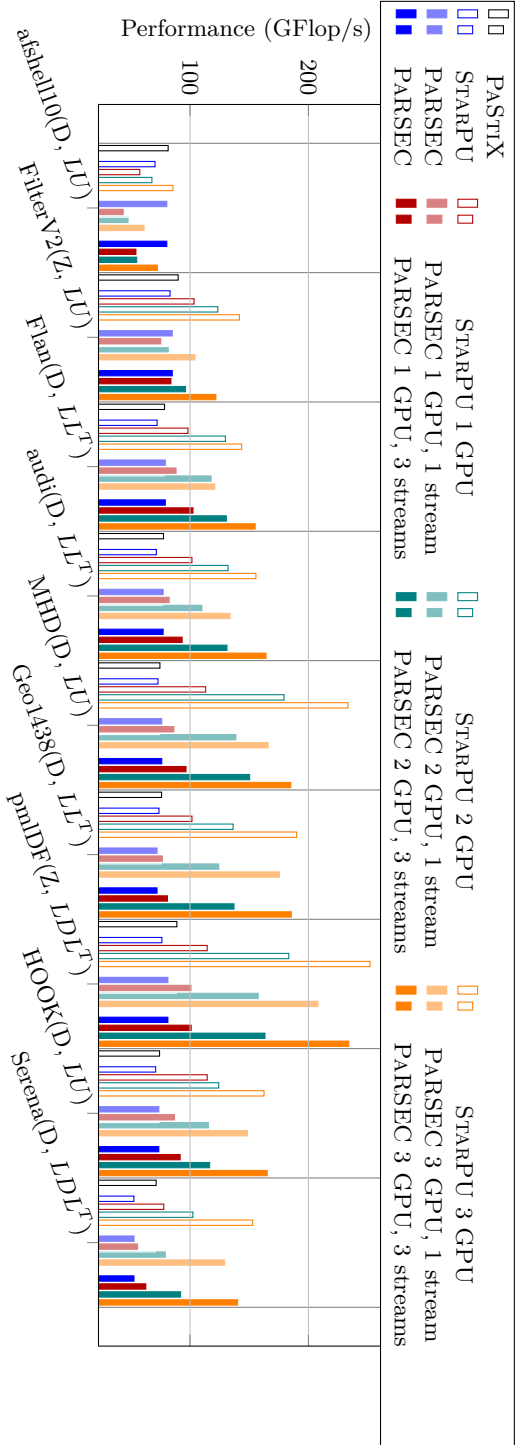


Figure 2.11: GPU scaling study: GFlop/s performance of the factorization step with the three schedulers on a set of 10 matrices. Experiments exploit twelve CPU cores and from zero to three additional GPUs.

- the coefficients of the factorized matrix which are allocated at the beginning of the computation and is the largest part of the memory;
- the structure of the factorized matrix also built and allocated before the factorization is performed;
- user's **CSC** (Compress Sparse Column) matrix which is the input given to PASTIX;
- internal block distributed **CSC** matrix which corresponds to the input matrix and is used to compute the relative error or to perform iterative refinement;
- a last part of memory that includes the scheduler overhead.

As shown in the plot, a large part of the memory corresponds to the first four categories and is independent of the runtime used.

The last part of the bars corresponds to the overhead of the scheduler.

The values on top of the bars are the overhead ratio compared to memory overhead obtained with the PASTIX native scheduler. We can see that we obtained a small overhead with PARSEC whereas STARPU allocate about 7% more memory than PASTIX.

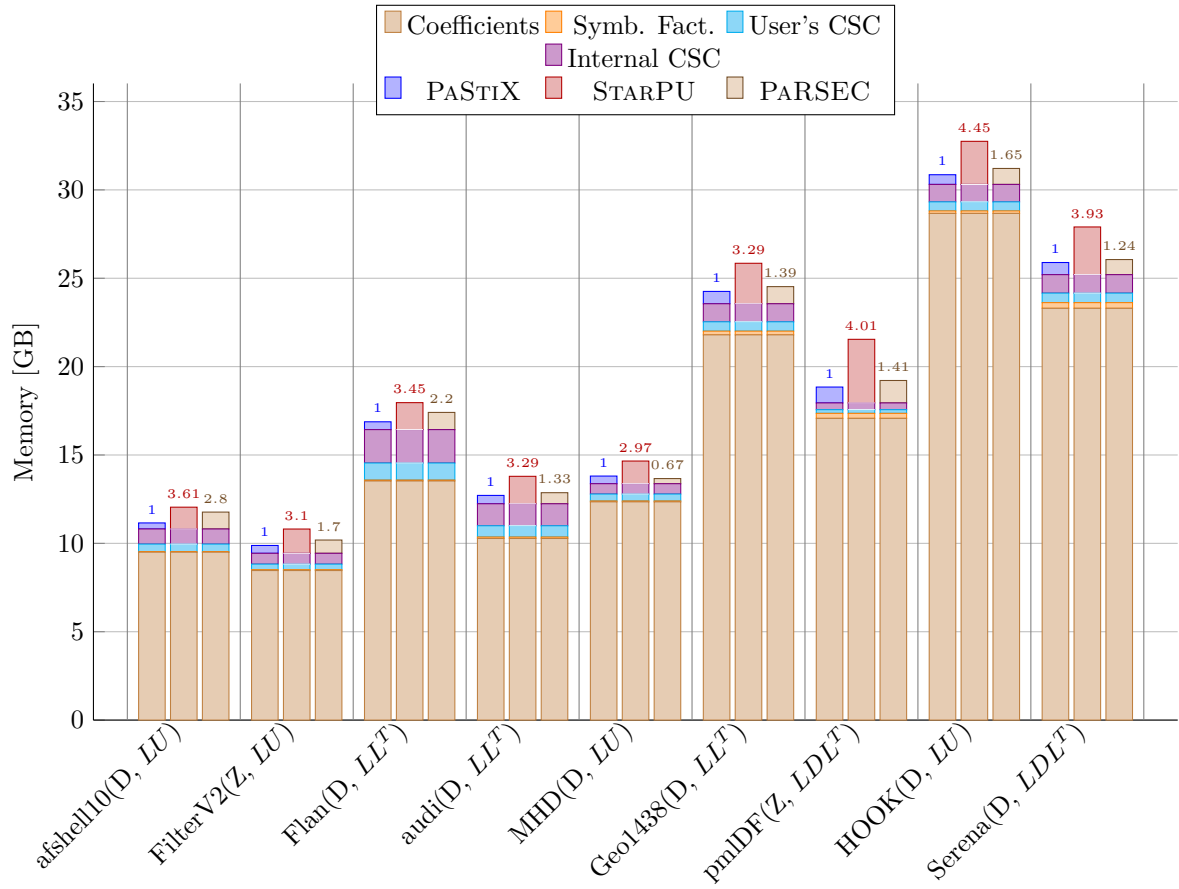


Figure 2.12: Memory consumption, common data structures are detailed, overhead ratio on top of bar chart



## Chapter 3

# Incomplete factorization and domain decomposition

The first part of this chapter presents the joint work with Pascal Hénon to implement an  $ILU(k)$  algorithm in the PASTIX solver [77].

Please look at [http://www.labri.fr/perso/ramet/restricted/HDR\\_PC08.pdf](http://www.labri.fr/perso/ramet/restricted/HDR_PC08.pdf) for a full version of this work with some experiments.

The second part of this chapter presents work that has been developed in the PhD thesis of Astrid Casadei [31] (in french) that I have co-advised. Some contributions have been published in [32].

Please look at [http://www.labri.fr/perso/ramet/restricted/HDR\\_HIPC14.pdf](http://www.labri.fr/perso/ramet/restricted/HDR_HIPC14.pdf) for a full version of this work with some experiments.

### 3.1 Amalgamation algorithm for $iLU(k)$ factorization

Solving large sparse linear systems by iterative methods [129] has often been unsatisfactory when dealing with practical “industrial” problems. The main difficulty encountered by such methods is their lack of robustness and, generally, the unpredictability and inconsistency of their performance when they are used over a wide range of different problems. Some methods can work quite well for certain types of problems but can fail on others. This has delayed their acceptance as “general-purpose” solvers in a number of important applications.

Meanwhile, significant progress has been made in developing parallel direct methods for solving sparse linear systems, due in particular to advances made in both the combinatorial analysis of Gaussian elimination process, and on the design of parallel block solvers optimized for high-performance computers. For example, it is now possible to solve real-life three-dimensional problems with several million unknowns, very effectively, with sparse direct solvers. This is achievable by a combination of state of the art algorithms along with careful implementations which exploit superscalar effects of the processors and other features of modern architectures [11, 64, 75, 76, 99]. However, direct methods will still fail to solve very large three-dimensional problems, due to the potentially huge memory requirements for these cases.

On the other hand, the iterative methods using a generic preconditioner like an  $ILU(k)$  factorization [129] require less memory, but they are often unsatisfactory when the simulation needs a solution with a good precision or when the systems are ill-conditioned. The incomplete factorization technique usually relies on a scalar implementation and thus does not benefit from the superscalar effects provided by the modern high performance architectures. Furthermore, these methods are difficult to parallelize efficiently, more particularly for high values of level-of-fill. Some improvements to the classical scalar incomplete factorization have been studied to reduce the gap between the two classes of methods. In the context of domain decomposition, some algorithms that can be parallelized in an efficient way have been investigated in [110]. In [124], the authors proposed to couple incomplete factorization with a selective inversion to replace the triangular solutions (that are not as scalable as the factorization) by scalable matrix-vector multiplications. The multifrontal method has also been adapted for incomplete factoriza-



tion with a threshold dropping in [89] or with a fill level dropping that measures the importance of an entry in terms of its updates [30]. In [34], the authors proposed a block ILU factorization technique for block tridiagonal matrices.

The approach investigated in this work consists in exploiting the parallel blockwise algorithmic approach used in the framework of high performance sparse direct solvers in order to develop robust parallel incomplete factorization based preconditioners [129] for iterative solvers. The idea is then to define an adaptive blockwise incomplete factorization that is much more efficient than the scalar incomplete factorizations commonly used to precondition iterative solvers. Indeed, by using the same ingredients which make direct solvers effective, these incomplete factorizations exploit the latest advances in sparse direct methods, and can be very competitive in terms of CPU time due to the effective usage of CPU power. At the same time, this approach can be far more economical in terms of memory usage than direct solvers. Therefore this should allow us to solve systems of much larger dimensions than those that are solved by the direct solvers.

The section is organized as follows: Section 3.1.1 gives the principles of the block ILU factorization based on the level of fill, Section 3.1.2 presents our algorithms to obtain the approximate supernode partition which aims at creating the sparse block structure of the incomplete factors and finally, in Section 3.1.3, we present some experiments obtained with our method.

### 3.1.1 Methodology

Preconditioned Krylov subspace methods utilize an accelerator and a preconditioner [129]. The goal of the ILU-based preconditioners is to find approximate LU factorizations of the coefficient matrix which are then used to facilitate the iterative process.

Incomplete LU (ILU) or Incomplete Cholesky (IC) factorization are based on the premise that most of the fill-in entries generated during a sparse direct factorization will tend to be small. Therefore, a fairly accurate factorization of  $A$  can be obtained by dropping most of the entries during the factorization. There are essentially two classical ways of developing incomplete LU factorizations.

The first (historically) consists of dropping terms according to a recursive definition of a level: a fill-in which is itself generated from another fill-in will tend to be smaller and smaller as this chain of creation continues. The notion of level-of-fill, first suggested by engineers is described next, as it is the stepping stone into the approach described in this work.

The second is based on the use of thresholds during the factorization. Thus,  $ILU(\tau, p)$  [128] is commonly implemented as an upward-looking row-oriented algorithm which computes the ILU factorization row by row. It utilizes two parameters, the first  $\tau$  being used as tolerance for dropping small terms relative to the norm of the row under consideration, and the second  $p$  determines the maximum number of nonzero elements to keep in each row.

#### ILU(k) preconditioners

The incomplete LU factorization  $ILU(k)$  implements dropping with the help of a *level-of-fill* associated with each fill-in introduced during the factorization. Initially, each nonzero element has a level-of-fill of zero, while each zero element has (nominally) an infinite level-of-fill. Thereafter, the level-of-fill of  $l_{ij}$  is defined from the formula:

$$\text{levf}(l_{ij}) = \min\{\text{levf}(l_{ij}); \text{levf}(l_{ki}) + \text{levf}(l_{jk}) + 1\} \quad (3.1)$$

This definition and its justification were originally given by Watts for problems arising in petroleum engineering [142]. Later Forsyth and Tang provided a graph-based definition, which was then reinterpreted by Hysom and Pothen [82] within the framework of the fill-path theorem [126]. The interpretation of the level-of-fill is that it is equal to  $\text{len}(i, j) - 1$  where  $\text{len}$  is the length of the shortest fill-path between  $i$  and  $j$ . It can be easily seen that the path-lengths follow the simpler update rule:  $\text{len}(i, j) = \min\{\text{len}(i, j); \text{len}(i, k) + \text{len}(k, j)\}$ . During Gaussian elimination, we eliminate nodes  $k$ , labelled before a certain pair of nodes  $(i, j)$ . Then, it can be proved that the shortest fill-path from  $i$  to  $j$  is the shortest of all shortest fill-paths from  $i$  to some  $k$  plus the shortest fill-path from  $k$  to  $j$ . This is illustrated in Figure (3.1).

The incomplete symbolic  $ILU(k)$  factorization has a theoretical complexity similar to the numerical factorization, but based on the graph interpretation of the level-of-fill, an efficient algorithm that leads

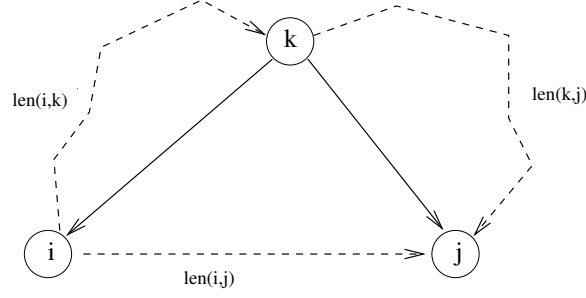


Figure 3.1: Fill-paths from  $i$  to  $j$ .

to a practical implementation, that can be easily parallelized, has been proposed in [82]. Thus, the symbolic factorization for ILU(k) method, though more costly than in the case of exact factorizations, is not a limitation in our approach.

### Block-ILU(k)

The idea of level-of-fill has been generalized to blocks in the case of block matrices with dense blocks of equal dimensions, see, e.g., [37]. Such matrices arise from discretized problems when there are  $m$  degrees of freedom per mesh-point, such as fluid velocities, pressure etc. This is common in particular in Computational Fluid Dynamics.

It is clear that for such matrices, it is preferable to work with the quotient graph, since this reduces the dimension of the problem. It is clear that the factorization ILU(k) obtained using the quotient graph and the original are then identical. In other words, we consider the partition  $\mathcal{P}_0$  constructed by grouping set of unknowns that have the same row and column pattern in  $A$ ; these set of unknowns are the cliques of  $G$ . In this case, if we denote by  $G^k$  the adjacency graph of the elimination graph for the ILU(k) factorization, then we have:

$$Q(G^k, \mathcal{P}_0) = Q(G, \mathcal{P}_0)^k.$$

For coarser partition than  $\mathcal{P}_0$ , those properties are not true anymore in the general case.

Therefore, the ILU(k) symbolic factorization can be performed with a significant lower complexity than the numerical factorization algorithm. In addition, by using the algorithm presented in [82] that is easily parallelizable, the symbolic block incomplete factorization is not a bottleneck in our approach.

For direct factorization, the supernode partition usually produces blocks that have a sufficient size to obtain a good superscalar effect using the BLAS 3 subroutines. The exact supernodes that are generated in the incomplete factor nonzero pattern are usually very small. Consequently, a blockwise implementation of the ILU(k) preconditioner based on the exact supernode partition would not be very efficient and can even be worse than a classical columnwise implementation due to the overhead of calling the BLAS subroutines. A remedy to this problem is to merge supernodes that have *nearly the same structure*. This process induces some *extra fill-in* compared to the exact ILU(k) factors but the increase in the number of operations is largely compensated by the gain in time achieved thanks to BLAS subroutines. The convergence of our Block-ILU(k) preconditioner is at least as good as that obtained by scalar ILU(k). Furthermore, it can also improve the convergence of the solver since the extra-fill admitted in the factors mostly corresponds to numerically non-null entries that may improve the accuracy of the preconditioner.

The principle of our heuristics to compute the new supernode partition is to iteratively merge supernodes for which nonzero patterns are the most similar until we reach a desired extra fill-in tolerance. To summarize, our incomplete block factorization consists of the following steps:

1. find the partition  $\mathcal{P}_0$  induced by the supernodes of  $A$ ;
2. compute the block symbolic incomplete factorization  $Q(G, \mathcal{P}_0)^k$ ;
3. find the exact supernode partition in  $Q(G, \mathcal{P}_0)^k$ ;

4. given a *extra fill-in* tolerance  $\alpha$  , construct an approximate supernode partition  $\mathcal{P}_\alpha$  to improve the block structure of the incomplete factors (detailed in next section);
5. apply a block incomplete factorization using the parallelization techniques developed for our direct solver PASTIX.

The incomplete factorization can then be used to precondition a Krylov method to solve the system. The next section will focus on the step 4; it gives the details of an amalgamation algorithm that is used to find an approximate supernode partition.

### 3.1.2 Amalgamation algorithm

A blockwise implementation of the ILU(k) factorization is directly obtained using the direct blockwise algorithm 3. In fact, the exact supernodes that are generated in the symbolic ILU(k) factor are usually too small to allow good BLAS efficiency in the numerical factorization and in the triangular solves. To address this problem we propose an amalgamation algorithm which aims to group some exact supernodes that have similar nonzero pattern in order to get bigger supernodes. By construction, the exact supernode partition found in an ILU(k) factor is always a sub-partition of the *direct supernode partition* (i.e. corresponding to the direct factorization) since  $G^k$  can be obtained by removing some edges from  $G^*$ .

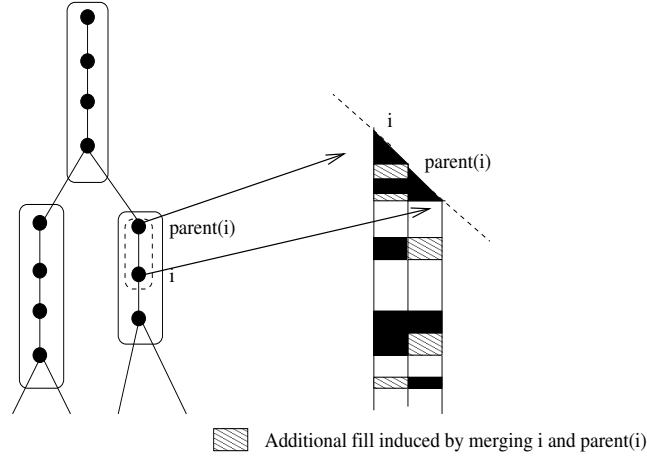


Figure 3.2: Additional fill created when merging the supernodes  $i$  and  $\text{parent}(i)$ .

As mention before, the amalgamation problem consists in merging as many supernodes as possible while adding only a few extra nonzeros in the sparse block pattern of the incomplete factors.

We propose a heuristics based on a greedy strategy. Here is some extra notation used in algorithm 5:

- $[k]$ ,  $\text{parent}(k)$  and  $\mathbf{Bmerge}$  are defined in the same way as in Section 1.2;
- $\text{nnz}_A$  is the number of nonzeros in  $A$ ;
- $\text{merge\_cost}(k)$  is the cost of merging the supernode  $k$  with its father in terms of extra-fill;
- $\text{son}(k)$  is the set of supernode indices corresponding to the sons of supernode  $k$  in the block elimination tree;
- by convention, if  $k$  is the root of the block elimination tree then  $\text{parent}(k) = k$  and  $\text{merge\_cost}(k) = \infty$ .

---

**Algorithm 5:** Amalgamation algorithm

---

```
nnz = 0 ;  
Compute  $Q(G, \mathcal{P}_0)^k$  and find  $S$  the set of all exact supernodes in  $G^k$ ;  
while  $nnz < \alpha * nnz_A$  and  $S \neq \emptyset$  do  
    Choose  $k$  /  $\text{merge\_cost}(k) = \min_{i \in S} \{\text{merge\_cost}(i)\}$  ;  
     $[k] := \text{Bmerge}([k], [\text{parent}(k)])$ ;  
     $S = S - \{\text{parent}(k)\}$  ;  
     $\text{son}(k) := \text{son}(k) \cup \text{son}(\text{parent}(k))$  ;  
     $\text{parent}(k) := \text{parent}(\text{parent}(k))$ ;  
     $nnz := nnz + \text{merge\_cost}(k)$  ;  
    Recompute  $\text{merge\_cost}(k)$ ;  
    for  $i \in \text{son}(k)$  do  
        | Recompute  $\text{merge\_cost}(i)$ ;
```

---

Given the set of all exact supernodes, it consists in iteratively merging the couple of supernodes  $(i, \text{parent}(i))$  which creates as few additional fill in the factor as possible (see Figure 3.2) while the extra fill tolerance  $\alpha$  is respected. Each time two supernodes are merged into a single one, the total amount of extra-fill is increased: the same operation is repeated until the amount of additional fill entries reaches the tolerance  $\alpha$  (given as a percentage of the number of nonzero elements found by the ILU(k) symbolic factorization). We denote by  $\text{merge\_cost}(i)$  the number of extra fill created when the supernodes  $(i, \text{parent}(i))$  are merged into a single one. Thus, the algorithm consists in choosing at each step the supernode  $k$  such that  $\text{merge\_cost}(k)$  is minimum (line 4) and to merge its father with it (line 5). The supernode  $k$  is then replaced by the new merged supernode and the supernode  $\text{parent}(k)$  is deleted from  $S$  (line 5, 6). The increasing of the global number of extra nonzeros is given by  $\text{merge\_cost}(k)$  (line 9). Since the sparse block structure of  $k$  has changed, its  $\text{merge\_cost}$  has to be recomputed (line 10) and the  $\text{merge\_cost}$  of its sons too (lines 11-13).

### Complexity of the amalgamation algorithm

We denote by  $\mathcal{P}_e$  the exact supernode partition of  $G^k$  (line 2),  $N_e$  the cardinal of  $\mathcal{P}_e$  and  $d$  the maximum degree of a vertex in  $Q(G^k, \mathcal{P}_e)$ . The amalgamation algorithm requires the set  $S$  to be sorted with respect to the  $\text{merge\_cost}$  metric and we have to keep  $S$  sorted each time a merge operation is done. One can use a heap to implement the set  $S$ ; therefore the cost to add or update an element in  $S$  will be at most  $O(\log(N_e))$  and the cost to get the lowest element is constant.

Computing  $\text{merge\_cost}()$  or  $\text{Bmerge}()$  requires merging two sorted lists of at most  $d$  intervals (a block is represented by an integer interval) so this operation is bounded by  $O(d)$ . In line 2, all the exact supernodes have to be sorted by increasing order of  $\text{merge\_cost}$  in  $S$ . This operation is thus  $O(N_e \cdot (\log(N_e) + d))$ .

Inside the **while** loop, each time a supernode is merged with its father there is a **Bmerge** operation (complexity of  $O(d)$ ) and if we make the assumption that the cardinality of  $\text{son}(k)$  is bounded by a constant (for a separator tree obtained by nested dissection, the constant will be 2 in most of the cases) then the cost of recomputing the  $\text{merge\_cost}$  of the supernode and its sons is also  $O(d)$  and the cost to update the heap  $S$  is  $O(\log(N_e))$ . The global cost of an iteration of the **while** loop is then  $O(d + \log(N_e))$ . Since in the worst case (where all the exact supernodes would be merged in a single one, leading to a dense matrix) only  $N_e - 1$  iterations can be done, a complexity bound of the amalgamation algorithm is  $O(N_e \cdot (\log(N_e) + d))$ .

### A variant of the amalgamation algorithm

The amalgamation algorithm 5 aims at minimizing the number of supernodes according to an extra fill tolerance  $\alpha$ . The assumption made here is that the triangular solution and the incomplete block factorization will all be more efficient if the supernode partition is coarser. A variant to the amalgamation objective is to merge some supernodes in order to minimize as far as possible the CPU time to apply the triangular solve or the incomplete factorization. Usually in an iterative method, the total time spent in the iterations is more than the time to compute the preconditioner. So we will focus on reducing the time of the triangular solves. To estimate the time spent in the triangular solves we use a time model

of the BLAS2 routines used in the blockwise triangular solve algorithm. The time model of a BLAS routine consists of a polynomial that interpolates the curve of the CPU times spent in the routine as a function of the block dimensions. These polynomials are obtained on a given architecture (such models are already used in PASTIX to balance the workload and schedule the computational tasks before the parallel factorization). For example, the time to compute a dense matrix-vector product  $M.v$  (GEMV BLAS subroutine) mostly depends on the dimensions  $(x, y)$  of  $M$ . Since the complexity of this operation is in  $O(x.y)$ , we use a polynomial model  $a.x.y + b.x + c.y + d$ . Thanks to experimental measurements, a multi-variable regression is used to set the coefficients of the polynomial. Figure 3.3 illustrates the model obtained on the IBM Power5 architecture and the experimental measurements.

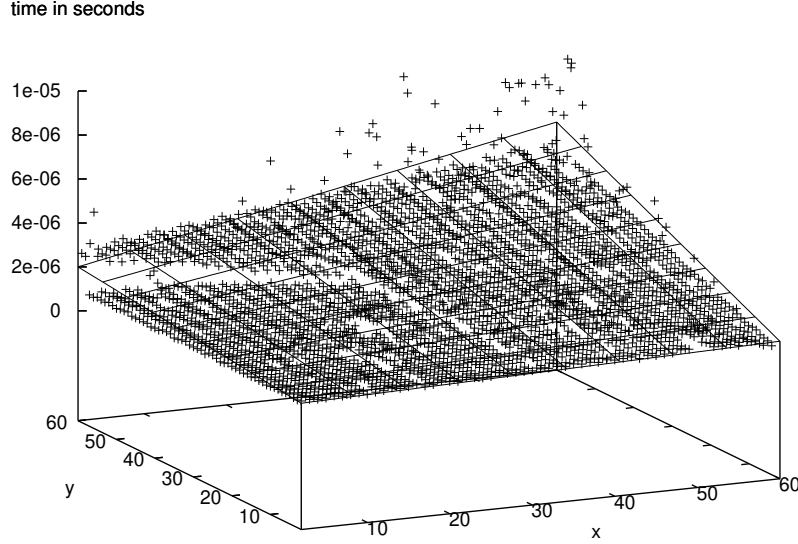


Figure 3.3: Polynomial model (surface) and experimental measurements (crosses) for GEMV obtained on IBM Power5.

Thanks to this polynomial BLAS time model, we can estimate the CPU time  $W_i$  that corresponds to the time spent in the supernode  $i$  in the triangular solve. What we seek, in this variant, is to merge two supernodes  $(k, parent(k))$  such that the gain in *CPU time per additional nonzero* allowed in the sparse block structure is the best. So, we evaluate the gain of merging  $k$  with  $parent(k)$  by the function :

$$\text{merge\_gain}(k) = \frac{W_k + W_{parent(k)} - W_{\text{Bmerge}([k],[parent(k)])}}{\text{merge\_cost}(k)}$$

Thus, if  $\text{merge\_gain}(k) > 0$ , it means that merging  $k$  and  $parent(k)$  will lower the CPU time in the triangular solves; the higher this value the better the trade-off (CPU time)/(extra nonzeros stored). On the contrary, if  $\text{merge\_gain}(k) < 0$  then it indicates that one should not merge  $k$  and its father because the number of additional floating operations induced by the extra nonzeros in the block structure is too much to be balanced by the superscalar effects in the BLAS routines.

The amalgamation Algorithm 6 aims to reduce the CPU time of the triangular solve for a given additional fill tolerance. The difference from Algorithm 5 is that the two supernodes to be merged are chosen as those that have the higher merge\_gain (line 4). Another difference is that any two supernodes that would increase the CPU time if they were merged are removed from the possible choices (line 2, 12 and 15) in order to decrease the number of operations. This means that we make the approximation that a supernode will never get a positive gain even if its father becomes bigger thanks to amalgamation.

In practice, this approximation is verified most of the time according to the BLAS model we obtained.

---

**Algorithm 6:** Amalgamation algorithm variant

---

```

 $nnz = 0$  ;
Compute  $Q(G, \mathcal{P}_0)^k$  and find  $S$  the set of all exact supernodes in  $G^k$  that have a
merge_gain  $> 0$ ;
while  $nnz < \alpha * nnz_A$  and  $S \neq \emptyset$  do
    Choose  $k/\text{merge\_gain}(k) = \max_{i \in S} \{\text{merge\_gain}(i)\}$  ;
     $[k] := \text{Bmerge}([k], [\text{parent}(k)])$ ;
     $S = S - \{\text{parent}(k)\}$  ;
     $\text{son}(k) := \text{son}(k) \cup \text{son}(\text{parent}(k))$  ;
     $\text{parent}(k) := \text{parent}(\text{parent}(k))$ ;
    Compute merge_cost( $k$ );
     $nnz := nnz + \text{merge\_cost}(k)$  ;
    Recompute merge_gain( $k$ );
    if  $\text{merge\_gain}(k) \leq 0$  then  $S = S - \{k\}$ ;
    ;
    for  $i \in \text{son}(k)$  do
        Recompute merge_gain( $i$ );
        if  $\text{merge\_gain}(i) \leq 0$  then  $S = S - \{i\}$ ;
        ;
    ;

```

---

In the case of Algorithm 5, if we set  $\alpha = \infty$  then it would merge all the supernodes and the sparse matrix  $L$  (resp.  $U$ ) would be considered as a dense matrix. An interesting property of Algorithm 6 is that if we set  $\alpha = \infty$  then it stops as soon as it cannot find any amalgamation of supernodes such that the global CPU time decreases (test  $S = \emptyset$  in line 3) or as soon as it reaches the extra fill tolerance given by  $\alpha$ . Thus it provides a convenient way to use the amalgamation algorithm without having to choose an arbitrary  $\alpha$  (that corresponds to  $\alpha = \infty$ ) parameter.

Algorithm 6 requires us to keep  $S$  sorted by increasing merge\_gain; though the merge\_gain is more costly than the merge\_cost it has also a complexity of  $O(d)$ ; therefore Algorithm 6 has the same asymptotic complexity as Algorithm 5.

### 3.1.3 Numerical experiments

We consider the AUDI test case (see Table 2.1) for the numerical validation of our block preconditioner.

Numerical experiments were performed on an IBM Power5 SMP node (16 processors per node) at the computing center of Bordeaux 1 University, France. We used a GMRES version without "restart". The stopping iteration criterion used in GMRES is that the right-hand-side relative residual norm should be less than  $10^{-7}$ .

As some matrices are symmetric definite positive, one could use a preconditioned conjugate gradient method; but at this time we have only implemented the GMRES method in order to treat unsymmetric matrices as well. The choice of the iterative accelerator is not in the scope of this study.

Graphical representations are provided in Figures 3.4, 3.5, 3.6 and 3.7 for the AUDI problem. We give according to the fill-in ratio:

- the number of iterations,
- the time of sequential incomplete factorization in seconds,
- the time of sequential triangular solve in seconds,
- the total sequential time in seconds,

for both scalar (with level-of-fill  $k = 1, 2, \dots, 7$ ) and block implementations (with level-of-fill  $k = 1, 2, 3$ ). For the block implementation, at each level-of-fill, the amalgamation ratio varies between 10% and 120% and for the scalar implementation the level-of-fill  $k$  varies between 1 to 7. We also add to these graphics the values obtained by our automatic criteria (large dots) based on algorithm 6 ( $\alpha = \infty$ ).

The scalar implementation has better total time, for each level-of-fill value, when the amalgamation ratio  $\alpha$  is set to 0% or 10%, but is not competitive for higher values. This is also verified for the

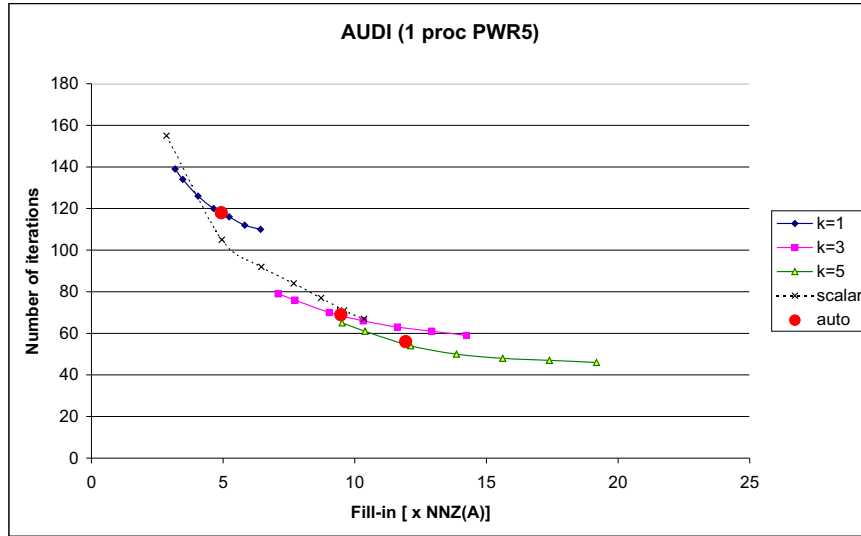


Figure 3.4: Number of iterations for AUDI problem

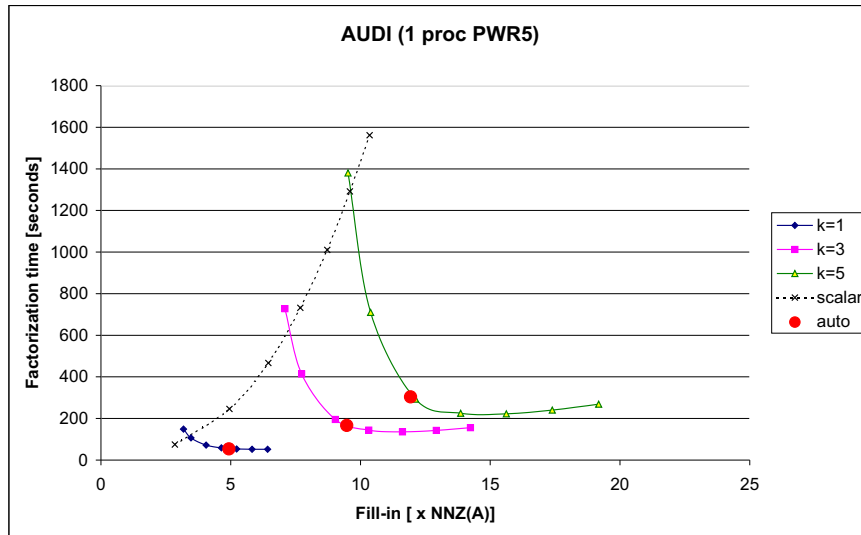


Figure 3.5: Time of sequential incomplete factorization for AUDI problem

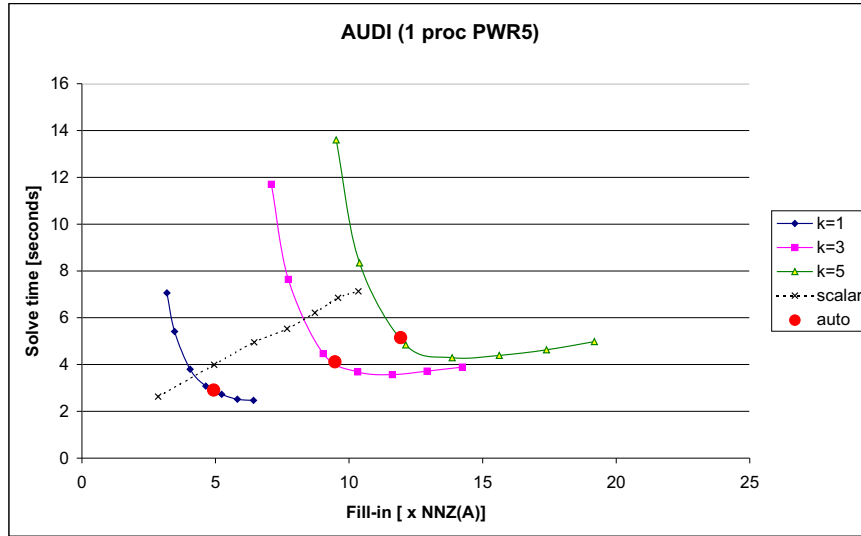


Figure 3.6: Time of sequential triangular solve for AUDI problem

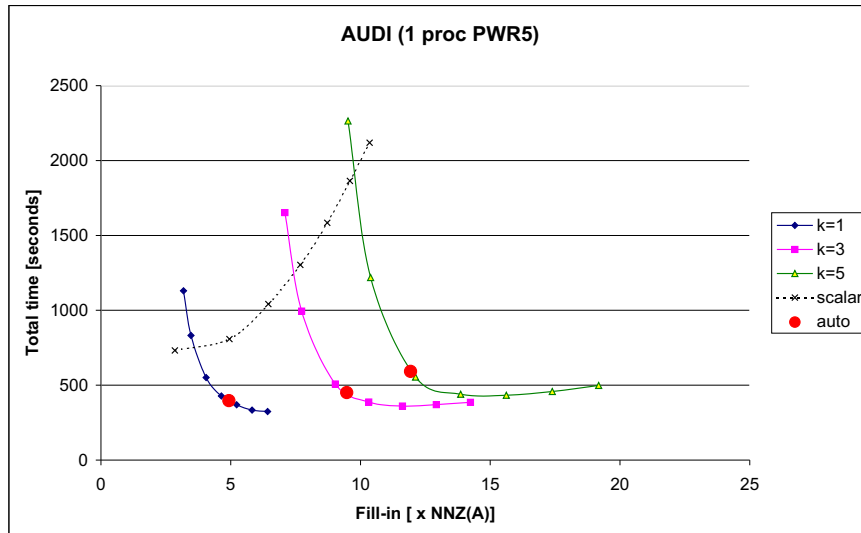


Figure 3.7: Total sequential time for AUDI problem



incomplete factorization time. We can see the real improvement provided by the amalgamation: for instance, when  $k = 5$ , by allowing some extra fill-in, the time can be divided by almost 4.

A great difference is observed in the incomplete factorization between the scalar implementation and the blockwise implementation. The BLAS-3 subroutines offer a great improvement over the scalar implementation especially for the higher level-of-fill values that provide the bigger dense blocks and number of floating point operations in the factorization. For the triangular solves, the results are less favorable since an amalgamation ratio greater than 40% is needed to improve the time of the scalar implementation. This is certainly due to the fact that the size of the blocks must be sufficient for BLAS-2 efficiency.

Our automatic criteria (based on time optimization) for amalgamation is a good compromise between minimizing the fill-in and optimizing the total time. For a given value of  $k$ , the variation between the time achieved by this automatic method and the best observed time for  $0\% \leq \alpha \leq 120\%$  is always lower than 25%. We will use this automatic criteria for the next experiments concerning the parallel implementation.

Another interesting remark is that for small values of  $\alpha$  ( $\leq 40\%$ ), the number of iterations for the blockwise implementation follows the curve of the scalar implementation. But, for higher values, one should prefer to increase the level-of-fill value to improve the convergence with the same fill-in ratio.

The main aims of this work have been reached. The blockwise adaptation of the  $ILU(k)$  factorization presented in this work allows us to significantly reduce the time to solve linear systems compared to the classical columnwise algorithm. It also benefits from the parallelization techniques developed for direct solvers (in our case PASTIX). We think that this approach is rather simple and could be adapted to other direct solvers (in particular others supernodal solvers) and thus provides a generic way to build efficient and parallel iterative solvers.

## 3.2 Graph partitioning for well balanced domain decomposition

Nested Dissection ( $ND$ ) was introduced to our community by A. George in 1973 [52] and is a well-known and very popular heuristic for sparse matrix ordering to reduce both fill-in and operation count during Cholesky factorization. This method is based on graph partitioning and the basic idea is to build a “good separator” that is to say a “small size separator”  $S$  of the graph associated with the original matrix in order to split the remaining vertices in two parts  $P_0$  and  $P_1$  of “almost equal sizes”. The vertices of the separator  $S$  are ordered with the largest indices, and then, the same method is applied recursively on the two subgraphs induced by  $P_0$  and  $P_1$ . Good separators can be built for classes of graphs occurring in finite-element problems based on meshes which are special cases of bounded density graphs[109] or more generally of overlap graphs[108]. In  $d$ -dimensions, such  $n$ -node graphs have separators whose size grows as  $\mathcal{O}(n^{(d-1)/d})$ . In this work, we focus on the cases  $d = 2$  and  $d = 3$  which correspond to the most interesting practical cases for numerical scientific applications.  $ND$  has been implemented by graph partitioners such as METIS<sup>1</sup> [87] or SCOTCH<sup>2</sup> [115].

Moreover,  $ND$  is based on a divide and conquer approach and is also very well suited to maximize the number of independent computational tasks for parallel implementations of direct solvers. Then, by using the block data structure induced by the partition of separators in the original graph, very efficient parallel block solvers have been designed and implemented according to supernodal or multifrontal approaches. To name a few, one can cite MUMPS<sup>3</sup> [6], PASTIX<sup>4</sup> [75] and SUPERLU<sup>5</sup> [63]. One can also find in [70] a survey of partitioning methods and models for the distribution of computations and communications in a parallel framework.

However, if we examine precisely the complexity analysis for the estimation of asymptotic bounds for fill-in or operation count when using  $ND$  ordering[100], we notice that the size of the halo of the separated subgraphs (set of external vertices adjacent to the subgraphs and previously ordered) plays a crucial role in the asymptotic behavior achieved. The minimization of the halo is in fact never considered

---

<sup>1</sup><http://www.cs.umn.edu/~metis>

<sup>2</sup><http://gforge.inria.fr/projects/scotch>

<sup>3</sup><http://graal.ens-lyon.fr/MUMPS/>

<sup>4</sup><http://pastix.gforge.inria.fr/>

<sup>5</sup><http://crd-legacy.lbl.gov/~xiaoye/SuperLU/>

in the context of standard graph partitioning and therefore in sparse direct factorization studies.

In this work, we focus on hybrid solvers combining direct and iterative methods and based on domain decomposition and Schur complement approaches. The goal is to provide robustness similar to sparse direct solvers, but memory usage and scalability more similar to preconditioned iterative solvers. Several sparse solvers like HIPS<sup>6</sup> [51], MAPHYS [2, 58], PDSLIN [144] and SHYLU<sup>7</sup> [125] implement different versions of this hybridification principle.

For generic hybrid solvers, a good tradeoff must be found between the number of subdomains which influences the numerical robustness in terms of rate of convergence in the iterative part of the solver and the size of the subdomains which influences the computational and memory costs for each subdomain direct solver. A classical first coarse grain level of parallelism is achieved by distributing the subdomains on different processors, but if we must consider medium or large subdomain sizes for numerical issues, one can use a parallel sparse direct solver for each subdomain leading to the use of a second level of parallelism. In this case and for today's architectures based on large clusters of SMP multicore nodes, one can associate each subdomain with a SMP node, thus leading to a hybrid programming approach (MPI between subdomains and threads for the sparse parallel direct solver for each subdomain).

In this context, the computational cost associated with each subdomain for which a sparse direct elimination based on  $ND$  ordering is carried out mainly depends on both the internal node set size and on the halo size of the subdomain. Indeed, the complexity analysis demonstrates that the computational cost for the construction of the local Schur complement (whose size is given by the halo size) grows as the computational cost of the sparse direct elimination of the internal nodes.

The construction of a domain decomposition tool leading to a good balancing of both the internal node set size and the halo node size for all the domains is then a critical point for load balancing and efficiency issues in a parallel computation context. To our knowledge, such a tool does not exist and standard partitioning techniques, even by using a  $k$ -way partitioning approach that intends to construct directly a domain decomposition of a graph in  $k$  sets of independent vertices [88], do not lead in general to good results for the two coupled criteria, for general irregular graphs coming from real-life scientific applications.

For this purpose, we revisit the original algorithm introduced by Lipton, Rose and Tarjan[100] in 1979 which performed the recursion for nested dissection in a different manner: at each level, we apply recursively the method to the subgraphs induced by  $P_0 \cup S$  on the one hand, and  $P_1 \cup S$  on the other hand (see Figure 3.8 on the right). In these subgraphs, vertices already ordered (and belonging to previous separators) are the halo vertices. The partition of these subgraphs will be performed with three objectives: balancing of the two new parts  $P'_0$  and  $P'_1$ , balancing the halo vertices in these parts  $P'_0$  and  $P'_1$ , and minimizing the size of the separator  $S'$ .

We implement this strategy in the SCOTCH partitioner. The SCOTCH strategy is based on the multilevel method[68, 86] which consists of three main steps: the (sub)graph is coarsened multiple times until it becomes small enough, then an algorithm called greedy graph growing is applied to the coarsest graph to find a good separator, and finally the graph is uncoarsened, projecting at each level the coarse separator on a finer graph and refining it using the Fiduccia-Mattheyses algorithm[69]. This work studies variations of these three algorithmic steps in order to take into account the balancing criteria for both the internal and halo nodes, the goal being to achieve in the end a well balanced domain decomposition well suited for parallel hybrid solvers. However, as we consider a bi-partitioning method, the number of subdomains generated will be  $2^k$  if we stop the recursion at some level  $k$ .

The sections are organized as follows. In Section 3.2.1, we focus on the coarsening and the uncoarsening steps, and we present the modifications compared to standard multilevel partitioning strategies. Section 3.2.2 presents greedy graph growing approaches for the coarsest graph and several adaptations developed to get balanced halo and interior node sizes. Some experimental results illustrate the different studied strategies.

---

<sup>6</sup><http://hips.gforge.inria.fr/>

<sup>7</sup><http://trilinos.sandia.gov/packages/shylu/>

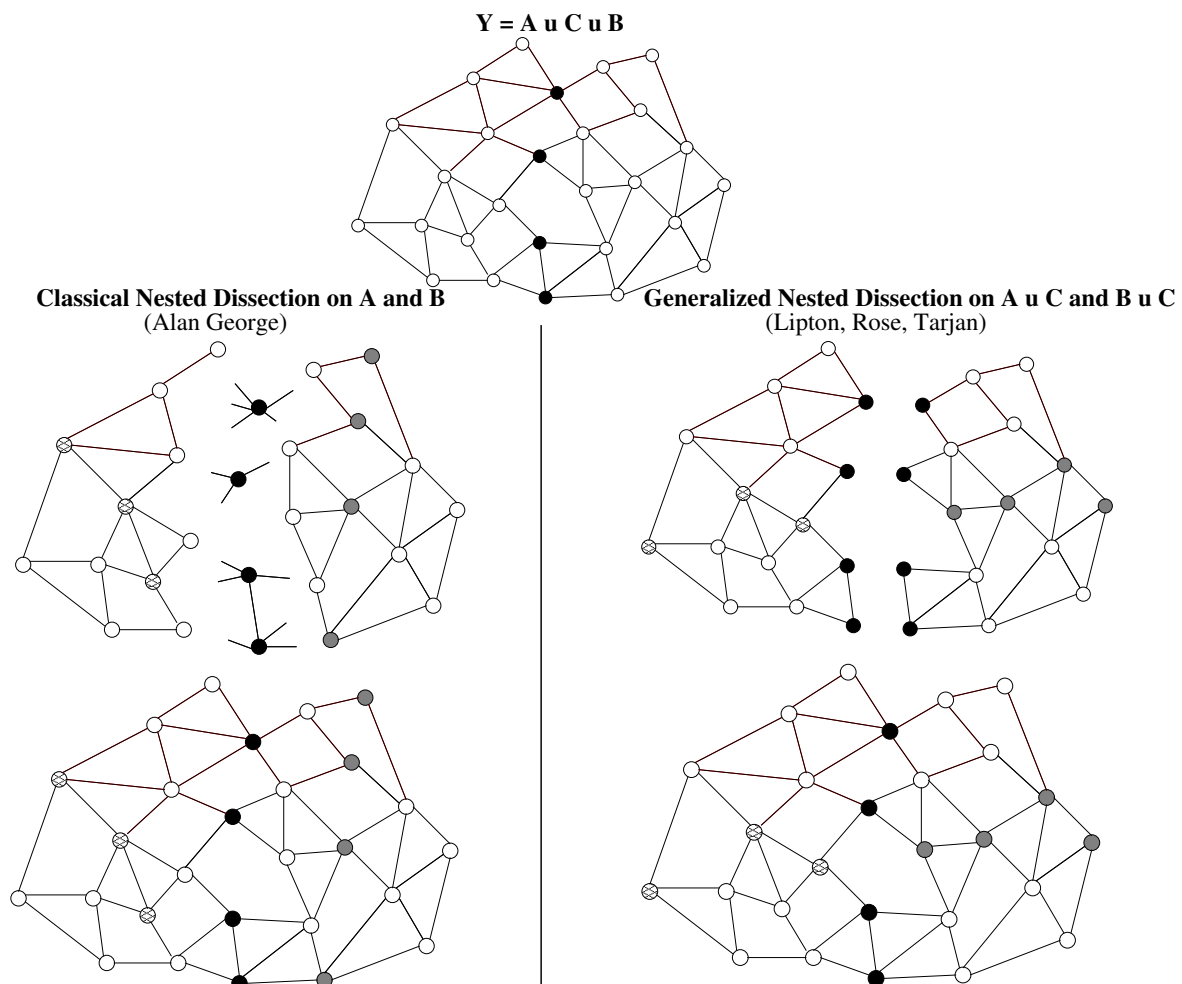


Figure 3.8: *On the left:* classical recursion which is performed on  $P_0$  and  $P_1$ . Objectives are to balance the sizes of the subgraphs and to minimize the separator size. However, halo sizes, represented by the nodes in black and grey, can be unbalanced: they are respectively 4, 5, 6 and 8. *On the right:* recursion is performed here on  $P_0 \cup S$  and  $P_1 \cup S$  and the halo vertices are balanced among the parts, leading to interface sizes equal to 5, 5, 6 and 6.

### 3.2.1 Multilevel Framework

The SCOTCH default strategy consists in a multilevel method, which is one of the best ways to find good separators. This takes two sub-methods as parameters: an effective partitioning strategy, which is a greedy graph growing algorithm (*GG*) by default in SCOTCH; and a method allowing us to enhance an existing separator, here the Fiduccia-Mattheyses algorithm (*FM*). The idea is to coarsen the graph multiple times to simplify it, then to apply the effective partitioning strategy *GG* on the coarsest graph, and finally to project the separator back on finest graphs. At each level, the projection is refined with the *FM* algorithm.

► More specifically, at each step of the coarsening stage, a matching of the vertices is performed, and the matched vertices are merged, summing their weight, to form the weight of the new vertices. This process is repeated until the graph obtained is small enough. Then, *GG* is applied on the (weighted) coarsest graph, making a first guess for the final separator. At each stage of the uncoarsening, two vertices that were matched at a finer level are assigned to the same part as their coarse equivalent. This way, if the global balance was achieved in the coarser graph, it is still there in the finer; yet, the uncoarsening may lead to a thick locally non-optimal separator, requiring the use of a refinement algorithm. To reduce the search domain of the algorithm, SCOTCH builds a band graph of width 3 around the uncoarsened separator and runs *FM* on it. Note that to have a good separator, this refinement is applied at each step of the uncoarsening, not only on the finest graph.

Our aim to balance the halo vertices requires modifying slightly the multilevel framework. Indeed, some halo vertices may be matched with non-halo vertices, and the sum of their weights would not mean anything. Thus, vertices have now two weights: a non-halo and a halo weight. When two vertices are matched, the two non-halo weights are added together, and the same is done for their halo weights. If the initial graph is unweighted, the non-halo weight of a vertex is one if it is out of the halo, zero otherwise; the halo weight of a vertex is one if the vertex is in the halo, zero otherwise. In the context of these two different kinds of weight, we redefine a halo vertex as *a vertex which has a nonzero halo weight*. Since the matching procedure treats halo and non-halo vertices the same way, we expect that the ratio of halo vertices is almost the same in the finest and the coarsest graphs.

In the following, if  $C$  is a set of vertices, we denote by  $\overline{C}$  its subset of halo vertices.  $|C|$  is the sum of the non-halo weights of vertices in  $C$  and  $|\overline{C}|$  the sum of halo weights.

► In order to maintain the balance achieved during the uncoarsening process, the Fiduccia-Mattheyses has also been modified. The *FM* method is an algorithm implemented in SCOTCH to refine an existing separator. It is based on a local search around the initial separator. A *move* of the search consists in picking a vertex from the current separator and putting it in one of the two parts. To keep a correct separator, the neighbours of the vertex in the other part also need to enter it. The *FM* algorithm makes several passes (set of consecutive moves) and keeps going until the maximum number of passes is reached and the last pass brings improvement; the next pass begins from the best separator ever found (and found in the last pass). Moreover, even passes have a slight preference for moving vertices in part 0, while odd passes favor part 1 instead.

*FM* has three objectives when it moves a vertex: getting a reasonable imbalance  $\Delta = |P_0| - |P_1|$ , minimizing the separator  $S$  and moving a vertex to the preferred *pref* part<sup>8</sup>. More specifically, *FM* ensures that once the move is done, the new imbalance do not exceed  $\max(|\Delta|, \Delta_{th})$ , where  $\Delta$  is the current imbalance and  $\Delta_{th}$  a fixed imbalance given by user. This means that if current imbalance is outside the scope of  $\Delta_{th}$ , it will not be degraded, and if it is within, it will remain within. If there is no possible move respecting this rule, the pass ends. Otherwise, *FM* takes, among valid choices, one that leads to the smallest possible new separator (which can be larger than the current one). If there are still several possibilities, *FM* eventually selects a move to the preferred part of the pass.

In order to prevent the local search making the same choices several times, a *Tabu* search is implemented. A set of *tabu* vertices is maintained and reset at each new pass. Whenever a vertex is chosen, it is put in the *tabu* set and will not be allowed to move again until next pass. This way, during a pass, a vertex may enter the separator, be chosen to leave it, and re-enter by the move of some of its neighbours, but then it will remain in the separator. A pass stops when either there is no possible move remaining, or the last *movenbr* moves did not bring any improvement. Giving the possibility of continuing a pass for *movenbr* moves after the last improvement may allow us to get out of a local minimum.

<sup>8</sup>Note that *FM* has some exceptions for isolated vertices, *i.e.* separator vertices which are adjacent to only one of the two parts. In practice, we have special treatment that avoids several difficulties that will not be described in this work.

---

**Algorithm 7:** modified *FM*

---

**Input:** graph:  $G = (V, E)$ , number of passes:  $passnbr$ , number of hill-climbing moves by pass:  $movenbr$ , maximum acceptable imbalance:  $\Delta_{th}$  and  $\bar{\Delta}_{th}$ , initial partition:  $(P_0, S, P_1)$  with  $S \neq \emptyset$

**Output:** partition  $(P_0, S, P_1)$  of  $V$  such as  $S$  is a (small) separator and  $|P_0| \approx |P_1|$

$(P_0^*, S^*, P_1^*) \leftarrow (P_0, S, P_1)$ ;

$passnum \leftarrow 0$ ;

**repeat**

$(P_0, S, P_1) \leftarrow (P_0^*, S^*, P_1^*)$ ;

$\Delta \leftarrow |P_0| - |P_1|$ ,  $\bar{\Delta} \leftarrow |P_0|_h - |P_1|_h$ ;

$tabu \leftarrow \emptyset$ ;

$movenum \leftarrow 0, enhanced \leftarrow false$ ;

$pref \leftarrow mod(passnum, 2)$ ;

**while**  $movenum < movenbr$  **do**

$f \leftarrow false$ ;

**if**  $|\bar{\Delta}| > \bar{\Delta}_{th}$  **then**

$(f, v, i) \leftarrow getHalo(S \setminus tabu, \bar{\Delta})$ ;

**if**  $\neg f$  **then**

$(f, v, i) \leftarrow getSep(S \setminus tabu, \max(\Delta_{th}, |\Delta|), pref)$ ;

**if**  $\neg f$  **then** /\* No movable vertex \*/

**break**;

        /\* Move  $v$  from separator to part  $i$  \*/  $R \leftarrow \{w | (v, w) \in E \text{ and } w \in P_{\neg i}\}$ ;

$S \leftarrow S \setminus \{v\} \cup R$ ;

$P_i \leftarrow P_i \cup \{v\}$ ,  $P_{\neg i} \leftarrow P_{\neg i} \setminus R$ ;

$\Delta \leftarrow |P_0| - |P_1|$ ,  $\bar{\Delta} \leftarrow |P_0|_h - |P_1|_h$ ;

$movenum++$ ;

$tabu \leftarrow tabu \cup \{v\}$ ;

**if**  $(P_0, S, P_1)$  is better than  $(P_0^*, S^*, P_1^*)$  **then**

$(P_0^*, S^*, P_1^*) \leftarrow (P_0, S, P_1)$ ;

$movenum \leftarrow 0, enhanced \leftarrow true$ ;

$passnum++$ ;

**until**  $\neg enhanced$  or  $(passnum = passnbr)$ ;

**return**  $(P_0^*, S^*, P_1^*)$ ;

---

Our modified *FM* algorithm is presented in Algorithm 7. The choice of a vertex  $v$  to move from the separator to a part  $i$  is revisited. If the current partition does not have an absolute halo imbalance  $|\bar{\Delta}|$  below the threshold  $\bar{\Delta}_{th}$  (chosen by user), then the function *getHalo* is called line 7. This function tries to fix the halo imbalance. It uses the sign of  $\bar{\Delta} = |P_0|_h - |P_1|_h$  to know the part where a vertex must be moved: a move to part 0 increases  $\bar{\Delta}$ , a move to part 1 decreases it. Then, it picks a vertex whose move to part  $i$  will minimize the new halo imbalance. If there is no such move that improves  $\bar{\Delta}$  strictly, then the function fails. Here, or if the partition had already a reasonable halo imbalance, the function *getSep* is called instead (line 7), which works as described in the unmodified version.

We conclude this section by giving our strategy to choose the *better* partition as indicated at line 7 of Algorithm 7. We proceed as follows:

- if we never found a partition in which  $|\Delta| \leq \Delta_{th}$ , we keep the partition whose  $|\Delta|$  is the smallest.
- if we already found a partition satisfying  $|\Delta| \leq \Delta_{th}$ , but never a partition satisfying both  $|\Delta| \leq \Delta_{th}$  and  $|\bar{\Delta}| \leq \bar{\Delta}_{th}$ , then we keep a partition with  $|\Delta| \leq \Delta_{th}$  whose  $|\bar{\Delta}|$  is the smallest.
- if we already found a partition satisfying both  $|\Delta| \leq \Delta_{th}$  and  $|\bar{\Delta}| \leq \bar{\Delta}_{th}$ , we keep only partitions satisfying these two conditions; among them, we choose the one which has the smallest separator. In case of equality, we pick the one with the smallest  $|\bar{\Delta}|$ , and if there is still a tie, the one with the smallest  $|\Delta|$ .

### 3.2.2 Graph Partitioning Algorithms

We also need to adapt the greedy graph growing (*GG*) algorithm in order to compute a partitioning which takes halo weight into account. The next subsection will present the *GG* algorithm and a straightforward adaptation. Some unsatisfactory results lead us to consider two other approaches that are presented in the last two subsections and named double *GG* and halo-first *GG* respectively. The first one shares the idea of the "bubble" algorithm of [45, 107] to do *GG* with one seed per part, although it is based on a different approach.

Table 3.1 presents all the testing matrices, giving their size and their number of nonzero entries. The *id* number will be used to identify matrices in the following. For each matrix  $A$ , the symmetric graph of  $A + A^t$  is used. Matrices 1-20 come from the University of Florida Sparse Matrix Collection, and the last set of ten matrices comes from PARASOL collection, industrial collaborations or partners.

Algorithms will be judged on two criteria. For each domain, the sizes of the interior and of the halo are measured. Then, we compute the difference between the maximum and the minimum for both, providing two metrics: *interface imbalance*, and *interior imbalance*. For example, on the bottom-right graph in Figure 3.8, interior sizes are all equal to 4, thus the interior imbalance is null, and halo sizes are 5, 5, 6, and 6 respectively, giving a halo imbalance equal to 1.

Note that the graph partitioning technique used for *ND* is designed for reordering purpose. In this context, the main objective of SCOTCH software is to minimize the size of the separator while keeping a local imbalance for interior sizes that does not exceed a fixed percentage, named *bal*. The recursion is performed until a fixed number of vertices is reached. Thus, the branches of the decomposition tree may have different heights. On the contrary, we focus in this work on decomposition domain : so we want to choose the number of domains and thus the number of levels in the recursion. Furthermore, a default value for the local constraint on the interior imbalance ( $bal = 10\%$ ) accumulates through levels of the recursion: at level  $i$ , imbalance between minimum and maximum subgraph sizes may reach roughly  $bal \times i$  percents. This is too loose for our purpose. We cannot decrease *bal* too much because the constraint would be too tight for having a chance to minimize the separator. Thus, to achieve good balancing, we use a constraint that depends on the level: on the higher levels, subgraphs are big, so we can use a tighter constraint while giving the possibility of optimizing the separator size; on the bottom levels, subgraphs are small and we use a looser constraint. More precisely, if  $p$  levels are requested, level  $i$  will try to get a local imbalance of at most  $\max(\frac{bal}{2^{p-i+1}}, minbal)$ , where *minbal* is a threshold ensuring that the constraint does not become too small.

Table 3.1: Set of test matrices. 1-20 come from the University of Florida Sparse Matrix Collection. 21-30 come from industrial collaborations or partners.

<b>id</b>	<b>Matrix</b>	<b>n</b>	<b>nnz</b>
1	Dubcova3	146689	3489960
2	wave	156317	2118662
3	dj_pretok	182730	1512512
4	turon_m	189924	1557062
5	stomach	213360	3236576
6	BenElechi1	245874	12904622
7	torso3	259156	4372658
8	mario002	389874	1867114
9	helm2d03	392257	2349678
10	kim2	456976	10905268
11	mc2depi	525825	3148800
12	tmt_unsym	917825	3666976
13	t2em	921632	3673536
14	ldoor	952203	45570272
15	bone010	986703	70679622
16	ecology1	1000000	39996000
17	dielFilterV3real	1102824	88203196
18	thermal2	1228045	7352268
19	StocF-1465	1465137	19540252
20	Hook_1498	1498023	59419422
<b>21</b>	<b>NICE-25</b>	140662	5547944
<b>22</b>	<b>MHD</b>	485597	23747544
<b>23</b>	<b>Inline</b>	503712	36312630
<b>24</b>	<b>ultrasound</b>	531441	32544720
<b>25</b>	<b>Audikw_1</b>	943695	76708152
<b>26</b>	<b>Haltere</b>	1288825	18375900
<b>27</b>	<b>NICE-5</b>	2233031	175971592
<b>28</b>	<b>Almond</b>	6994683	102965400
<b>29</b>	<b>NICE-7</b>	8159758	661012794
<b>30</b>	<b>10millions</b>	10423737	157298268

In the following, all tests are done with a fixed number of levels of recursion. The column *GG* (standing for Greedy Graph Growing) in the results refers to the unmodified SCOTCH strategy, with *bal* = 10%. The column *GG\** and the other columns use the level-dependent constraint described above with *bal* = 10% and a threshold of 1%. *GG\** thus refers to a modified SCOTCH strategy with default graph partitioning algorithms but using the level-dependent *bal* constraint.

## Greedy Graph Growing

The algorithm implemented by the SCOTCH software to find a good separator in a graph  $G = (V, E)$  at the bottom of the multilevel technique is the greedy graph growing method. The idea is to pick a random seed vertex in the graph, and to make a part grow from this seed, until it reaches half of the graph size. It is described in Algorithm 8. At line 8, the seed  $w$  is chosen. Singleton  $\{w\}$  is the initial separator  $S$  between the parts  $P_1$ , empty, and  $P_0$ , containing all other vertices. Then, at each step, a vertex  $v$  from current separator  $S$  is chosen (l. 8), and passed from the separator  $S$  to the growing part  $P_1$  (l. 8 and 8). The choice is oriented by the minimization of the current separator. Additionally, the set  $N$  of all neighbours of  $v$  in  $P_0$  are retrieved from  $P_0$  (l. 8) and added to  $S$  (l. 8), so that  $S$  remains a separator for the parts. The process is repeated until both parts have almost the same size.

The result of this algorithm is very dependent on the random seed chosen at the beginning. Thus, SCOTCH tries several passes with different seeds (l. 8), and it eventually selects the best partition  $(P_0, S, P_1)$  found in all passes (l. 8).

**Algorithm 8:** GreedyGraphGrowing

```

Input: graph  $G = (V, E)$ , number of passes passnbr
Output: partition  $(P_0, S, P_1)$  of  $V$  such as  $S$  is a (small) separator and  $|P_0| \approx |P_1|$ 
 $(P_0^*, S^*, P_1^*) \leftarrow (\emptyset, V, \emptyset)$ ;
for  $p = 1$  to passnbr do
     $w \leftarrow \text{RandomSeed}(V)$  ;
     $P_0 \leftarrow V \setminus \{w\}$ ;
     $P_1 \leftarrow \emptyset$ ;
     $S \leftarrow \{w\}$ ;
    while  $|P_0|$  and  $|P_1|$  are not balanced do
         $v \leftarrow \text{getVertex}(S)$  ;
         $N \leftarrow \{j | (v, j) \in E \text{ and } j \in P_0\}$  ;           /* neighbours of  $v$  in  $P_0$  */
         $S \leftarrow S \setminus \{v\} \cup N$ ;
         $P_0 \leftarrow P_0 \setminus N$ ;
         $P_1 \leftarrow P_1 \cup \{v\}$ ;
    if  $(P_0, S, P_1)$  is better than  $(P_0^*, S^*, P_1^*)$  then
         $(P_0^*, S^*, P_1^*) \leftarrow (P_0, S, P_1)$ ;
return  $(P_0^*, S^*, P_1^*)$ ;

```

In a first attempt to adapt this algorithm to our purpose of balancing the halo, we made the following changes. First, the choice of the vertex to move from  $S$  to  $P_1$  was now oriented by the halo balance. More specifically, if  $P_1$  had not as many halo vertices as  $P_0$  (relative to the respective size of the parts), then we preferably chooses a vertex  $v$  inside the halo. Secondly, note that it is needed to have both the halo and the non-halo vertices in the separator for this strategy to work well. We thus choose the random seed inside halo, since halo vertices are often close to each other.

We tested this adapted algorithm. Unfortunately, it often fails to improve the default partitioning strategy.

## Double Greedy Graph Growing with Halo Care

The previous algorithm managed a good halo balance in general, but often at the price of a disconnected part  $P_0$ . We thus decided to use two initial seeds, one for each part, and to make both parts grow simultaneously. However, this new strategy can lead to blocking. Indeed, when growing, one part may block the progression of the other: this happens when  $V \setminus (P_0 \cup P_1)$  is not empty but has no vertex



reachable from some part  $P_i$ . To avoid this problem, we need to delay, as much as possible, the moment when parts meet each other.

Algorithm 9 describes the new method. Line 9 picks the two seeds  $w_i$  and  $w_{-i}$  in the halo. They are also chosen as far as possible from each other, so that parts meet as late as possible. Both parts, initially empty, are grown from their respective seed vertex. At each step, we choose the smallest part  $i$  (l. 9-9), and a vertex  $v$  from its boundary  $S_i$  (l. 9).  $v$  is chosen according to the halo balance situation; if part  $i$  has less halo vertices than part  $-i$ , a halo vertex is taken if possible, and if it has more halo vertices, a non-halo vertex is picked preferably. If several choices of vertices remain, then the vertex which is the nearest from  $w_i$  and the farthest from  $w_{-i}$  (i.e. the vertex  $v$  with the smallest value  $\text{dist}(v, w_i) - \text{dist}(v, w_{-i})$ ) is taken. This is still with the purpose of making the parts meet as late as possible. Like the single-seed greedy graph growing presented before,  $v$  is then added to  $P_i$  (l. 9), retrieved from  $S_i$ , and  $S_i$  is updated to remain the boundary of  $P_i$  (l. 9). The process is carried on until all vertices are in one of the two parts, meaning  $V \setminus (P_0 \cup P_1) = \emptyset$  (end of while loop l. 9), or we are blocked, namely  $S_i = \emptyset$  (l. 9).

In the latter case, a solution would be to put all remaining vertices of  $V \setminus (P_0 \cup P_1)$  in the part to which they are adjacent. If few vertices remain, this is actually the solution we take lines 9-9. Otherwise, we empty  $P_0$  and  $P_1$  (l. 9) and retry to grow the parts from  $w_0$  and  $w_1$ , using some additional information to avoid getting blocked again. More specifically, we define a set of *control points* for each part  $i$ , containing only their respective seed at the beginning. When blocked, we add a new control point to the part  $i$  which could not grow. This control point is defined by the vertex of  $P_i$  which is the nearest from the untaken vertices. Then, parts are made grown again. When we choose a vertex to add to part  $i$  (l. 9), the first criterion is still the halo situation, and the second criterion is now the vertex  $v$  with the smallest value  $\min_j \{\text{dist}(v, \text{ctrlpts}_i[j])\} - \min_j \{\text{dist}(v, \text{ctrlpts}_{-i}[j])\}$ . In other words, part  $i$  will be *attracted* by its own control points, and *repulsed* by the control points of  $-i$ . (Note that this rule is in fact a generalization of the previous one).

The strategy described before is repeated until we either succeed to construct a partition  $(P_0, P_1)$  of  $V$  from  $(w_0, w_1)$ , or we reach *triesnb* tries, meaning we failed. If we succeed, we can construct a separator  $S$  by applying a minimum vertex cover algorithm on the edges on the frontier of  $P_0$  and  $P_1$  (l. 9).

Like in the previous algorithm, several passes are made with different couples of seed vertices. We eventually select the best partition found among the successful passes on line 9.

We tested double greedy graph growing on 4 levels of recursion (i.e. 16 domains). The results are presented in Table 3.2. The columns *GG* give the interface and interior imbalance of unmodified SCOTCH with  $\text{bal} = 10\%$ . Other columns only give a percentage relative to the corresponding *GG* column. For example, for the matrix *ecology1* (16), double greedy graph growing (denoted by the *DG* column) achieves a halo imbalance 62,9% better than unmodified *GG*, that is a halo imbalance of  $(1 - 0.629) \times 564 \simeq 209$ . The column *GG\** refers to a modified SCOTCH with a balance depending on the level (see introduction of this section). For each criterion, we highlighted in bold the best result.

We can see that interface balancing of *DG* is much better than unmodified *GG* and *GG\** for all but two matrices. The gain can be up to 78,5% on matrix *MHD* (22), with an average of 40% over all matrices. *DG* also achieves a better interior balancing in general compared to *GG*, on all but two matrices; the average gain for this column is 45%. It is also better than *GG\** on one third of the test cases, which is rather good since it has one more criterion to optimize. Moreover, we can see that on all but one of the industrial matrices (which are of particular interest for us), gains are very good on both criteria.

## Halo-first Greedy Graph Growing

In the previous section, we have studied an algorithm that constructs a separator for the parts and for the halo at once. This gives priority to minimizing the separator, while trying to balance the halo when possible. In this section, we review another approach, which consists in finding a halo separator first. Once this is done, we construct a separator for the whole graph, making the parts grow from the parts induced by this halo separator.

Before splitting the graph of the halo, we first have to build the graph. We could take the graph  $(V_h = \overline{V}, E_h = E \cap (V_h \times V_h))$ , defined by the restriction of the whole graph to the halo vertices and the edges connecting them. Nevertheless, this graph may not be connected, even if the whole graph is. In the worst case, it can be totally disconnected, and considering the far-away neighbourhood may not be

---

**Algorithm 9:** DoubleGreedyGraphGrowing

---

**Input:** graph  $G = (V, E)$ , number of passes  $passnbr$

**Output:** partition  $(P_0, S, P_1)$  of  $V$  such as  $S$  is a (small) separator,  $|P_0| \approx |P_1|$  and  $|\overline{P_0}| \approx |\overline{P_1}|$   
 $(P_0^*, S^*, P_1^*) \leftarrow (\emptyset, V, \emptyset)$ ;

**for**  $p = 1$  **to**  $passnbr$  **do**

$(w_0, w_1) \leftarrow RandomSeeds(V)$  ;

$ctrlpts_0 \leftarrow \{w_0\}, ctrlpts_1 \leftarrow \{w_1\}$ ;

$success \leftarrow false$ ;

**for**  $q = 1$  **to**  $triesnb$  **do**

$P_0, P_1 \leftarrow \emptyset$ ;

$S_0 \leftarrow \{w_0\}, S_1 \leftarrow \{w_1\}$ ;

$ctrldist \leftarrow computeDistances(G, ctrlpts_0, ctrlpts_1)$ ;

**while**  $V \setminus (P_0 \cup P_1) \neq \emptyset$  **do**

**if**  $|P_0| < |P_1|$  **then**

$i \leftarrow 0$ ;

**else**

$i \leftarrow 1$ ;

**if**  $S_i = \emptyset$  **then**

$break$ ;

$v \leftarrow getVertex(S_i, ctrldist)$  ;

$S_i \leftarrow S_i \setminus \{v\} \cup \{j | (v, j) \in E \text{ and } j \in V \setminus (P_0 \cup P_1)\}$  ;

$P_i \leftarrow P_i \cup \{v\}$  ;

**if**  $|V \setminus (P_0 \cup P_1)| \leq 0.1|V|$  **then**

$P_{\neg i} \leftarrow V \cup P_i$ ;

$success \leftarrow true$ ;

$break$ ;

**else**

$ctrlpts_i \leftarrow ctrlpts_i \cup findNewControlPoint(G, P_i, P_{\neg i})$ ;

**if**  $success$  **then**

$S \leftarrow MinVertexCover(E \cap (P_0 \times P_1))$ ;

$P_0 \leftarrow P_0 \setminus S, P_1 \leftarrow P_1 \setminus S$ ;

**if**  $(P_0, S, P_1)$  is better than  $(P_0^*, S^*, P_1^*)$  **then**

$(P_0^*, S^*, P_1^*) \leftarrow (P_0, S, P_1)$ ;

**return**  $(P_0^*, S^*, P_1^*)$ ;

---

Table 3.2: Results with double greedy graph growing compared to Scotch greedy graph growing

id	interface imbalance			interior imbalance		
	<i>GG</i>	% <i>GG</i> *	% <i>DG</i>	<i>GG</i>	% <i>GG</i> *	% <i>DG</i>
1	297	7,4	<b>-19,2</b>	1311	<b>-69,1</b>	-23,3
2	1112	1,6	<b>-40,0</b>	4678	<b>-66,5</b>	-78,9
3	522	-11,3	<b>-39,7</b>	1635	<b>-13,9</b>	-13,0
4	244	-9,0	<b>-11,5</b>	1568	-23,7	<b>-31,1</b>
5	475	<b>-17,9</b>	-3,8	4605	<b>-85,6</b>	-62,3
6	869	-21,3	<b>-41,3</b>	4107	<b>-78,5</b>	-49,6
7	<b>905</b>	49,4	26,4	4942	<b>-69,1</b>	-63,7
8	261	0,0	<b>-46,7</b>	420	<b>0,0</b>	79,8
9	365	-3,8	<b>-44,9</b>	8128	<b>-82,8</b>	-65,2
10	1002	14,0	<b>-32,1</b>	4852	<b>-73,2</b>	-44,6
11	509	-3,7	<b>-44,4</b>	2831	<b>-84,1</b>	27,5
12	569	-25,0	<b>-59,1</b>	22416	<b>-79,5</b>	-67,5
13	532	-11,8	<b>-58,5</b>	12049	<b>-69,0</b>	-49,5
14	756	-23,1	<b>-46,3</b>	17458	-61,9	<b>-66,6</b>
15	6678	6,6	<b>-29,8</b>	35466	<b>-73,9</b>	-68,4
16	564	-11,9	<b>-62,9</b>	15092	<b>-65,5</b>	-58,0
17	2130	18,6	<b>-50,4</b>	32202	<b>-72,9</b>	-67,7
18	335	17,0	<b>-19,7</b>	28057	<b>-70,1</b>	-64,9
19	2604	-16,4	<b>-42,0</b>	25853	<b>-66,5</b>	-59,5
20	9990	-14,2	<b>-25,8</b>	73635	<b>-80,7</b>	-16,5
<b>21</b>	927	0,6	<b>-40,9</b>	2377	-58,6	<b>-59,5</b>
<b>22</b>	3468	5,0	<b>-78,5</b>	<b>3336</b>	4,3	18,2
<b>23</b>	1869	7,1	<b>-3,2</b>	14424	<b>-73,3</b>	-64,4
<b>24</b>	2460	-9,1	<b>-73,4</b>	8940	-44,1	<b>-60,6</b>
<b>25</b>	6837	-11,6	<b>-69,7</b>	26877	-63,0	<b>-68,9</b>
<b>26</b>	780	-15,9	<b>-53,8</b>	24987	-58,3	<b>-65,2</b>
<b>27</b>	6168	-27,5	<b>-68,4</b>	67721	-68,7	<b>-76,2</b>
<b>28</b>	4344	-15,6	<b>-41,4</b>	240729	-76,9	<b>-77,1</b>
<b>29</b>	11539	8,6	<b>-51,3</b>	244959	-73,9	<b>-77,2</b>
<b>30</b>	9936	-6,9	<b>-52,0</b>	286992	<b>-72,6</b>	-8,5

enough to reconnect it. However, it is important to take graph connections into account because choosing which of the halo vertices will be in each part at random would often lead to a very poor separator of the whole graph.

To deal with this issue, we use the following algorithm to build a graph containing all relevant information about the halo vertices. A partition of the halo vertices is maintained. At the beginning, each halo vertex is in a different set of the partition, and a set  $V'_h$  is initialized with all halo vertices. Then, we make simultaneous breadth-first searches from all the sets of the partition. When two search bubbles corresponding to different sets meet, this means a shortest-path between any two sets of the partition has been found. All vertices of this path are added to  $V'_h$ . The sets which have met are merged, and the breadth-first-search is continued. The process stops when either all sets of the partition have merged - meaning the graph is connected -, or all breadth-first searches have finished. Finally, the graph of the halo is defined by  $(V'_h, E'_h = E \cap (V'_h \times V'_h))$ . Ignoring the time for partition managing operations (which is almost constant), the complexity to build the halo graph is equivalent to a single global breadth-first search, that is  $\Theta(|V| + |E|)$ .

Now, let *buildConnectedHalo* be a function building such a graph  $(V'_h, E'_h)$ . Algorithm 10 gives the main steps to find a separator. A first greedy graph growing algorithm is performed to compute a cut of the halo  $(V'_{h0}, S'_h, V'_{h1})$ . Next, a kind of double greedy graph growing is done, beginning with the set of seed  $V'_{h0}$  for part 0, and  $V'_{h1}$  for part 1. Finally, we get a partition  $(P_0, S, P_1)$ . As in the other algorithms, these steps can be repeated, doing several passes and keeping the best one.

---

**Algorithm 10:** HaloFirstGreedyGraphGrowing

---

**Input:** graph  $G = (V, E)$ , number of passes *passnbr*

**Output:** partition  $(P_0, S, P_1)$  of  $V$  such as  $S$  is a (small) separator,  $|P_0| \approx |P_1|$  and  $|\overline{P_0}| \approx |\overline{P_1}|$

$(P_0^*, S^*, P_1^*) \leftarrow (\emptyset, V, \emptyset);$

$(V'_h, E'_h) \leftarrow \text{buildConnectedHalo}(V, E, V_h);$

**for**  $p = 1$  **to** *passnbr* **do**

$(V'_{h0}, S'_h, V'_{h1}) \leftarrow \text{greedyGraphGrowing}(V'_h, E'_h);$

$(P_0, S, P_1) \leftarrow \text{doubleGreedyGraphGrowing}(V, E, V'_{h0}, V'_{h1});$

**if**  $(P_0, S, P_1)$  *is better than*  $(P_0^*, S^*, P_1^*)$  **then**

$(P_0^*, S^*, P_1^*) \leftarrow (P_0, S, P_1);$

**return**  $(P_0^*, S^*, P_1^*);$

---

We have applied the same testing protocol as in the previous subsection 3.2.2. The results are shown in Table 3.3 where the column *HF* refers to the halo-first greedy graph growing algorithm. A sign has been added to the right of each column of *HF*: a '+' means that this gain is better (i.e. smaller) than the corresponding *DG* gain and a '-' that *DG* is better.

On the interface criterion, the *HF* approach is better than unmodified *GG* and *GG\** in all but four matrices. The worst case is the *turon\_m* (4), but this apparent failure is due to the fact that *GG* performs very well on this matrix: the interface imbalance is only 244 for 189924 vertices. Globally, the average gain of *HF* over unmodified *GG* on interface imbalance is 38%, with a maximum of 75,4%; this is almost as good as *DG*. If we compare gains of *HF* over *DG* on this criteria, we have 16 '+' out of 30, which confirms this tendency.

Moreover, *HF* achieves gains on the interior imbalance in all but one matrix. On average, interior imbalance gain of *HF* is 56%. This is about 10% better than *DG*, and if gains are compared one by one, *HF* beats *DG* on two thirds of the matrices. *DG* is not obsolete however: for instance, on matrix *ultrasound* (24), *DG* performs better than *HF* on both criteria.

### 3.2.3 Experimental Results

In order to see what are the characteristics of *GG*, *DG* and *HF*, we drew the partitioning performed by these algorithms on 16 domains on a small mesh called *darcy003*, without the multilevel framework. Figure 3.9 gives the results obtained. It can be seen that *GG* makes domains with irregular shapes,

Table 3.3: Results with halo first greedy graph growing compared to Scotch greedy graph growing

id	interface imbalance			interior imbalance		
	<i>GG</i>	% <i>GG</i> *	% <i>HF</i>	<i>GG</i>	% <i>GG</i> *	% <i>HF</i>
1	297	7,4	<b>-29,3</b> +	1311	-69,1	<b>-73,5</b> +
2	1112	1,6	<b>-34,9</b> -	4678	-66,5	<b>-74,2</b> -
3	522	-11,3	<b>-63,4</b> +	1635	<b>-13,9</b>	-7,2 -
4	244	<b>-9,0</b>	103,3 -	1568	-23,7	<b>-24,5</b> -
5	475	-17,9	<b>-26,7</b> +	4605	<b>-85,6</b>	-74,3 +
6	869	-21,3	<b>-48,2</b> +	4107	<b>-78,5</b>	-65,6 +
7	905	49,4	<b>-24,2</b> +	4942	-69,1	<b>-72,2</b> +
8	261	0,0	<b>-69,0</b> +	420	0,0	<b>-11,4</b> +
9	365	-3,8	<b>-41,4</b> -	8128	<b>-82,8</b>	-69,2 +
10	1002	14,0	<b>-66,9</b> +	4852	<b>-73,2</b>	-47,5 +
11	509	-3,7	<b>-50,3</b> +	2831	<b>-84,1</b>	-19,1 +
12	569	-25,0	<b>-70,1</b> +	22416	<b>-79,5</b>	-72,9 +
13	532	-11,8	<b>-37,0</b> -	12049	<b>-69,0</b>	-52,3 +
14	756	<b>-23,1</b>	-20,4 -	17458	-61,9	<b>-67,2</b> +
15	6678	6,6	<b>-22,4</b> -	35466	<b>-73,9</b>	-68,2 -
16	564	-11,9	<b>-54,4</b> -	15092	<b>-65,5</b>	-59,2 +
17	2130	18,6	<b>-44,8</b> -	32202	-72,9	<b>-73,0</b> +
18	<b>335</b>	17,0	14,6 -	28057	<b>-70,1</b>	-68,3 +
19	2604	<b>-16,4</b>	-15,8 -	25853	<b>-66,5</b>	-49,7 -
20	9990	-14,2	<b>-55,4</b> +	73635	<b>-80,7</b>	-79,6 +
21	927	0,6	<b>-49,4</b> +	2377	-58,6	<b>-64,5</b> +
22	3468	5,0	<b>-75,4</b> -	<b>3336</b>	4,3	16,1 +
23	1869	7,1	<b>-24,2</b> +	14424	<b>-73,3</b>	-72,0 +
24	2460	-9,1	<b>-55,9</b> -	8940	-44,1	<b>-51,5</b> -
25	6837	-11,6	<b>-65,5</b> -	26877	-63,0	<b>-80,3</b> +
26	780	-15,9	<b>-33,6</b> -	24987	-58,3	<b>-66,0</b> +
27	6168	-27,5	<b>-73,6</b> +	67721	-68,7	<b>-74,5</b> -
28	4344	-15,6	<b>-47,9</b> +	240729	<b>-76,9</b>	-73,2 -
29	11539	8,6	<b>-57,0</b> +	244959	<b>-73,9</b>	-70,9 -
30	9936	-6,9	<b>-55,9</b> +	286992	<b>-72,6</b>	-71,4 +

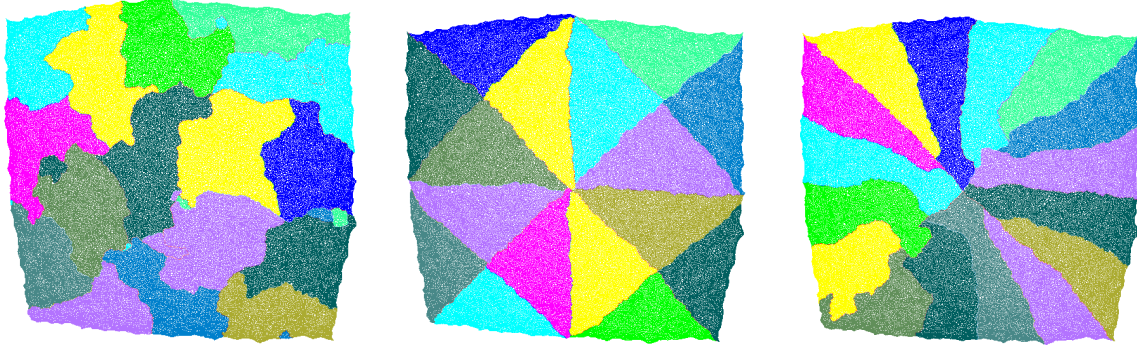


Figure 3.9: Partitioning of the graph of matrix `darcy003` in 16 domains with SCOTCH. From left to right, the method applied was greedy graph growing, double greedy graph growing and halo-first greedy graph growing.

leading to an interface imbalance of 224. On the contrary, *DG* performs better on this example, getting 16 triangular-shaped domains. The halo imbalance of 151 comes from the fact that the eight triangles in the center have their three edges touching other domains, whereas the eight on the corners have one edge on the border, touching no other domain. Finally, *HF* is the best with a halo imbalance of 145. To achieve that, it builds some kind of long-shaped domains around the "center" of the mesh.

We now present a complementary study with a variable number of domains. As previously said in the introduction, we are interested in domain decomposition for a hybrid solver where each domain will be factorized in parallel with the others. Each single factorization will be performed with a direct solver which can be parallel itself. So, we can exploit *two* levels of parallelism and thus we can afford to use larger domains. This is interesting when solving ill-conditioned linear systems for which too many domains often leads to bad convergence. For these reasons, we target a number of domains which is not too high, typically between 64 and 512.

Results are reported in Tables 3.4, 3.5 and 3.6. For this study, we focus on the three largest matrices in our pool: `Almond` (28), `NICE-7` (29) and `10millions` (30). The column *dom* gives the number of domains in which the graph was split. First, we can see that, in almost all configurations, one of our strategies outperforms *GG\**, and if not, at least one of them is very close. We remark that on more than 16 domains, double *DG* sometimes does not always work well: on the matrix `10millions` (30), both its interface and interior imbalance are worse than the original *GG*. *HF* provides better results, with significant gains on both criteria on most cases. In particular, it is the best (or very close to it) for 512 domains on all three matrices on both criteria. Thus, we think that for a large number of domains, *HF* should be favoured. However, in the context of parallel partitioning, one can consider trying both approaches and taking the best of *DG* and *HF*.

Table 3.4: Results of *DG* and *HF* with different numbers of domains, compared to Scotch greedy graph growing, for matrix `Almond`

dom	interface imbalance				interior imbalance			
	<i>GG</i>	% <i>GG*</i>	% <i>DG</i>	% <i>HF</i>	<i>GG</i>	% <i>GG*</i>	% <i>DG</i>	% <i>HF</i>
16	4344	-15,6	-41,4	<b>-47,9</b>	240729	-76,9	<b>-77,1</b>	-73,2
32	3179	<b>-34,8</b>	-31,5	-0,5	133886	-73,8	<b>-80,1</b>	-76,9
64	2258	-5,8	<b>-47,6</b>	-17,8	83819	<b>-80,5</b>	-79,2	-79,1
128	1822	-29,5	<b>-42,9</b>	-32,6	48087	-78,4	-77,6	<b>-80,9</b>
256	1071	-2,2	<b>-44,4</b>	2,5	27695	-81,6	-77,9	<b>-83,0</b>
512	910	0,8	-17,1	<b>-22,3</b>	16243	-83,8	-80,0	<b>-84,7</b>

Table 3.5: Results of  $DG$  and  $HF$  with different numbers of domains, compared to Scotch greedy graph growing, for matrix NICE-7

dom	interface imbalance				interior imbalance			
	$GG$	% $GG^*$	% $DG$	% $HF$	$GG$	% $GG^*$	% $DG$	% $HF$
16	11539	8,6	-51,3	<b>-57,0</b>	244959	-73,9	<b>-77,2</b>	-70,9
32	10991	-26,3	<b>-45,7</b>	-38,5	188834	-80,3	-81,0	<b>-81,6</b>
64	8997	-27,5	40,7	<b>-30,8</b>	101838	-75,9	-6,6	<b>-80,2</b>
128	5694	-14,4	11,7	<b>-26,9</b>	66792	-83,9	-1,9	<b>-84,3</b>
256	4554	-3,2	<b>-33,1</b>	-27,6	34314	-77,4	7,3	<b>-82,4</b>
512	3762	-16,7	-30,8	<b>-33,1</b>	19734	-79,1	-6,3	<b>-84,2</b>

Table 3.6: Results of  $DG$  and  $HF$  with different numbers of domains, compared to Scotch greedy graph growing, for matrix 10millions

dom	interface imbalance				interior imbalance			
	$GG$	% $GG^*$	% $DG$	% $HF$	$GG$	% $GG^*$	% $DG$	% $HF$
16	9936	-6,9	-52,0	<b>-55,9</b>	286992	<b>-72,6</b>	-8,5	-71,4
32	6666	-0,5	43,7	<b>-56,6</b>	188900	-69,5	13,0	<b>-77,7</b>
64	7036	-13,3	<b>-47,4</b>	-31,1	125444	-76,9	-18,8	<b>-78,4</b>
128	4564	-11,2	4,0	<b>-48,7</b>	79754	<b>-82,9</b>	-52,9	-78,8
256	3114	-6,2	163,5	<b>-32,5</b>	42931	-79,5	-30,2	<b>-80,8</b>
512	2336	-19,5	22,2	<b>-54,2</b>	25800	<b>-83,5</b>	49,3	-83,4

## Chapter 4

# Towards $\mathcal{H}$ -matrices in sparse direct solvers

This chapter presents the work that is currently developed in the PhD thesis of Grégoire Pichon that I co-advise. The first part of this chapter have been published in [120] and the second part in [119].

Please look at [http://www.labri.fr/perso/ramet/restricted/HDR\\_SIMAX17.pdf](http://www.labri.fr/perso/ramet/restricted/HDR_SIMAX17.pdf) and also at [http://www.labri.fr/perso/ramet/restricted/HDR\\_PDSEC17.pdf](http://www.labri.fr/perso/ramet/restricted/HDR_PDSEC17.pdf) for a full version of this work with some experiments.

### 4.1 Reordering strategy for blocking optimization

The block-symbolic factorization [38] analytically computes the block-structure of the factorized matrix from the reordering step and from a supernode partition of the unknowns. It allows the solver to create the data structure that will hold the final matrix instead of allocating it at runtime. The goal of this step is also to block the data in order to efficiently apply matrix-matrix operations, also known as BLAS Level 3, on those blocks instead of scalar operations. For this purpose, extra fill-in, and by extent extra computations, might be added in order to reduce the time to solution. However, the size of these blocks might not be sufficiently large to obtain the full performance from the BLAS kernels.

Modern architectures, whether based on CPUs, GPUs, or Intel Xeon Phi may be efficient with a performance close to the theoretical peak. This can be achieved only if the data size is large enough to take advantage of caches, vector units, and provides a large ratio of computation per byte. Accelerators such as GPUs or Intel Xeon Phi require even larger blocking sizes than those for CPUs due to their particular architectural features.

In order to obtain block sizes more suited to kernel operations, we propose in this work an algorithm that reorders the unknowns of the problem to increase the average size of the off-diagonal blocks in block-symbolic factorization structures. The major feature of this solution is that, based on an existing nested dissection ordering for a given problem, our solution will keep constant the amount of fill-in generated during the factorization. Therefore, the amount of memory and computation to store and compute the factorized matrix is invariant. The consequence of this increased average size is that the number of off-diagonal blocks is significantly reduced, diminishing the memory overhead of the data structures used by the solver and the number of tasks required to compute the solution in task-based implementations.

#### 4.1.1 Intra-node reordering

Let us now illustrate the problem of current ordering solutions and how to overcome this problem. For this purpose, we consider a regular 3D cube of  $n^3$  vertices presented in Figure 4.1. We apply the nested dissection process to this cube. Naturally, the first separator, in gray, is a plane of  $n^2$  vertices cutting the cube into two halves of balanced parts. Then, by recursively applying the nested dissection process, we partition the two-halves' subparts with the two red separators, and again dissect the resulting partitions by the four third-level green separators giving us eight final partitions. We know from this process that each separator will be ordered with higher indices than those in lower levels.



Inside each separator, vertices have to be ordered as well, and it is common to use techniques such as the Reverse Cuthill-McKee [54] (RCM) algorithm in order to have an internal separator ordering “as contiguous as possible” to limit the number of off-diagonal blocks in the associated column block. This strategy works with only the local graph induced by the separator. It starts from a peripheral vertex and orders, consecutively, vertices at distance 1, then at distance 2, and so on, giving indices in reverse order. It is close to a Breadth-First Search (BFS) algorithm. However, such an algorithm uses only interactions within a supernode, without taking into account contributing supernodes. On the quotient graph, it means that this will reorder unknowns inside a node of this graph without considering interactions with other nodes of this graph. However, these interactions are those related to off-diagonal blocks in the factorized matrix. Therefore, it is important to note that the ordering inside a supernode can be rearranged to take into account interactions with vertices outside its local graph without changing the final fill-in of the  $L$  block-structure used by the solver. Then, we can expect that complete knowledge of the local graph and of its outer interactions will lead to a better quality ordering in terms of the number of off-diagonal blocks.

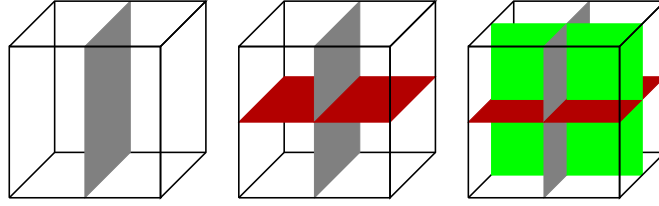


Figure 4.1: Three-levels of nested dissection on a regular cube.

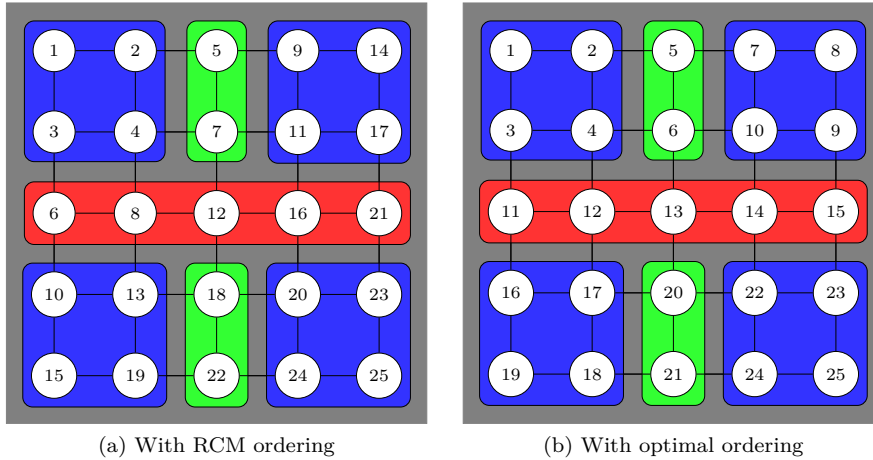


Figure 4.2: Projection of contributing supernodes and ordering on the first separator (gray in Figure 4.1).

Figure 4.2 presents the vertices of the gray separator from the 3D cube case with  $n = 5$ . The projection of contributing supernodes on this separator is shown. The blue parts are the vertices connected only to the leaves of the elimination tree. Thanks to the nested dissection process, the nodes of the gray separator have the largest numbers and their connections to other supernodes represent the off-diagonal contributions. Based on this, we propose an optimal ordering, in Figure 4.2b, computed by hand, as opposed to an RCM algorithm, in Figure 4.2a. One can note that RCM will not order, consecutively, vertices that will receive contributions from the same supernodes, leading to a substantially larger number of off-diagonal blocks than the optimal solution. For instance, the four blue vertices in the top right of the RCM ordering will create four different off-diagonal blocks. The general idea is that some projections will be cut by RCM following the neighborhood, while those vertices could have been ordered together to reduce the number of off-diagonal blocks. On the right, the optimal ordering tries to consider this rule by ordering vertices with similar connections in a contiguous manner. This leads to a smaller number of

off-diagonal blocks as shown in the block-data structure computed by the block-symbolic factorization for these two orderings in Figures 4.3a and 4.3b.

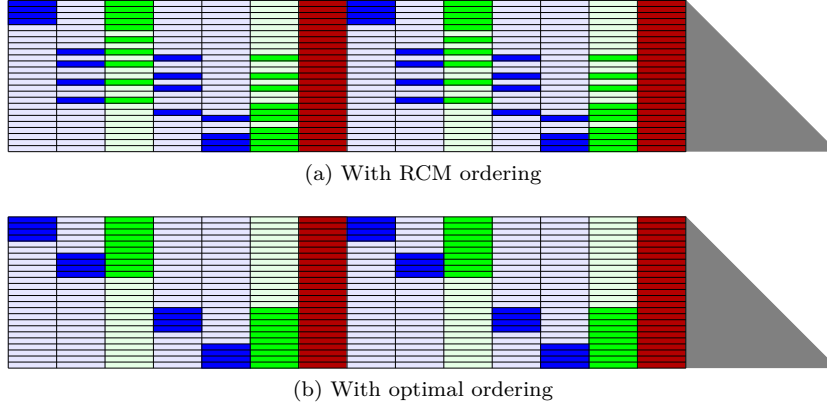


Figure 4.3: Off-diagonal blocks contributing to the first separator in Figure 4.1.

We have demonstrated with this simple example that RCM does not fulfill the correct objective in a more global view of the problem. This is especially true in the context of 3D graphs, where the separator is a 2D structure, receiving contributions from 3D structures on both sides. With 2D graphs, the separator is a 1D structure and in such a case, RCM will generally provide a good solution by following the neighborhood in the BFS algorithm. However, it often happens that the separators found by generic tools such as SCOTCH or METIS are disconnected making this previous statement incorrect.

Note that if it is quite easy to manually compute the optimal ordering on our example, it is harder in practice. Indeed, given an initial partition  $V = A \cup B \cup C$ , nothing guarantees that subparts  $A$  and  $B$  will be partitioned in a similar fashion, and that the resulting projection will match. For instance, Figure 4.4 presents the projection of level-1 (in red) and level-2 (in green) supernodes on the first separator of a  $40 \times 40 \times 40$  Laplacian partitioned with SCOTCH. One can note that there are crossed contributions, meaning that subparts  $A$  and  $B$  are partitioned differently.

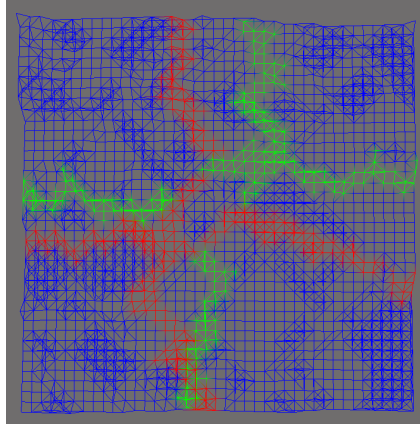


Figure 4.4: Projection of contributing supernodes on the first separator of a 3D Laplacian of size  $40 \times 40 \times 40$ , using SCOTCH.

In the next section, we propose a new reordering strategy that permutes the rows to reduce the off-diagonal information. Note that such a reordering strategy will not impact the global fill-in as long as the diagonal blocks are considered as dense blocks. The first solution that appears in Figure 4.4 would be to cluster vertices by common connections to nodes of the quotient graph. However, in most cases, that would result in clusters of  $O(1)$  size that would still need to be ordered correctly, taking into account their level in the elimination tree of the connected supernodes. The solution we propose to remedy this problem relies on the computed block-data structure. Our objective is to express an algorithm providing the optimal solution before proposing a heuristic with reasonable complexity.

### 4.1.2 Related work

Studying the structure of off-diagonal blocks was used in different contexts. In [55], the purpose was to reduce the overhead associated with each single off-diagonal block. The authors proposed a reordering strategy that refines the ordering provided by the minimum degree algorithm. Their experiments have been applied to 2D graphs and successfully reduce the number of off-diagonal blocks. However, the authors did not provide a theoretical study of their reordering algorithm and their solution did not apply in the context of 3D graphs. In [134], the authors introduce reordering in the context of a multifrontal solver. A front is ordered according to its two sons (in the nested dissection process), starting with the largest son, in order to limit the scatter operation when updating the front with the son's contributions. A similar approach was studied in [131] for the MUMPS solver, to reorder blocks in order to reduce the communication volume induced by the fronts in a distributed context.

### 4.1.3 Improving the blocking size

As presented in section 4.1.1, the RCM algorithm – widely used to order supernodes – generates many extra diagonal blocks by not considering supernode interactions, which leads to an increased number of less efficient block operations. In this section, we present an algorithm that reorders supernodes using a global view of the nested dissection partition. We expect that considering contributing supernodes will lead to a better quality — a smaller number of larger blocks. Our proposition is to consider the set of contributions for each line of a supernode, before using a distance metric to minimize the creation of off-diagonal blocks when permuting lines.

#### Problem modeling

The main idea is to rely on the block-symbolic factorization of  $L$  instead of the original graph of  $A$ . Indeed, it allows us to take into account fill-in elements that were computed in the block-symbolic factorization process instead of re-computing those elements with the matrix graph. Let us consider the  $\ell^{th}$  diagonal block  $C_\ell$  of the factorized matrix that corresponds to a supernode, and the set of supernodes  $C_k$  with  $k < \ell$  corresponding to the supernodes in levels of the elimination tree lower than  $C_\ell$ . Note that we refer to  $N$  as the total number of diagonal blocks appearing in the structure of the factorized matrix, as opposed to  $n$  for the total number of unknowns.

We define for each supernode  $C_\ell$ :

$$row_{ik}^\ell = \begin{cases} 1 & \text{if vertex } i \text{ from } C_\ell \text{ is connected to } C_k \\ 0 & \text{otherwise} \end{cases}, k \in \llbracket 1, \ell - 1 \rrbracket, i \in \llbracket 1, |C_\ell| \rrbracket. \quad (4.1)$$

$row_{ik}^\ell$  is then equal to 1 when the vertex  $i$ , or row  $i$ , of the supernode  $C_\ell$  is connected to any vertex of the supernode  $k$  belonging to a lower level in the elimination tree. It is equal to 0, if not, meaning that no nonzero element connects the two in the initial matrix, or no fill-in will create that connection. Let's now define for each vertex the set  $B_i^\ell = (row_{ik}^\ell)_{k \in \llbracket 1, \ell - 1 \rrbracket}$ . We can then define  $w_i^\ell$ , the weight of a row  $i$ , as in equation (4.2), that represents the number of supernodes contributing to that row  $i$ , and the distance between two rows  $i$  and  $j$ ,  $d_{i,j}^\ell$ , as in equation (4.3). It is known as the Hamming distance [66] between two binary vectors, and allows for measuring the number of off-diagonal blocks induced by the succession of two rows  $i$  and  $j$ . Indeed,  $d_{i,j}^\ell$  represents the number of off-diagonal blocks that belongs to only one of the two rows, which can be seen as the number of blocks that end at row  $i$  or start at row  $j$ .

$$w_i^\ell = \sum_{k=1}^{\ell-1} row_{ik}^\ell, \quad (4.2)$$

$$d_{i,j}^\ell = d(B_i^\ell, B_j^\ell) = \sum_{k=1}^{\ell-1} row_{ik}^\ell \oplus row_{jk}^\ell, \quad (4.3)$$

where  $\oplus$  is the exclusive **or** operation.

Thus, the total number of off-diagonal blocks,  $odb^\ell$ , contributing to the diagonal block  $C_\ell$  can be defined as:

$$odb^\ell = \frac{1}{2}(w_1^\ell + \sum_{i=1}^{|C_\ell|-1} d_{i,i+1}^\ell + w_{|C_\ell|}^\ell), \quad (4.4)$$

where the Hamming weights of the first and last row of the supernode  $C_\ell$  correspond respectively to the number of blocks in the first row and in the last one, and the distances between two consecutive rows gives the evolution in the number of blocks when traveling through them.

Then, to reduce the total number of off-diagonal blocks in the final structure, the goal is to minimize this metric  $odb^\ell$  for each supernode, by computing a minimal path visiting each node, with a constraint on the first and the last node. This problem is known as the Shortest Hamiltonian Path Problem, and is an NP-hard problem.

### Proposed heuristic

We first propose to introduce an extra fictitious vertex,  $S_0$ , for which  $B_0$  is the null set. Thus, we have:

$$\forall i \in \llbracket 1, |C_\ell| \rrbracket, d_{0,i} = d_{i,0} = w_i, \quad (4.5)$$

The problem can now be transformed into a Travelling Salesman Problem [17] (TSP):

$$\sum_{i=0}^{|C_\ell|} d_{i,(i+1)}^\ell, \quad (4.6)$$

which is also an NP-Hard problem, but for which many heuristics have been proposed in the literature [84], contrary to the Shortest Hamiltonian Path Problem. Furthermore, our problem presents properties that make it compatible for better heuristics and theoretical models that guarantee the maximum distance to the optimal solution. Firstly, our problem is symmetric because:

$$d_{ij}^\ell = d_{ji}^\ell, \forall (i, j) \in \llbracket 1, |C_\ell| \rrbracket^2, \quad (4.7)$$

and secondly, it respects the triangular inequality:

$$d_{ij}^\ell \leq d_{ik}^\ell + d_{kj}^\ell, \forall (i, j, k) \in \llbracket 1, |C_\ell| \rrbracket^3. \quad (4.8)$$

This means our problem is an Euclidean TSP, and so heuristics for this specific case can be used.

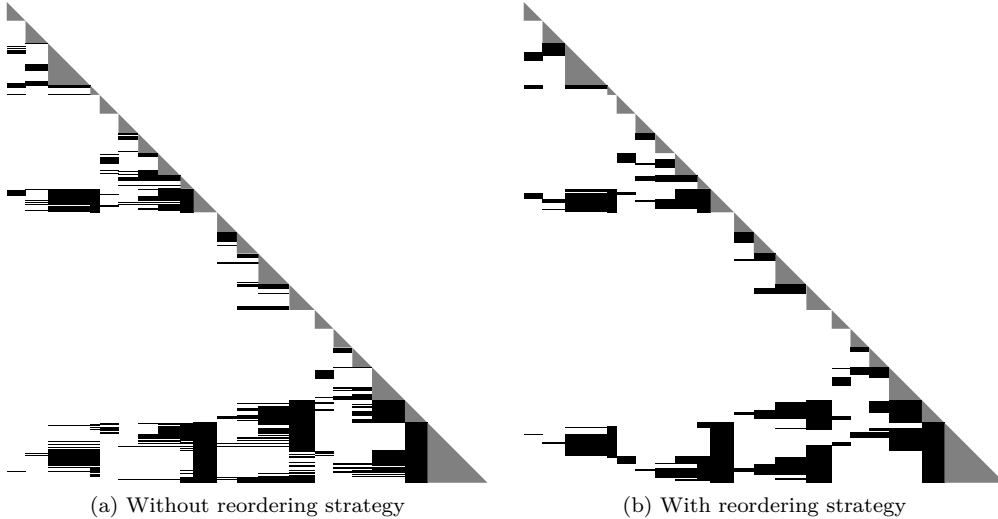


Figure 4.5: Block-symbolic factorization of  $8 \times 8 \times 8$  Laplacian initially reordered with SCOTCH.

Figure 4.5 presents the block-symbolic factorization of a 3D Laplacian of size  $8 \times 8 \times 8$  reordered with the SCOTCH nested dissection algorithm. In Figure 4.5a, our reordering algorithm has not been applied,

and supernodes ordering comes only from the local RCM applied by SCOTCH. One can notice that some rows can be easily aggregated to reduce the number of off-diagonal blocks. In Figure 4.5b, our algorithm has to reorder unknowns within each supernode. The final structure exhibits more compact blocks that are larger. Note that the fill-in of the matrix has not changed due to the dense storage of the diagonal blocks. Our algorithm does not impact the fill-in outside those diagonal blocks.

## 4.2 On the use of low rank approximations in PASTIX

In the context of sparse direct solvers, some recent work has investigated the low-rank representations of dense blocks appearing during the sparse matrix factorization, by compressing blocks through many possible compression formats such as Block Low-Rank (BLR),  $\mathcal{H}$ ,  $\mathcal{H}^2$ , HSS, HODLR... These different approaches allow a reduction of the memory requirement and/or the time to solution. Depending on the compression strategy, solvers require knowledge of the underlying geometry to tackle the problem or can do it in a purely algebraic fashion.

Hackbusch [65] introduced the  $\mathcal{H}$ -LU factorization for dense matrices, which compresses the matrix into a hierarchical matrix before applying low-rank operations instead of classic dense operations. In the same paper, an extension of the dense version was designed for sparse matrices using a nested dissection ordering. In [61],  $\mathcal{H}$ -LU factorization is used in an algebraic context. Performance, as well as a comparison of  $\mathcal{H}$ -LU with some sparse direct solvers is presented in [62]. Kriemann [93] implemented this algorithm using Directed Acyclic Graphs.

The Hierarchically Off-Diagonal Low-Rank (HODLR) compression technique was used in a multi-frontal sparse direct solver in [12] to accelerate the elimination of large fronts. It was fully extended for a sparse purpose in [13] and uses Boundary Distance Low-Rank (BDLR) to allow both time and memory savings. A supernodal solver using a compression technique similar to HODLR was presented in [33]. The proposed approach allows memory savings and can be faster than standard preconditioned techniques. However, it is slower than the direct approach in the benchmarks and requires an estimation of the rank to use randomized techniques and accelerate the solver.

There has been different work around the use of Hierarchically Semi-Separable (HSS) matrices in sparse direct solvers. In [143], Xia et al. presented a solver for 2D geometric problems, where all operations are realized algebraically. In [141], a geometric solver was developed, but contribution blocks are not compressed, making memory savings impossible. [57] proposed an algebraic code that uses randomized sampling to manage low-rank blocks and to allow memory savings.

$\mathcal{H}^2$  arithmetic has also been applied to sparse solvers. In [122], a fast sparse  $\mathcal{H}^2$  solver, called LoRaSp, based on extended sparsification was introduced. In [146], a variant of LoRaSp, aimed at improving the quality of the solver when used as a preconditioner, was presented, as well as a numerical analysis of the convergence with  $\mathcal{H}^2$  preconditioning. In particular, this variant was shown to lead to a bounded number of iterations irrespective of problem size and condition number (under certain assumptions). In [79] a fast sparse solver was introduced based on interpolative decomposition and skeletonization. It was optimized for meshes that are perturbations of a structured grid. In [135], an  $\mathcal{H}^2$  sparse algorithm was described. It is similar in many respects to [122], and extends the work of [79]. All these solvers have a guaranteed linear complexity, for a given error tolerance, and assuming a bounded rank for all well-separated pairs of clusters (the admissibility criterion in Hackbusch et al.'s terminology).

Block Low-Rank compression has also been investigated for dense matrices [14], and for sparse linear systems when using a multifrontal method [9]. Considering that these approaches are close to the current study, a detailed comparison will be described in Section 4.2.4.

The first objective of this work is to combine a generic sparse direct solver with recent work on matrix compression to come up with a way to solve larger problems, overcoming the memory limitations and accelerating the time-to-solution. The second objective is to keep the black-box algebraic approach of sparse direct solvers, by relying on methods that are independent of the underlying problem geometry. In this paper, we consider the multi-threaded sparse direct solver PASTIX [75] and we introduce a BLR compression strategy to reduce its memory and computational cost. We developed two strategies: *Minimal Memory*, which focuses on reducing the memory consumption, and *Just-In-Time* which focuses on reducing the time-to-solution (factorization and solve steps).

During the factorization, the first strategy compresses the sparse matrix from the beginning and exploits complicated low-rank numerical operations to keep the memory cost of the factorized matrix

as low as possible. The second one compresses the information as late as possible to avoid the cost of low-rank update operations. The resulting solver can be used either as a direct solver for low accuracy solutions or as a high-accuracy preconditioner for iterative methods, requiring only a few iterations to reach machine precision.

The two strategies, introduced in PASTIX, are then presented in Section 4.2.1, before describing in detail the low-rank kernels in Section 4.2.2. In Section 4.2.3, we perform experiments comparing the two BLR strategies with the original approach — that uses only dense blocks — in terms of memory consumption, time-to-solution and numerical behavior. Section 4.2.4 surveys in more details related work on BLR for dense and/or sparse direct solvers, highlighting the differences with our approach, before discussing how to extend this work to a hierarchical format ( $\mathcal{H}$ , HSS, HODLR...).

### 4.2.1 Block Low-Rank solver

In this section, we describe the main contribution of this work which is a BLR solver developed within the PASTIX library. First we introduce the notation and the basics used to integrate low-rank blocks in the solver. Then, using the newly introduced structure, we describe two different strategies leading to a sparse direct solver that optimizes the memory consumption or the time-to-solution.

#### Notation

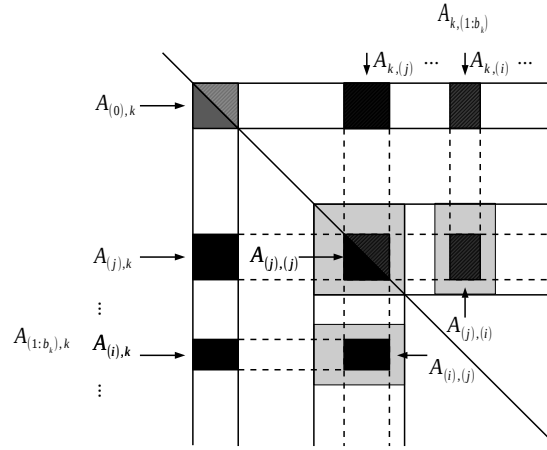


Figure 4.6: Symbolic block structure and notation used for the algorithms for one column block  $k$ , and its associated blocks.

Let us consider the symbolic block structure of a factorized matrix  $L$ , obtained through the symbolic block factorization. Initially, we allocate this structure initialized with the entries of  $A$  and perform an in-place factorization. We denote initial blocks by  $A$  and when a block corresponds to its final state, it becomes  $L$  (or  $U$ ). The matrix is composed of  $N_{cblk}$  column blocks, where each column block is associated with a supernode, or to a subset of unknowns in a supernode when the latter is split to create parallelism. Each column block  $k$  is composed of  $b_k + 1$  blocks, as presented in Figure 4.6 where:

- $A_{(0),k}(= A_{k,(0)})$  is the dense diagonal block;
- $A_{(j),k}$  is the  $j^{th}$  off-diagonal block in the column block with  $1 \leq j \leq b_k$ , ( $j$ ) being a multi-index describing the row interval of each block, and respectively,  $A_{k,(j)}$  is the  $j^{th}$  off-diagonal block in the row block;
- $A_{(1:b_k),k}$  represents all the off-diagonal blocks of the column block  $k$ , and  $A_{k,(1:b_k)}$  all the off-diagonal blocks of the symmetric row block;
- $A_{(i),(j)}$  is the rectangular dense block corresponding to the rows of the multi-index ( $i$ ) and to the columns of the multi-index ( $j$ ).

In addition, we denote by  $\hat{A}$  the compressed representation of a matrix  $A$ .

## Sparse direct solver using BLR compression

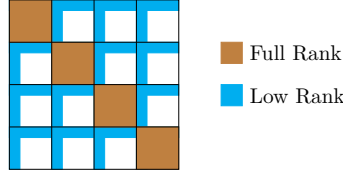


Figure 4.7: Block Low-Rank compression.

The BLR compression scheme is a flat, non-hierarchical format, unlike others mentioned in the introduction. If we consider the example of a dense matrix, the BLR format clusters the matrix into a set of smaller blocks, as presented in Figure 4.7. Diagonal blocks are kept dense and off-diagonal blocks, which represent long distance interactions in the graph, are low-rank. Thus, these off-diagonal blocks can be represented through a low-rank form  $uv^t$ , obtained with a compression technique such as Singular Value Decomposition (SVD) or Rank-Revealing QR (RRQR) factorization. Compression techniques are detailed in Section 4.2.2.

We propose in this work to similarly apply this scheme to the symbolic block structure of sparse direct solvers. First, diagonal blocks of the largest supernodes in the block elimination tree can be considered as large dense matrices which are compressible with the BLR approach. In fact, as we have seen previously, it is common to split these supernodes into a set of smaller column blocks in order to increase the level of parallelism. Thus, the block structure resulting from this operation gives the cluster of the BLR compression format. Secondly, interaction blocks from two large supernodes are by definition long distance interactions, and thus can be represented by a low-rank form. It is then natural to store them as low-rank blocks as long as they are large enough. To summarize, if we take the final symbolic block structure (after splitting) used by the PASTIX solver, all diagonal blocks are considered dense, and all off-diagonal blocks might be stored using a low-rank structure. In practice, we limit this compression to blocks of a minimal size, and all blocks with relatively high ranks are kept dense.

Relying on the original block structure, adapting the solver to block low-rank compression mainly relies on the replacement of the dense operations with the equivalent low-rank operations. Still, different variants of the final algorithm can be obtained by changing *when and how* the low-rank compression is applied. We introduce two scenarios: *Minimal Memory*, which compresses the blocks before any other operations, and *Just-In-Time* which compresses the blocks after they received all their contributions.

---

**Algorithm 11:** Right looking block sequential LU factorization with *Minimal Memory* scenario.

---

```

▷ /* Initialize A (L structure) compressed */
For k = 1 to Nblk
     $\hat{A}_{(1:b_k),k} = \text{Compress}(A_{(1:b_k),k})$ 
     $\hat{A}_{k,(1:b_k)} = \text{Compress}(A_{k,(1:b_k)})$ 
End For
For k = 1 to N
    Factorize  $A_{(0),k} = L_{(0),k}U_{k,(0)}$ 
    Solve  $\hat{L}_{(1:b_k),k}U_{k,(0)} = \hat{A}_{(1:b_k),k}$ 
    Solve  $L_{(0),k}\hat{U}_{k,(1:b_k)} = \hat{A}_{k,(1:b_k)}$ 
    For j = 1 to bk
        For i = 1 to bk
            ▷ /* LR to LR updates (extend-add) */
             $\hat{A}_{(i),(j)} = \hat{A}_{(i),(j)} - \hat{L}_{(i),k}\hat{U}_{k,(j)}$ 
            ▷ LR2LR
        End For
    End For
End For
End For

```

---

### Minimal Memory

This scenario, described by Algorithm 11, starts by compressing the original matrix  $A$ . Thus, all low-rank blocks that are large enough are compressed directly from the original sparse form to the low-rank representation (lines 1 – 4). Note that for a matter of conciseness, loops of compression and solve over all off-diagonal blocks are merged into a single operation. In this scenario, compression kernels and later operations could have been performed using a sparse format, such as CSC for instance, until we get some fill-in. However, for the sake of simplicity we use a low-rank form throughout the entire algorithm to rely on blocks and not just on sets of values. Then, each classic dense operation on a low-rank block is replaced by a similar kernel operating on low-rank forms, even for the usual matrix-matrix multiplication (*GEMM*) kernel that is replaced by the equivalent *LR2LR* kernel operating on three low-rank matrices (cf. Section 4.2.2).

---

**Algorithm 12:** Right looking block sequential LU factorization with *Just-In-Time* scenario.

---

```

For  $k = 1$  to  $N_{cblk}$ 
  Factorize  $A_{(0),k} = L_{(0),k} U_{k,(0)}$ 
  ▷ /* Compress L and U off-diagonal blocks */
   $\hat{A}_{(1:b_k),k} = \text{Compress}(A_{(1:b_k),k})$ 
   $\hat{A}_{k,(1:b_k)} = \text{Compress}(A_{k,(1:b_k)})$ 
  Solve  $\hat{L}_{(1:b_k),k} U_{k,(0)} = \hat{A}_{(1:b_k),k}$ 
  Solve  $L_{(0),k} \hat{U}_{k,(1:b_k)} = \hat{A}_{k,(1:b_k)}$ 
  For  $j = 1$  to  $b_k$ 
    For  $i = 1$  to  $b_k$ 
      ▷ /* LR to dense updates */
       $A_{(i),j} = A_{(i),j} - \hat{L}_{(i),k} \hat{U}_{k,(j)}$  ▷ LR2GE
    End For
  End For
End For

```

---

### Just-In-Time

This second scenario, described by Algorithm 12, delays the compression of each supernode after all contributions have been accumulated. The algorithm is thus really close to the previous one with the only difference being in the update kernel, *LR2GE*, at line 9, which accumulates contributions on a dense block, and not on a low-rank form.

This operation, as we describe in Section 4.2.2, is much simpler than the *LR2LR* kernel, and is faster than a classic *GEMM*. However, by compressing the initial matrix  $A$ , and maintaining the low-rank structure throughout the factorization with the *LR2LR* kernel, *Minimal Memory* can reduce more drastically the memory footprint of the solver. Indeed, the final *dense* structure of the factorized matrix is never allocated, as opposed to *Just-In-Time* that requires it to accumulate the contributions. The final matrix is compressed with similar sizes in both scenarios.

### 4.2.2 Low-rank kernels

We introduce in this section the low-rank kernels used to replace the dense operations, and we present a complexity study of these kernels. Two families of operations are studied to reveal the rank of a matrix: Singular Value Decomposition (SVD) which leads to smaller ranks, and Rank-Revealing QR (RRQR) which allows a faster implementation.

#### Compression

The goal of low-rank compression is to represent a general dense matrix  $A$  of size  $m_A$ -by- $n_A$  by its compressed version  $\hat{A} = u_A v_A^t$ , where  $u_A$ , and  $v_A$ , are respectively matrices of size  $m_A$ -by- $r_A$ , and  $n_A$ -by- $r_A$ , with  $r_A$  being the rank of the block supposed to be small with respect to  $m_A$  and  $n_A$ . In order



to keep a given numerical accuracy we have to choose  $r_A$  such that  $\|A - \hat{A}\| \leq \tau \|A\|$ , where  $\tau$  is the prescribed tolerance.

**SVD**  $A$  is decomposed as  $U\sigma V^t$ . The low-rank form of  $A$  consists of the first  $r_A$  singular values and their associated singular vectors such that:  $\sigma_{r_A+1} \leq \tau$ ,  $u_A = U_{r_A}$ , and  $v_A^t = \sigma_{1:r_A} V_{r_A}^t$  with  $U_{r_A}$  being the first  $r_A$  columns of  $U$ , and respectively for  $V$ . This process requires  $\Theta(m_A^2 n_A + n_A^2 m_A + n_A^3)$  operations.

**RRQR**  $A$  is decomposed as  $PQR$ , where  $P$  is a permutation matrix, and  $QR$  the QR decomposition of  $P^{-1}A$ . The rank- $r_A$  form of  $A$  is then formed by  $u_A = Q_{r_A}$ , the first  $r_A$  columns of  $Q$ , and  $v_A^t = R_{r_A}$ , the first  $r_A$  rows of  $R$ . The main advantage of this process is that it can stop the factorization as soon as the norm of the trailing submatrix  $\tilde{A}_{(r_A+1:m_A, r_A+1:n_A)} = A - PQ_{r_A}R_{r_A}$  is lower than  $\tau$ . Thus, the complexity is lowered to  $\Theta(n_A r_A^2)$  operations.

SVD compression is much more expensive than RRQR. However, for a given tolerance, SVD returns lower ranks. Put another way, for a given rank, SVD will have better numerical accuracy. Thus, there is a trade-off between time-to-solution (RRQR) versus memory consumption and numerical accuracy (SVD).

Note that for the *Minimal Memory* scenario, the first compression (of sparse blocks) may be realized using Lanczos's methods, to take advantage of sparsity. However, both SVD and RRQR algorithms inherently take advantage of these zeros. In addition, most of the low-rank compressions are applied to blocks stored as dense blocks and represent the main part of the computations.

## Solve

The solve operation for a generic lower triangular matrix  $L$  is applied to blocks in low-rank forms in our two scenarios:  $L\hat{x} = \hat{b} \Leftrightarrow Lu_x v_x^t = u_b v_b^t$ . Then, with  $v_x^t = v_b^t$ , the operation is equivalent applying a dense solve only to  $u_b^t$ , and the complexity is only  $\Theta(m_L^2 r_x)$ , instead of  $\Theta(m_L^2 n_L)$  for the dense representation.

## Update

Let us consider the generic update operation,  $C = C - AB^t$ . Note that the PASTIX solver stores  $L$ , and  $U^t$  if required. Then, the same update is performed for Cholesky and LU factorizations. We break the operation into two steps: the product of two low-rank blocks, and the addition of a low-rank block and either a dense block (*LR2GE*), or a low-rank block (*LR2LR*).

**Low-rank matrices product** This operation can simply be expressed as two dense matrix products:  $\hat{A}\hat{B}^t = (u_A(v_A^t v_B))u_B^t = u_A((v_A^t v_B)u_B^t)$  where  $u_A$  is kept unchanged if  $r_A \leq r_B$  ( $u_B^t$  is kept otherwise) to lower the complexity.

However, it has been shown in [14] that the rank  $r_{AB}$  of the product of two low-rank matrices of ranks  $r_A$  and  $r_B$  is usually smaller than  $\min(r_A, r_B)$ . Moreover,  $u_A$  and  $u_B$  are both orthogonal, so the matrix  $T = (v_A^t v_B)$  has the same rank as  $\hat{A}\hat{B}^t$ . Thus, the complexity can be further reduced by transforming the matrix product to the following series of operations:

$$T = v_A^t v_B \quad (4.9)$$

$$\hat{T} = \widehat{v_A^t v_B} = u_T v_T^t \quad (4.10)$$

$$u_{AB} = u_A u_T \quad (4.11)$$

$$v_{AB}^t = v_T^t v_B^t. \quad (4.12)$$

**Low-rank matrices addition** Let us consider the next generic operation  $C' = C - u_{AB}v_{AB}^t$ , with  $m_{AB} \leq m_C$  and  $n_{AB} \leq n_C$  as it generally happens in supernodal methods. This is illustrated for example by the update block  $A_{(i),(j)}$  in Figure 4.6.

If  $C$  is not compressed as in the *LR2GE* kernel,  $C'$  will be dense too, and the addition of the two matrices is nothing else than a *GEMM* kernel. The complexity of this operation grows as  $\Theta(m_{AB} n_{AB} r_{AB})$ .

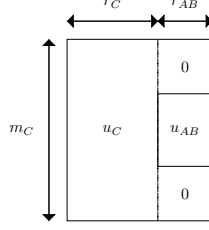


Figure 4.8: Accumulation of two low-rank matrices when sizes do not match.

If  $C$  is compressed as in the  $LR2LR$  kernel,  $C'$  will be compressed too, and

$$\hat{C}' = u_C v_C^t - u_{AB} v_{AB}^t \quad (4.13)$$

$$u_{C'} v_{C'}^t = [u_C, u_{AB}]([v_C, -v_{AB}])^t \quad (4.14)$$

where  $[,]$  is the concatenation operator. This is the commonly named *extend-add* operation. Without further optimization, this operation costs only two copies. In the case of supernodal method, adequate padding is also required to align the vectors coming from the  $AB$  and  $C$  matrices as shown in Figure 4.8 for the  $u$  vectors. The operation on  $v$  is similar.

One can notice that, kept as this, the rank of the updated  $C$  is now  $r_C + r_{AB}$ . When accumulating multiple updates, the rank grows quickly and the storage exceeds the original dense version. In order to maintain a small rank for  $C$ , recompression techniques are used. As for the compression kernel, both SVD and RRQR algorithms can be used.

**Recompression using SVD** first requires us to compute a QR decomposition for both matrices:

$$[u_C, u_{AB}] = Q_1 R_1 \text{ and } [v_C, -v_{AB}] = Q_2 R_2. \quad (4.15)$$

Then, the temporary matrix  $T = R_1 R_2^t$  is compressed using the SVD algorithm described previously. This gives the final  $\hat{C}'$  with:

$$u_{C'} = (Q_1 u_T) \text{ and } v_{C'} = (Q_2 v_T). \quad (4.16)$$

The complexity of this operation is decomposed as follows:  $\Theta((m_C + n_C)(r_C + r_{AB})^2)$  for the QR decomposition of equation (4.15),  $\Theta((r_C + r_{AB})^3)$  for the SVD decomposition, and finally  $\Theta((m_C + n_C)(r_C + r_{AB})r_{C'})$  for the application of both  $Q_1$  and  $Q_2$ .

**Recompression using RRQR** takes advantage of the orthogonality of both  $u_C$  and  $u_{AB}$  to first orthogonalize  $u_{AB}$  with respect to  $u_C$ :

$$u_{AB}^* = u_{AB} - u_C(u_C^t u_{AB}). \quad (4.17)$$

We obtain an orthonormal basis  $[u_C, u_{AB}^*]$  such that:

$$[u_C, u_{AB}] = [u_C, u_{AB}^*] \times \begin{pmatrix} I & u_C^t u_{AB} \\ 0 & I \end{pmatrix}. \quad (4.18)$$

We follow by applying the RRQR algorithm to:

$$\begin{pmatrix} I & u_C^t u_{AB} \\ 0 & I \end{pmatrix} \times ([v_C, v_{AB}])^t = PQR. \quad (4.19)$$

As for the compression, we keep the  $k = r_{C'}$  first columns of  $Q$  and rows of  $R$  to form the final  $C'$ :

$$u_{C'} = ([u_C, u_{AB}^*] P Q_k) \text{ and } v_{C'}^t = R_k. \quad (4.20)$$

Note that  $u_{C'}$  is kept orthogonal for future updates.

When the RRQR algorithm is used, the complexity of the recompression is then composed of:  $\Theta(r_C r_{AB} m_{AB})$  to form the intermediate product  $u_C^t u_{AB}$ ,  $\Theta(m_C r_C r_{AB})$  to form the orthonormal basis,  $\Theta(n_{AB} r_{AB} r_C)$  to generate the temporary matrix used in (4.19),  $\Theta((r_C + r_{AB})n_C r_{C'})$  to apply the RRQR algorithm, and finally again  $\Theta((r_C + r_{AB})n_C r_{C'})$  to compute the final  $u_{C'}$ .

## Summary

Table 4.1 presents the computational complexity for the two low-rank strategies with respect to the original version of the solver. To get the main factor of the complexity, we make the assumption that  $m_C \geq m_A \geq m_B$ ,  $r_A \geq r_B$ ,  $m_C \geq n_C$ , and  $r_C \leq r_{C'}$ . One can note that the *Just-In-Time* strategy performs the calculation of the low-rank contribution before assembling the matrix explicitly to apply a dense modification. The main factor of the complexity does not depend on  $n_A$  but on the ranks  $r_A$  and  $r_B$ : there are fewer operations to be performed. On the other hand, the *Minimal Memory* strategy requires using either the SVD or RRQR recompression, for which the complexity depends on  $m_C$  and  $n_C$ , the dimensions of the block  $C$ . This explains why this strategy is of higher complexity than the original solver.

When considering dense matrices, a low-rank matrix is usually modified by a contribution of the same size: the low-rank extend-add process may be efficient and lead to performance gain [14]. It is also the case for the CUFS strategy in BLR-MUMPS, which compresses a dense front before applying operations between low-rank blocks of the same size.

In our case, a block  $C$  receives many small contributions as stated by the separator theorem [101] describing how the size of supernodes is evolving during the nested dissection process. According to our experiments, it is still interesting to have low-rank blocks at the end of the factorization, meaning that ranks remain lower than  $\min(m_C, n_C)/4$  (otherwise compression will not help), even if blocks received a large number of contributions. Thus,  $r_{C'}$  is often close to or equal to  $r_C$  and lower than  $r_C + r_{AB}$ : the rank is often invariant to applying a small contribution. So it is less expensive to use RRQR recompression (and operations are more suitable for the performance). In terms of complexity, the recompression depends on the size of the target block  $C$  and not on the size of the contribution blocks  $A$  and  $B$ . As huge low-rank blocks are recompressed many times, it makes the *Minimal Memory* scenario slower than the dense version, but allows consequent memory savings.

Finally, the main advantage of the *Minimal Memory* scenario is that it can drastically reduce the memory footprint of the solver, since it compresses the matrix before the factorization. Thus, the final structure of the dense factorized matrix is never allocated, and the low-rank structure needs to be maintained throughout the factorization process to lower the memory peak.

In order to overcome the issue of expensive low-rank additions, an idea would be to consider randomized techniques to allow an extend-add process depending on the size of contributing blocks and not on the size of the target block.

### 4.2.3 Numerical experiments

Experiments were conducted on the *Plafrim*<sup>1</sup> supercomputer, and more precisely on the *miriel* cluster. Each node is equipped with two INTEL Xeon E5-2680 v3 12-cores running at 2.50 GHz and 128 GB of memory. The INTEL MKL 2016 is used for BLAS and SVD kernels. The RRQR kernel is coming from the BLR-MUMPS solver [9], and is an extension of the block rank-revealing QR factorization subroutines from LAPACK 3.6.0 (xGEQP3).

The PASTIX version used for our experiments is available on the public git repository<sup>2</sup> as the tag `papers/pdsec17`. The multi-threaded version used is the static scheduling version presented in [95].

For the initial ordering step, we used SCOTCH [118] 5.1.11 with the configurable strategy string from PASTIX to set the minimal size of non separated subgraphs, *cmin*, to 15. We also set the *frat* parameter to 0.08, meaning that column aggregation is allowed by SCOTCH as long as the fill-in introduced does not exceed 8% of the original matrix.

In experiments, blocks that are larger than 256 are split into blocks of size at most 128 to create more parallelism while keeping sizes large enough. The same 128 criteria is used to define the minimal width of the column blocks that are compressible. An additional limit on the minimal height to compress an off-diagonal block is set to 20.

Experiments were computed on a set of 3D matrices from The SuiteSparse Matrix Collection [43]:

- *Atmosmodj*: atmospheric model (1 270 432 dofs)
- *Audi*: structural problem (943 695 dofs)

<sup>1</sup><https://plafrim.bordeaux.inria.fr>

<sup>2</sup><https://gitlab.inria.fr/solverstack/pastix>

- *Hook*: model of a steel hook (1 498 023 dofs)
- *Serena*: gas reservoir simulation (1 391 349 dofs)
- *Geo1438*: geomechanical model of earth (1 437 960 dofs)

We also used 3D Laplacian generators (7 points stencils), and defined *lap120* as a Laplacian of size  $120^3$ . Note that when results showing numerical precision are presented, we used the backward error on  $b$ :  $\frac{\|Ax-b\|_2}{\|b\|_2}$ .

## SVD versus RRQR

The first experiment studies the behavior of the two compression methods coupled with both *Minimal Memory*, and *Just-In-Time* scenarios, on the matrix *Atmosmodj*. Table 4.2 presents the sequential timings of each operation of the numerical factorization with a tolerance of  $10^{-8}$ , as well as the memory used to store the final structure of the factorized matrix.

We can first notice that SVD compression kernels are much more time consuming than the RRQR kernels in both scenarios following the complexity study from Section 4.2.2. Indeed, RRQR compression kernels stop the computations as soon as the rank is found which reduces by a large factor the complexity, and this reduction is reflected in the time-to-solution. However, the SVD allows, for a given tolerance, to get a better memory reduction in both scenarios.

Comparing the *Minimal Memory* and the *Just-In-Time* scenario, the compression time is minimized in the *Minimal Memory* scenario because the compression occurs on the initial blocks which hold more zeros and are lower rank than when they have been updated. The time for the update addition, *extend-add* operation, becomes dominant in the *Minimal Memory* scenario, and even explodes when SVD is used. This is expected as the complexity depends on the largest blocks in the addition even for small contributions (see Section 4.2.2). Note that this ratio will evolve in favor of the *extend-add* operation on larger matrices where the ratio of updates of same size becomes dominant with respect to the number of updates from small blocks. For both compression methods, both scenarios compress the final coefficients with similar rates.

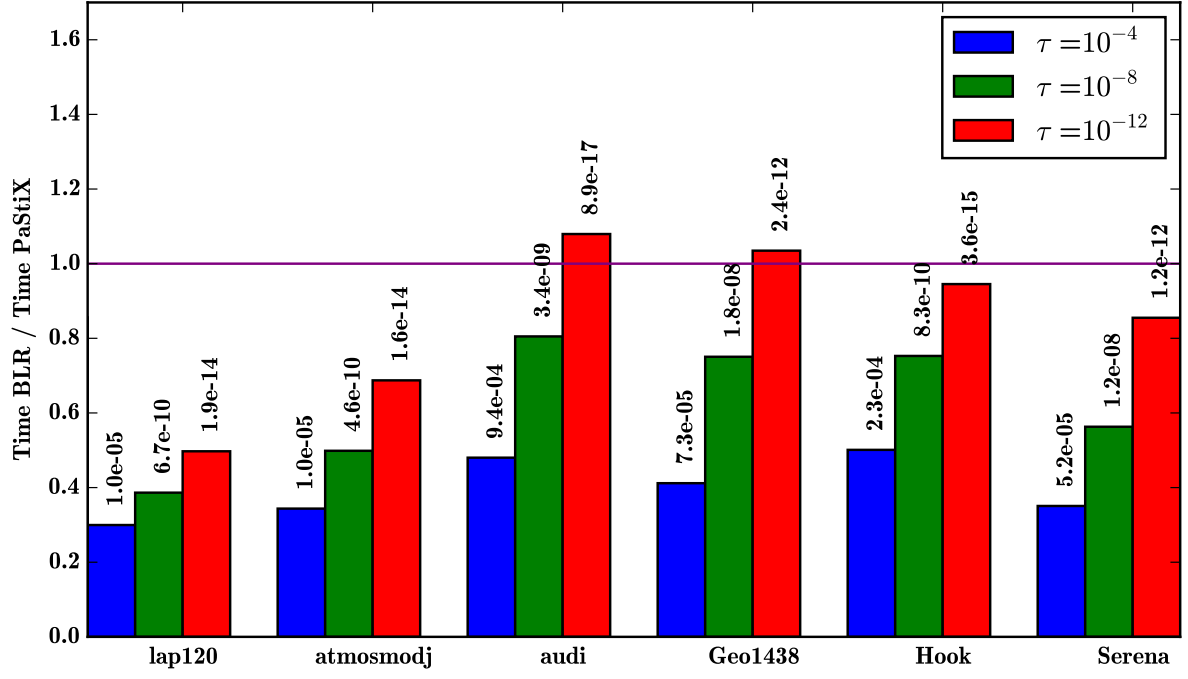
The diagonal block factorization time is invariant in the five strategies: the block sizes and kernels are identical. Panel solve, update product, and solve times are reduced in all low-rank configurations compared to the dense factorization and the timings follow the final size of the factors, since this size reflects the final ranks of the blocks.

To conclude, the *Minimal Memory* scenario is not able to compete with the original direct factorization due to the costly update addition. However, it reduced the memory peak of the solver to the final size of the factors. The *Minimal Memory*/RRQR offers a 25% memory reduction while doubling the sequential time-to-solution. The *Just-In-Time* scenario competes with the original direct factorization, and divides by two the time-to-solution with RRQR kernels.

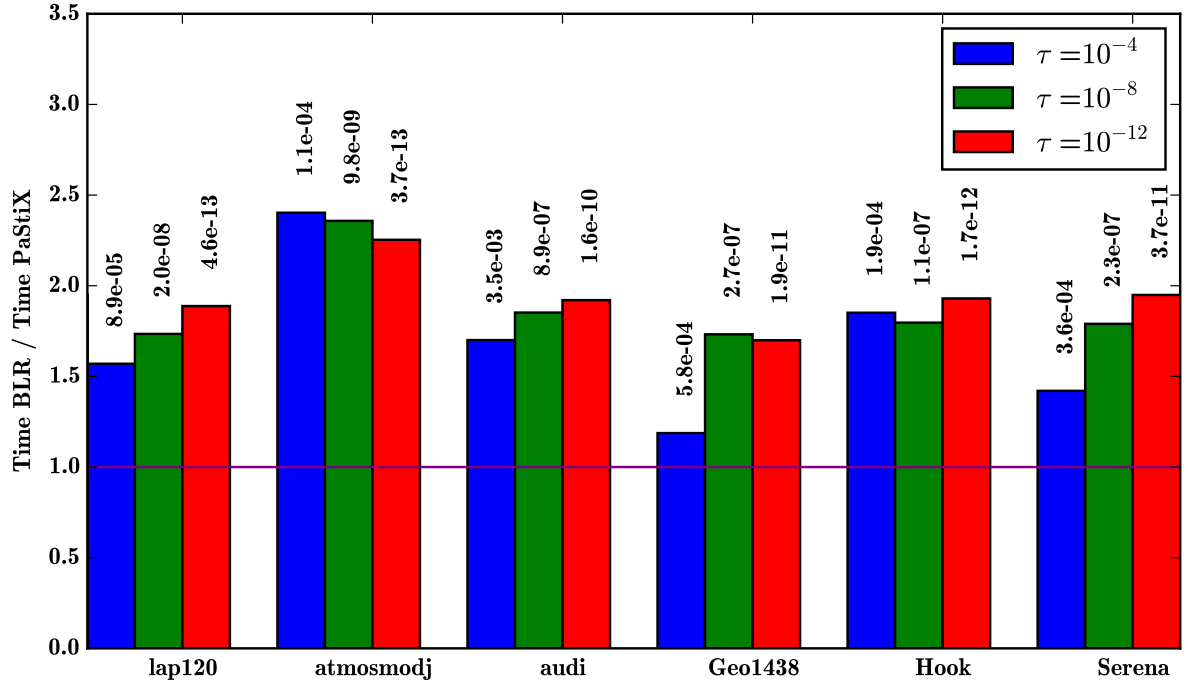
## Performance

Figure 4.9 presents the overall performance achieved by the two low-rank scenarios with respect to the original version of the solver (where lower is better) on the previously introduced set of 6 matrices. All versions are multi-threaded implementations and use all the 24 cores of one node. The scheduling used is the PASTIX static scheduler developed for the original version, this might have a negative impact on the low-rank implementations by creating a load imbalance. We study only the RRQR kernels as the SVD kernels have shown to be much slower. Three tolerance thresholds are studied for their impact on the time-to-solution, and the accuracy of the first residual of the solver, which went through one refinement step is shown with the backward errors printed on top of each bar.

Figure 4.9a shows that the *Just-In-Time*/RRQR scenario is able to reduce the time-to-solution in almost all cases of tolerance, and for all matrices which have a large spectrum of numerical properties. These results show that applications which requires low accuracy, as the seismic application for instance, can benefit by up to a factor of 3.3. Figure 4.9b shows that it is more difficult for the *Minimal Memory*/RRQR scenario to be competitive. The performance is always degraded with respect to the original PASTIX performance, with an average loss of around a factor of 1.8, and the tolerance has a much lower impact than for the previous case.



(a) *Just-In-Time* scenario using RRQR.



(b) *Minimal Memory* scenario using RRQR.

Figure 4.9: Performance of both strategies with 3 tolerance thresholds, backward error of the solution is printed on top of each bar.

For both scenarios, the backward error of the first solution is close to the entry tolerance. It is a little less accurate in the *Minimal Memory* scenario, because approximations are made earlier in the computation, and information is lost from the beginning. However, these results show that we are able to catch algebraically the information and forward it throughout the update process.

### Memory consumption

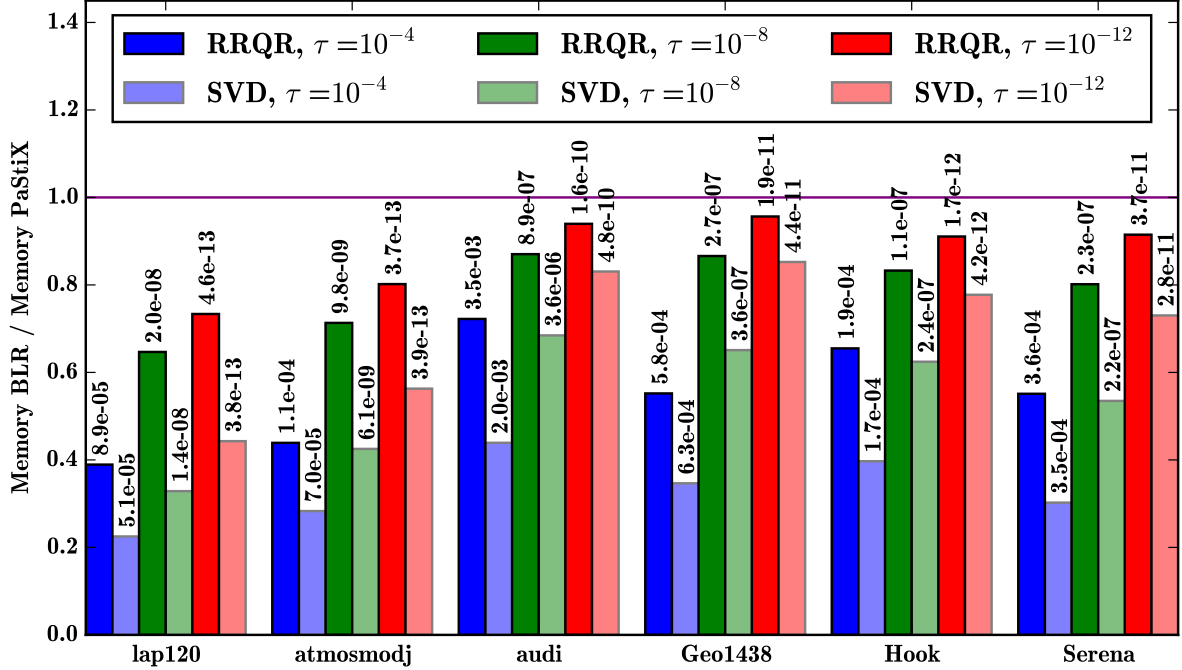


Figure 4.10: Memory peak for the *Minimal Memory* scenario with 3 tolerance thresholds and both SVD and RRQR kernels.

The *Minimal Memory* scenario is slower than the original solver, but it is a strategy that efficiently reduces the memory peak of the solver. Figure 4.10 presents the gain in the memory used to store the factors at the end of the factorization of the set of 6 matrices with respect to the *block dense* storage of PaStiX. In this figure, we also compare the memory gain of the SVD and RRQR kernels. We observe that in all cases, SVD provides a better compression rate by finding smaller ranks for a given matrix and a given tolerance. The quality of the first residual is also slightly better with the SVD kernels despite the smaller ranks. The second observation is that the smaller the tolerance ( $10^{-12}$ ), the larger the ranks and the memory consumption. However, the solver always presents a memory gain which can be more than 50% with larger tolerance ( $10^{-4}$ ).

Figure 4.11 presents the evolution of the size of the factors as well as the full consumption of the solver (factors and management structures) on 3D Laplacians with an increasing size. The memory limit of the system is 128GB. The original version is limited on this system to a 3D Laplacian of 4 million unknowns, and the size of the factors quickly increases for larger number of unknowns. With the *Minimal Memory/RRQR* scenario, we have now been able to run a 3D problem on up to 12 million unknowns when relaxing the tolerance to  $10^{-4}$ .

The memory of the *Just-In-Time* scenario has not been studied, since in our supernodal approach, each supernode is fully allocated in a dense fashion in order to accumulate the update before being compressed. Thus, the memory peak corresponds to the totality of the factorized matrix structure without compression and is identical to the original version. To reduce this memory peak, a solution would be to modify the scheduler to a *Left-Looking* approach that would delay the allocation and the compression of the original blocks. However, it would need to be carefully implemented to keep a certain amount of parallelism in order to save both time and memory. A possible solution are the scheduling strategies presented in [3] to keep the memory consumption of the solver under a given limit.

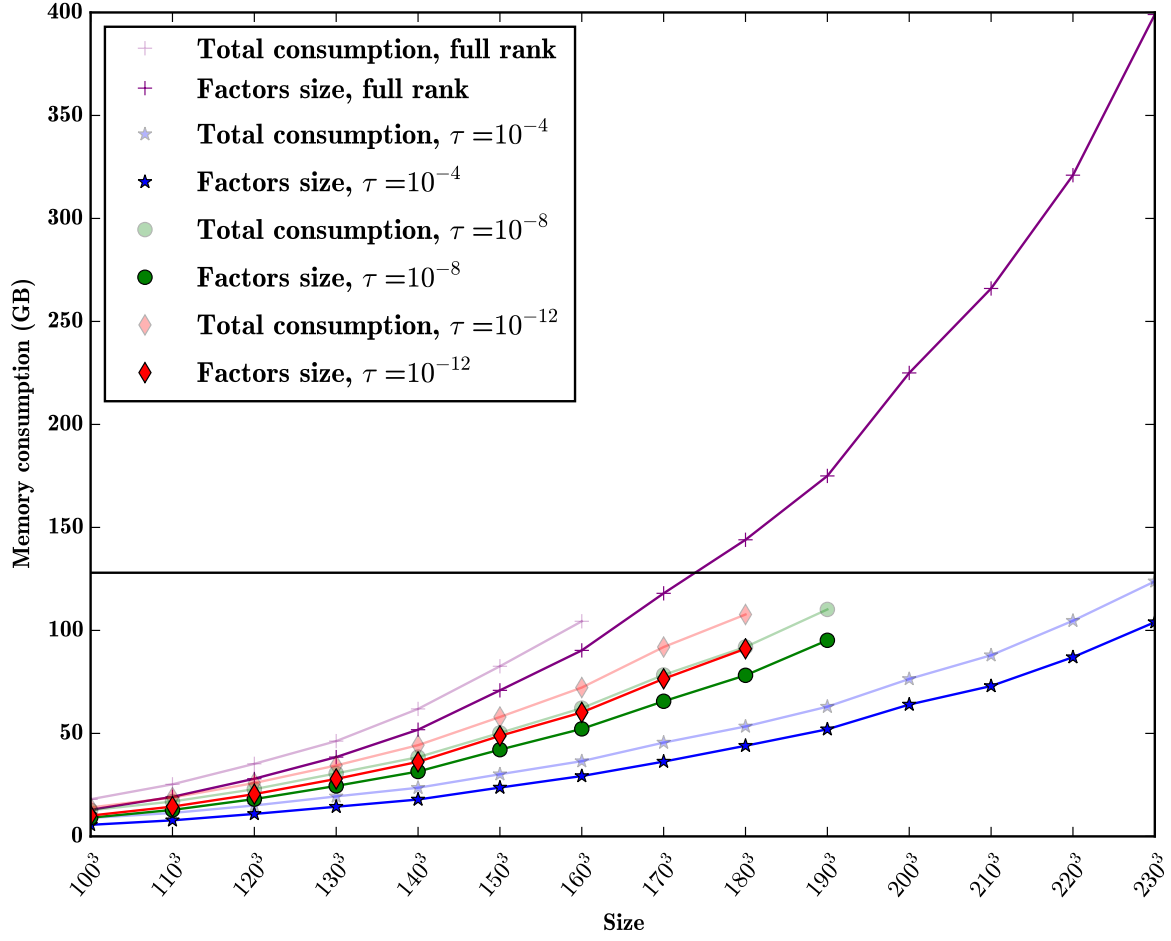


Figure 4.11: Memory scalability with 3 tolerance thresholds for the *Minimal Memory*/RRQR scenario when increasing the size of 3D Laplacians.

## Convergence and numerical stability

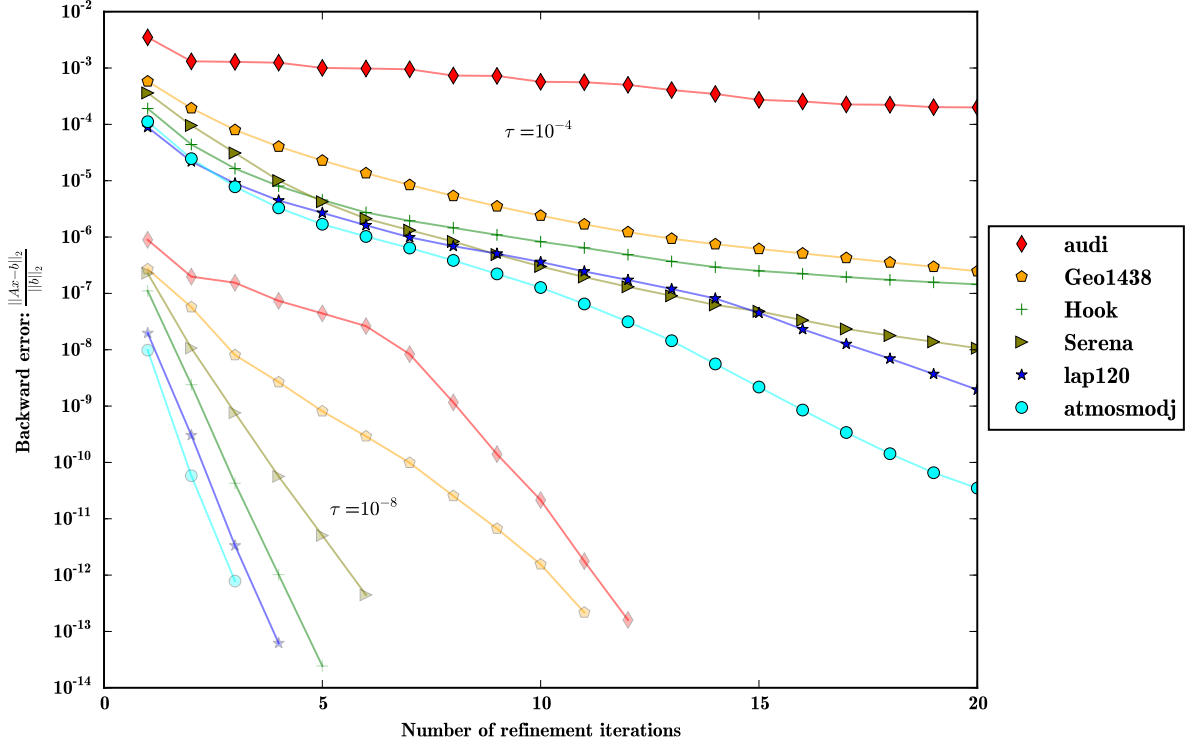


Figure 4.12: Convergence speed for the *Minimal Memory*/RRQR scenario with 2 tolerance thresholds.

Figure 4.12 presents the convergence of the iterative solver — GMRES for general matrices and Conjugate Gradient (CG) for SPD matrices — preconditioned with the low-rank factorization at tolerances of  $10^{-4}$  and  $10^{-8}$ . The iterative solver is stopped after reaching 20 iterations or a backward error lower than  $10^{-12}$ .

With a tolerance of  $10^{-8}$ , only a few iterations are required to converge to the solution. Note that on the *Audi* and *Geo1438* matrices, which are difficult to compress, a few more iterations are required to converge. With a larger tolerance  $10^{-4}$ , it is difficult to recover all the information lost during the compression, but this is enough to quickly get solutions at  $10^{-6}$  or  $10^{-8}$ . Note that the iterative refinement process benefits from the compression, as the solve step.

### 4.2.4 Discussion

In this section, we discuss the positioning of our solver with the closest related work and we give some limitations in extending this work to a hierarchical format.

Contrary to the approach studied in [65], we perform a symbolic block factorization. In their approach, as in our proposition, there is no fill-in between distinct branches of the elimination tree. However, contributions of a supernode to its ancestors are considered as full, in the sense that all structural zeros are included to generate the low-rank representation. Thus, they do not have extend-add (*LR2LR*) operation between low-rank blocks of different sizes, but the memory consumption is higher because some structural zeros are not managed.

A dense BLR solver was designed by Livermore Software Technology Corporation [14]. In this work, the full matrix is compressed at the beginning and operations between low-rank blocks are performed. This approach is similar to our *Minimal Memory* scenario in the context of dense matrices. Due to this restriction, the extend-add process concerns low-rank matrices of the same size, without zero padding. Thus, the *LR2LR* operation is less costly than the dense update in this context.

A BLR multifrontal sparse direct solver was designed for the MUMPS solver. The strategy is described in [9] and a theoretical study of the complexity of the solver is presented in [10]. When a front is



eliminated, different strategies are proposed to enhance the time-to-solution. Our scenario *Just-In-Time* is close to their FCSU (Factor, Compress, Solve, Update) strategy. The LUAR (Low-Rank Update Accumulation with Recompression) groups together multiple low-rank products to exploit the memory locality during the product recompression process. This could be similarly used in the *Just-In-Time*, but would imply larger ranks in the extend-add operations of the *Minimal Memory*. The CUFS (Compress, Update, Factor, Solve) is the strategy closest to our *Minimal Memory* scenario. However, only a dense front is fully compressed before being eliminated: contributing blocks are not compressed and low-rank operations occur within a dense matrix similarly to the previous work from LSTC. If the time-to-solution is better with BLR-MUMPS, there is more room for memory savings in our approach.

With the aim of extending our solver to hierarchical compression schemes, such as  $\mathcal{H}$ , HSS, or HODLR, we consider graphs coming from finite-element meshes from real-life simulations of 3D physical problems. From a theoretical point of view, the majority of these graphs have a bounded degree, and thus good separators respecting the separator theorems [101] can be built. For a  $n$ -vertices mesh, the time complexity of a direct solver is in  $\Theta(n^2)$ , and we expect to build a low-rank solver requiring  $\Theta(n^{\frac{4}{3}})$  operations. For the memory requirements, the direct approach leads to an overall storage of  $\Theta(n^{\frac{4}{3}})$ , while we target a  $\Theta(n \log(n))$  complexity. Let us consider the last separator of size  $\Theta(n^{\frac{2}{3}})$  for a 3D mesh, and one of the largest low-rank blocks of this separator. They are asymptotically the same size. Previous studies have shown that such a block may have a rank of order  $\Theta(n^{\frac{1}{3}})$ .

For the *Minimal Memory* scenario, we have seen that the time-to-solution is longer than the dense version. As low-rank blocks become larger in the hierarchy, it will be even worse than the solution we developed. For the *Just-In-Time* scenario, maintaining such a block in a dense form before compressing the block requires  $\Theta(n^{\frac{4}{3}})$  memory and does not satisfy the memory complexity we target. It also means that a compromise between *Minimal Memory* and *Just-In-Time* strategies using a *Left-Looking* approach might not be a relevant solution. Currently, no sparse solver is able to perform efficiently the extend-add operations using compression techniques such as SVD or RRQR, and it is still an open problem.

Table 4.1: Summary of the operation complexities when computing  $C = C - AB^t$ 

	GEMM ( <i>Dense</i> )	<i>LR2GE (Just-In-Time)</i>		<i>LR2LR (Minimal Memory)</i>	
		SVD	RRQR	SVD	RRQR
LR matrices product	–	(4.9): $\Theta(n_A \ r_A \ r_B)$		(4.9): $\Theta(n_A \ r_A \ r_B)$	
		(4.10): $\Theta(r_A^2 \ r_B)$	(4.10): $\Theta(r_A \ r_B \ r_{AB})$	(4.10): $\Theta(r_A^2 \ r_B)$	(4.10): $\Theta(r_A \ r_B \ r_{AB})$
		(4.11), (4.12): $\Theta(m_A \ r_A \ r_{AB})$		(4.11), (4.12): $\Theta(m_A \ r_A \ r_{AB})$	
LR matrices addition	–	–		(4.15): $\Theta(m_C(r_C + r_{AB})^2)$	(4.17): $\Theta(m_C \ r_C \ r_{AB})$
				(SVD): $\Theta((r_C + r_{AB})^3)$	(4.19): $\Theta(n_C(r_C + r_{AB})r_{C'})$
				(4.16): $\Theta(m_C(r_C + r_{AB})r_{C'})$	(4.20): $\Theta(m_C(r_C + r_{AB})r_{C'})$
Dense update	$\Theta(m_A \ m_B \ n_A)$	$\Theta(m_A \ m_B \ r_{AB})$		–	–
Main factor	$\Theta(m_A \ m_B \ n_A)$	$\Theta(m_A \ m_B \ r_{AB})$	$\Theta(m_A \ m_B \ r_{AB})$	$\Theta(m_C(r_C + r_{AB})^2)$	$\Theta(m_C(r_C + r_{AB})r_{C'})$

Table 4.2: Costs distribution on the Atmosmodj matrix with  $\tau = 10^{-8}$

	Full-rank	<i>Just-In-Time</i>		<i>Minimal Memory</i>	
		RRQR	SVD	RRQR	SVD
Factorization time (s)					
Compression	-	49.53	418.5	15.20	180.9
Block factorization	0.9635	1.000	1.003	1.074	1.104
Panel solve	15.80	6.970	6.526	11.16	6.946
LR product	-	64.10	91.15	193.1	94.36
LR addition	-	-	-	774.6	6523
Dense update	418.7	47.94	47.03	-	-
<i>Total</i>	<i>436</i>	<i>169</i>	<i>564</i>	<i>995</i>	<i>6806</i>
Solve time (s)	2.43	1.54	1.8	2.22	1.29
Factors final size (GB)	15.9	7.4	6.86	11.4	6.76

# Conclusion

► In Chapter 2, we presented a new implementation of a sparse direct solver with a supernodal method using a task-based programming paradigm. The programming paradigm shift insulates the solver from the underlying hardware. The runtime system takes advantage of the parallelism exposed via the graph of tasks to maximize the efficiency on a particular platform, without the involvement of the application developer. In addition to the alteration of the mathematical algorithm to adapt the solver to the task-based concept, and to provide an efficient memory-constraint sparse GEMM for the GPU, contributions to both runtimes (PARSEC and STARPU) were made such that they could efficiently support tasks with irregular duration, and minimize the non-regular data movements to, and from, the devices. While the current status of this development is already significant in itself, the existence of the conceptual task-based algorithm opened an astonishing new perspective for the seamless integration of any type of accelerator. Providing computational kernels adapted to specialized architectures has become the only obstruction to a portable, efficient, and generic sparse direct solver exploiting these devices. In the context of this study, developing efficient and specialized kernels for GPU allowed us a swift integration on hybrid platforms. Globally, our experimental results corroborate the fact that the portability and efficiency of the proposed approach are indeed available, elevating this approach to a suitable programming model for applications on hybrid environments.

Future work will concentrate on smoothing the runtime integration within the solver. First, in order to minimize the scheduler overhead, we plan to increase the granularity of the tasks at the bottom of the elimination tree. Merging leaves or subtrees together yields bigger, more computationally intensive tasks. Second, we will pursue the extension of this work in distributed heterogeneous environments. On such platforms, when a supernode updates another non-local supernode, the update blocks are stored in a local extra-memory space (this is called “fan-in” approach [18]). By locally accumulating the updates until the last updates to the supernode are available, we trade bandwidth for latency. The runtime will allow for studying dynamic algorithms, where the number of local accumulations has bounds discovered at runtime. Finally, the availability of extra computational resources highlights the potential to dynamically build or rebuild the supernodal structures according to the load on the cores and the GPUs. Simultaneously, we will work on the challenging problem of refining the initial mapping of the data based on the heterogeneous capabilities of the distributed memory architectures and to dynamically rebalance the data to match the computational power of the available resources.

► In Chapter 3, our objective was to build a good domain decomposition of a graph to be used as an entry by a hybrid solver. To get a good load balancing, we needed to get both balanced interior node and interface node set sizes. We decided to revisit the recursive algorithm introduced by Lipton et al. in the context of generalized nested dissection. This led us to keep track of the halo vertices during the recursion of the algorithm. In the software context of the SCOTCH partitioner, we modified the multilevel framework and adapted the Fiduccia-Mattheyses algorithm to refine separators during the uncoarsening steps. We also proposed two effective alternatives to the greedy graph growing algorithm for partitioning the coarsest graph. All those changes do not impact the computational complexity of the SCOTCH partitioner. We obtained very good balance gains on both criteria on most matrices and in particular on the biggest industrial test cases which have several million vertices. Our new algorithms keep behaving well even when we increase the number of domains.

In the short term, we will first study the impact of our work on the quality of the parallel performance on the MAPHYS hybrid solver which is developed in our research team. Secondly, our algorithms will be adapted in the parallel framework PT-SCOTCH in order to address larger problems. And finally,

we want to investigate the impact of these partitioning algorithms, especially the *HaloFirst* strategy, to build some improved cluster-trees in the context of hierarchical matrix approximations used in the Block Low-Rank version of the PASTIX solver.

► In Chapter 4, we presented a new Block Low-Rank sparse solver that combines an existing sparse direct solver PASTIX, and low-rank compression kernels. This solver reduces the memory consumption and/or the time-to-solution depending on the scenario. Two scenarios were developed. *Minimal Memory* saves memory up to a factor of 2.6 using RRQR kernels, with a time overhead that is limited to 2.4 despite the higher complexity. Large problems that could not fit into memory when the original solver was used can now be solved thanks to the lower memory requirements, especially when low accuracy solutions and/or a large number of right-hand sides are involved. *Just-In-Time* reduces both the time-to-solution by a factor up to 3.3, and the memory requirements of the final factorized matrix with similar factors to *Minimal Memory*. However, with the actual scheduling strategy, this gain is not reflected in the memory peak. Two compression kernels, SVD and RRQR, were studied and compared. We have shown that, for a given tolerance, both approaches provide correct solutions with the expected accuracy, and that RRQR despite larger ranks provides faster kernels. In addition, we demonstrated that the solver can be used either as a low-tolerance direct solver, or as a good preconditioner for iterative methods, that normally require only a few iterations before reaching the machine precision.

In the future, new kernel families, such as RRQR with randomization techniques, will be studied in terms of accuracy and stability in the context of a supernodal solver. To further improve the performance of *Minimal Memory* and close up the gap with the original solver, aggregation techniques on small contributions will also be studied. This will lead to the extension of this work to hierarchical compression in large supernodes that could further reduce the memory footprint, and the solver complexity. Regarding *Just-In-Time*, future work is focused on studying smart scheduling strategies that combines a *Right-Looking* and a *Left-Looking* approach in order to find a good compromise between memory and parallelism for the targeted architecture. The *Minimal Memory* strategy can be enhanced to achieve performance gains by aggregating small contributions together before applying a single recompression of a large low-rank structure. In addition, the *Just-In-Time* strategy can lead to memory savings with smart memory allocation to avoid the peak achieved during the factorization.

While the ongoing work, which consists in studying how to replace some classic dense linear algebra calculation by data sparse  $\mathcal{H}$ -arithmetic on the dense block that appears during the factorization, will be pursued; we also envisage a more disruptive approach where the  $\mathcal{H}$ -algebra will be fully integrated in the design of the solver. In this latter approach, the large dense block will be computed and handled directly in  $\mathcal{H}$ -form. This is a fundamental new direction that changes entirely the properties of the algorithm and could lead to significant speed-ups. PASTIX will be the main testbed and its future software releases will host the new capabilities and features enabled by  $\mathcal{H}$ -algebra.

From the software development point of view, the version 6.0 of PASTIX is now available at <https://gitlab.inria.fr/solverstack/pastix>. It has been fully redesigned by Mathieu Faverge with the main objectives to be easily maintained for next generation of architectures and to merge requests from external contributors. It relies on the same programming standards as the software developed at ICL (mainly PLASMA and PARSEC) and provides new GPUs kernels dedicated to our sparse direct solver and block low-rank compression methods. Based on runtime systems, this framework will enable the possibility of investigating combined strategies between right-looking and left-looking, but also mixed supernodal and multifrontal methods. Preliminary work on the solver has shown the benefit of using runtime systems to exploit accelerators efficiently, and fine granularity tasks of 2D schemes are essential to provide sufficient parallelism to feed all resources. In this context, we will investigate the use of a multilevel approach to control the number of tasks in the system. The objective is twofold: create enough parallelism to feed the large spectrum of resources, and keep the number of tasks to a level that can be efficiently handled by the runtime systems in terms of scheduling time, and memory overhead. This evolution in the programming model of our sparse direct solvers will lead to the development of new scheduling strategies tied to this multilevel approach. This programming model will enable a better scalability of today's problem to consider a better scalability at very large scale on homogeneous and heterogeneous clusters. New communication schemes will also be studied (Fan-out, Fan-both) to adapt to the new parallelism expressed by this multilevel algorithm. Both the multilevel algorithm and the communication strategy will adapt to the block low-rank capability of the solver in order to directly

provide the compressed solution to upper levels.

On the other hand, the NLAFET<sup>3</sup> project (Parallel Numerical Linear Algebra for Future Extreme-Scale Systems), follows clearly the same direction in a wider range of applications. It could be a great opportunity to consolidate our collaborations, or, at least, to exchange our expertise on the use of advanced scheduling strategies and runtime systems for linear algebra software.

Finally, in addition to numerical simulations of physical models of reality, the processing and analysis of very large amounts of data (Big Data analytics) is an important area with many new applications. For instance, in the last Inria's scientific strategic plan for 2018-2022, one of the scientific challenges is to jointly leverage the know-how and existing solutions from both High Performance Computing (HPC) and Data-intensive processing (Big Data). Some milestone and open questions are raised in this document that would help to identify the objectives and the computational challenges that could be the core of my long-term research project. Furthermore, many recent reports in the US lead to the same conclusion that we have to consider problems where data is the dominating factor. In this context, I would like to investigate how some of the numerical schemes we are working on can evolve when tensors have to be considered instead of classical 2-dimensional regular matrices. In particular, one class of applications concerns the factorization and parallel decomposition of sparse tensors where many people have started to work on. I could at least mention [90, 91, 132, 133] that come from the community of scheduling, parallel algorithms, graph partitioning and linear algebra.

---

<sup>3</sup><http://www.nlafet.eu/>



# Appendix A

## PASTIX 6.0 updated performance

### A.1 Experimental conditions

#### Set of matrices

- Subset of large matrices from SuiteSparse collection, around 1 million unknowns each

#### Architectures

- 2 dodecacore Intel Xeon E5-2680 v3 @ 2.50GHz + 4 NVIDIA K40
- 1 Intel KNL 7230 @ 1.30GHz, 64 cores

#### Implementation

- Factorization step only
- Implementation over the PARSEC runtime system
- Blocking sizes from 160 to 320 on low  $flops/nnz_L$  ratio
- Blocking sizes from 320 to 640 on high  $flops/nnz_L$  ratio

#### Lower level of the elimination tree

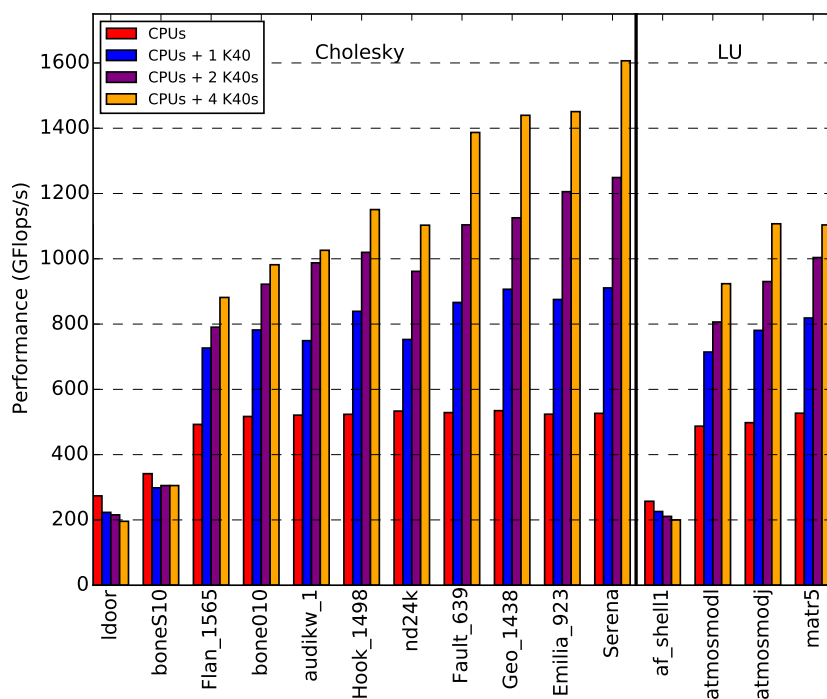
- Computed with 1D tasks (supernodal)
- Lower levels:
  - exhibits more parallelism
  - generates low efficiency updates

#### Higher level of the elimination tree

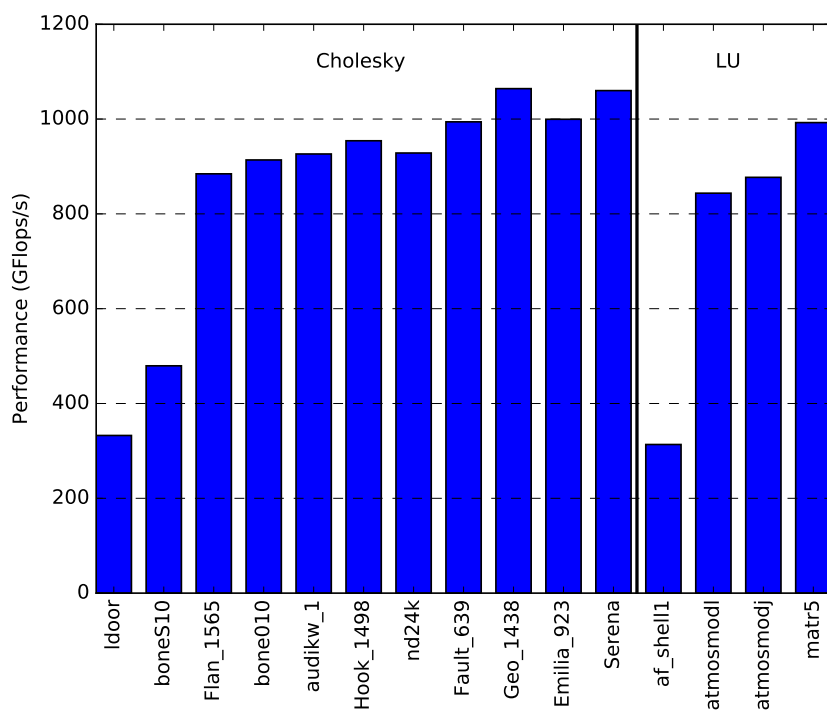
- Decomposed in 2D elementary tasks (xxTRF, TRSM, GEMM)
- Higher levels:
  - exhibits less parallelism in 1D
  - generates more compute intensive updates
- Use a compressed representation of the DAG:
  - Exploit the elimination tree
  - Exploit a double index CSC/CSR of the symbolic blocked structure of the matrix



## A.2 Performance on the Kepler architecture



## A.3 Performance on the KNL architecture



# Appendix B

## Bibliography

- [1] E. Agullo, J. Demmel, J. Dongarra, B. Hadri, J. Kurzak, J. Langou, H. Ltaief, P. Luszczek, and S. Tomov. Numerical linear algebra on emerging architectures: The PLASMA and MAGMA projects. *Journal of Physics: Conference Series*, Vol. 180(1):012037, 2009. [Cited on pages 29 and 30]
- [2] E. Agullo, L. Giraud, A. Guermouche, A. Haidar, and J. Roman. Parallel algebraic domain decomposition solver for the solution of augmented systems. *Advances in Engineering Software*, 60(Supplement C):23 – 30, 2013. CIVIL-COMP: Parallel, Distributed, Grid and Cloud Computing. [Cited on pages 3 and 53]
- [3] Emmanuel Agullo, Patrick R. Amestoy, Alfredo Buttari, Abdou Guermouche, Jean-Yves L’Excellent, and François-Henry Rouet. Robust Memory-Aware Mappings for Parallel Multifrontal Factorizations. *SIAM Journal on Scientific Computing*, 38(3), 2016. [Cited on page 81]
- [4] P. Amestoy, I.S. Duff, S. Pralet, and C. Voemel. Adapting a parallel sparse direct solver to SMP architectures. *Parallel Computing*, 29(11-12):1645–1668, 2003. [Cited on page 8]
- [5] P. R. Amestoy, T. Davis, and I. S. Duff. An approximate minimum degree ordering algorithm. *SIAM J. Matrix Anal. and Appl.*, 17:886–905, 1996. [Cited on pages 9 and 11]
- [6] P. R. Amestoy, I. S. Duff, and J.-Y. L’Excellent. Multifrontal parallel distributed symmetric and unsymmetric solvers. *Comput. Methods in Appl. Mech. Eng.*, 184:501–520, 2000. [Cited on pages 7 and 52]
- [7] P. R. Amestoy, I. S. Duff, J.-Y. L’Excellent, and X. S. Li. Analysis, tuning and comparison of two general sparse solvers for distributed memory computers. *ACM Trans. Math. Softw.*, 27(4):388–420, 2001. [Cited on page 8]
- [8] P. R. Amestoy, A. Guermouche, J.-Y. L’Excellent, and S. Pralet. Hybrid scheduling for the parallel solution of linear systems. *Parallel Computing*, 32(2):136–156, 2006. [Cited on page 9]
- [9] Patrick Amestoy, Cleve Ashcraft, Olivier Boiteau, Alfredo Buttari, Jean-Yves L’Excellent, and Clement Weisbecker. Improving Multifrontal Methods by Means of Block Low-Rank Representations. *SIAM Journal on Scientific Computing*, 37(3):A1451–A1474, 2015. [Cited on pages 72, 78, and 83]
- [10] Patrick Amestoy, Alfredo Buttari, Jean-Yves L’Excellent, and Theo Mary. On the Complexity of the Block Low-Rank Multifrontal Factorization. Research Report RT–2016–03–FR, IRIT, May 2016. [Cited on page 83]
- [11] Patrick R Amestoy, Iain S Duff, Stephane Pralet, and Christof Vomel. Adapting a parallel sparse direct solver to architectures with clusters of smps. *Parallel Computing*, 29(11):1645 – 1668, 2003. Parallel and distributed scientific and engineering computing. [Cited on page 43]
- [12] A. Aminfar, S. Ambikasaran, and E. Darve. A fast block low-rank dense solver with applications to finite-element matrices. *Journal of Computational Physics*, 304:170–188, 2016. [Cited on page 72]

- [13] AmirHossein Aminfar and Eric Darve. A fast, memory efficient and robust sparse preconditioner based on a multifrontal approach with applications to finite-element matrices. *International Journal for Numerical Methods in Engineering*, 2016. [Cited on page 72]
- [14] J Anton, C Ashcraft, and C Weisbecker. A Block Low-Rank Multithreaded Factorization for Dense BEM Operators. In *SIAM Conference on Parallel Processing for Scientific Computing (SIAM PP 2016)*, Paris, France, April 2016. [Cited on pages 72, 76, 78, and 83]
- [15] Gabriel Antoniu, Luc Bougé, and Raymond Namyst. *An efficient and transparent thread migration scheme in the PM2 runtime system*, pages 496–510. Springer Berlin Heidelberg, Berlin, Heidelberg, 1999. [Cited on page 2]
- [16] Joseph Antony, Pete P. Janes, and Alistair P. Rendell. Exploring thread and memory placement on NUMA architectures: Solaris and Linux, UltraSPARC/FirePlane and Opteron/HyperTransport. In *HiPC*, pages 338–352, 2006. [Cited on page 21]
- [17] David L. Applegate, Robert E. Bixby, Vasek Chvatal, and William J. Cook. *The Traveling Salesman Problem: A Computational Study (Princeton Series in Applied Mathematics)*. Princeton University Press, Princeton, NJ, USA, 2007. [Cited on page 71]
- [18] A. Ashcraft, S. C. Eisenstat, and J. W.-H. Liu. A fan-in algorithm for distributed sparse numerical factorization. *SIAM Journal on Scientific and Statistical Computing*, 11:593–599, 1990. [Cited on page 87]
- [19] C. Ashcraft, S. C. Eisenstat, J. W.-H. Liu, and A. Sherman. A comparison of three column based distributed sparse factorization schemes. In *Proc. Fifth SIAM Conf. on Parallel Processing for Scientific Computing*, 1991. [Cited on page 14]
- [20] Cleve Ashcraft. *The Fan-Both Family of Column-Based Distributed Cholesky Factorization Algorithms*, pages 159–190. Springer New York, New York, NY, 1993. [Cited on page 16]
- [21] Cédric Augonnet, Samuel Thibault, Raymond Namyst, and Pierre-André Wacrenier. StarPU: a unified platform for task scheduling on heterogeneous multicore architectures. *Concurrency and Computation: Practice and Experience*, 23(2), 2011. [Cited on pages 30 and 31]
- [22] Maxime Barrault, Bruno Lathuilière, Pierre Ramet, and Jean Roman. Efficient Parallel Resolution of The Simplified Transport Equations in Mixed-Dual Formulation. *Journal of Computational Physics*, 230(5):2004–2020, 2011. [Cited on page 5]
- [23] George Bosilca, Aurelien Bouteiller, Anthony Danalis, Mathieu Faverge, Azzam Haidar, Thomas Herault, Jakub Kurzak, Julien Langou, Pierre Lemarinier, Hatem Ltaief, Piotr Luszczek, Asim YarKhan, and Jack Dongarra. Flexible development of dense linear algebra algorithms on massively parallel architectures with DPLASMA. In *12th IEEE International Workshop on Parallel and Distributed Scientific and Engineering Computing (PDSEC’11)*, 2011. [Cited on pages 30 and 31]
- [24] George Bosilca, Aurelien Bouteiller, Anthony Danalis, Thomas Hérault, Pierre Lemarinier, and Jack Dongarra. DAGuE: A generic distributed DAG engine for High Performance Computing. *Parallel Computing*, 38(1-2), 2012. [Cited on page 30]
- [25] Jacques Briat, Ilan Ginzburg, Marcelo Pasin, and Brigitte Plateau. *Athapascan runtime: Efficiency for irregular problems*, pages 591–600. Springer Berlin Heidelberg, Berlin, Heidelberg, 1997. [Cited on page 2]
- [26] François Broquedis, Jérôme Clet-Ortega, Stéphanie Moreaud, Nathalie Furmento, Brice Goglin, Guillaume Mercier, Samuel Thibault, and Raymond Namyst. hwloc: A Generic Framework for Managing Hardware Affinities in HPC Applications. In *Proceedings of the 18th Euromicro International Conference on Parallel, Distributed and Network-Based Processing (PDP2010)*, pages 180–186, Pisa, Italia, February 2010. IEEE Computer Society Press. [Cited on page 30]
- [27] A. Buttari. Fine-grained multithreading for the multifrontal QR factorization of sparse matrices, 2013. To appear in SIAM SISC and APO technical report number RT-APO-11-6. [Cited on page 29]

- [28] A. Buttari, J. Dongarra, J. Kurzak, J. Langou, P. Luszczyk, and S. Tomov. The impact of multicore on math software. In *Proceedings of the 8th international conference on Applied parallel computing: state of the art in scientific computing*, PARA'06, pages 1–10, Berlin, Heidelberg, 2007. Springer-Verlag. [Cited on page 29]
- [29] Alfredo Buttari, Julien Langou, Jakub Kurzak, and Jack Dongarra. A class of parallel tiled linear algebra algorithms for multicore architectures. *Parallel Computing*, 35(1):38–53, 2009. [Cited on pages 29, 30, and 33]
- [30] Y. Campbell and T.A. Davis. Incomplete LU factorization: A multifrontal approach. Technical report, Technical Report TR-95-024, Computer and Information Sciences, Department University of Florida, Gainesville, FL, USA, October 1995. [Cited on page 44]
- [31] A. Casadei. *Optimizations of hybrid sparse linear solvers relying on Schur complement and domain decomposition approaches*. PhD thesis, LaBRI, Bordeaux University, Talence, France, October 2015. [Cited on page 43]
- [32] Astrid Casadei, Pierre Ramet, and Jean Roman. An improved recursive graph bipartitioning algorithm for well balanced domain decomposition. In *IEEE International Conference on High Performance Computing (HiPC 2014)*, pages 1–10, Goa, India, December 2014. [Cited on page 43]
- [33] J. N. Chadwick and D. S. Bindel. An Efficient Solver for Sparse Linear Systems Based on Rank-Structured Cholesky Factorization. *CoRR*, abs/1507.05593, 2015. [Cited on page 72]
- [34] Tony F. Chan and Panayot S. Vassilevski. A framework for block ilu factorizations using block-size reduction. *Mathematics of Computation*, 64(209):129–156, 1995. [Cited on page 44]
- [35] M. Chanaud. *Conception d'un solveur haute performance de systèmes linéaires creux couplant des méthodes multigrilles et directes pour la résolution des équations de Maxwell 3D en régime harmonique discrétisées par éléments finis*. PhD thesis, LaBRI, Bordeaux University, Talence, France, December 2009. [Cited on page 5]
- [36] M. Chanaud, L. Giraud, D. Goudin, J. J. Pesqué, and J. Roman. A parallel full geometric multigrid solver for time harmonic maxwell problems. *SIAM Journal on Scientific Computing*, 36(2):C119–C138, 2014. [Cited on page 5]
- [37] Andrew Chapman and Yousef Saad. Deflated and augmented krylov subspace techniques. *Numerical Linear Algebra with Applications*, 4(1):43–66, 1997. [Cited on page 45]
- [38] P. Charrier and J. Roman. Algorithmique et calculs de complexité pour un solveur de type dissections emboîtées. *Numerische Mathematik*, 55:463–476, 1989. [Cited on pages 10, 11, and 67]
- [39] Michel Cosnard, Emmanuel Jeannot, and Tao Yang. Compact dag representation and its symbolic scheduling. *Journal of Parallel and Distributed Computing*, 64(8):921–935, 2004. [Cited on page 31]
- [40] T. Davis. *Direct Methods for Sparse Linear Systems*. Society for Industrial and Applied Mathematics, 2006. [Cited on page 8]
- [41] T. Davis. Multifrontal sparse qr factorization: Multicore, and gpu work in progress. In *15th SIAM Conference on Parallel Processing for Scientific Computing*, Savannah, USA, February 2012. [Cited on page 30]
- [42] T. A. Davis. Algorithm 915, SuiteSparseQR: Multifrontal multithreaded rank-revealing sparse QR factorization. *ACM Trans. Math. Softw.*, 38(1):8, 2011. [Cited on page 29]
- [43] T. A. Davis and Y. Hu. The University of Florida sparse matrix collection. *ACM Trans. Math. Softw.*, 38(1):1:1–1:25, December 2011. [Cited on pages 33 and 78]
- [44] Timothy A. Davis, Sivasankaran Rajamanickam, and Wissam M. Sid-Lakhdar. A survey of direct methods for sparse linear systems. *Acta Numerica*, 25:383–566, 2016. [Cited on page 2]

- [45] R. Diekmann, R. Preis, F. Schlimbach, and C. Walshaw. Shape-optimized mesh partitioning and load balancing for parallel adaptive FEM. *Parallel Computing*, 26:1555–1581, 2000. [Cited on page 57]
- [46] I. S. Duff, A. M. Erisman, and J. K. Reid. Direct methods for sparse matrices. *Oxford University Press*, London 1986. [Cited on pages 7 and 8]
- [47] I. S. Duff and J. K. Reid. The multifrontal solution of indefinite sparse symmetric linear equations. *ACM Transactions on Mathematical Software*, 9:302–325, 1983. [Cited on page 7]
- [48] M. Faverge. *Ordonnancement hybride statique-dynamique en algèbre linéaire creuse pour de grands clusters de machines NUMA et multi-coeurs*. PhD thesis, LaBRI, Bordeaux University, Talence, France, December 2009. [Cited on page 19]
- [49] Mathieu Faverge and Pierre Ramet. Dynamic Scheduling for sparse direct Solver on NUMA architectures. In *PARA'08*, LNCS, Norway, 2008. [Cited on pages 19 and 29]
- [50] J. Gaidamour. *Conception d'un solveur linéaire creux parallèle hybride direct-itératif*. PhD thesis, LaBRI, Bordeaux University, Talence, France, December 2009. [Cited on page 3]
- [51] J. Gaidamour and P. Hénon. A parallel direct/iterative solver based on a Schur complement approach. In *IEEE 11th International Conference on Computational Science and Engineering*, pages 98–105, Sao Paulo, Brésil, July 2008. [Cited on pages 3 and 53]
- [52] A. George. Nested dissection of a regular finite element mesh. *SIAM Journal on Numerical Analysis*, 10(2):345–363, 1973. [Cited on page 52]
- [53] A. George, M. T. Heath, J. W.-H. Liu, and E. G.-Y. Ng. Sparse Cholesky factorization on a local memory multiprocessor. *SIAM Journal on Scientific and Statistical Computing*, 9:327–340, 1988. [Cited on page 7]
- [54] A. George and J. W.-H. Liu. *Computer Solution of Large Sparse Positive Definite Systems*. Prentice-Hall, Englewood Cliffs, NJ, 1981. [Cited on pages 7, 8, 9, and 68]
- [55] A. George and D. R. McIntyre. On the application of the minimum degree algorithm to finite element systems. *SIAM Journal on Numerical Analysis*, 15(1):90–112, 1978. [Cited on page 70]
- [56] T. George, V. Saxena, A. Gupta, A. Singh, and A. R. Choudhury. Multifrontal Factorization of Sparse SPD Matrices on GPUs. *2011 IEEE International Parallel & Distributed Processing Symposium*, pages 372–383, May 2011. [Cited on page 30]
- [57] Pieter Ghysels, Xiaoye S. Li, François-Henry Rouet, Samuel Williams, and Artem Napov. An Efficient Multicore Implementation of a Novel HSS-Structured Multifrontal Solver Using Randomized Sampling. *SIAM Journal on Scientific Computing*, 38(5):S358–S384, 2016. [Cited on page 72]
- [58] L. Giraud, A. Haidar, and Y. Saad. Sparse approximations of the Schur complement for parallel algebraic hybrid linear solvers in 3D. Rapport de recherche RR-7237, INRIA, March 2010. [Cited on page 53]
- [59] D. Goudin, P. Hénon, M. Mandallena, K. Mer, F. Pellegrini, P. Ramet, J. Roman, and J.-J. Pesqué. Outils numériques parallèles pour la résolution de très grands problèmes d'électromagnétisme. In *Séminaire sur l'Algorithmique Numérique Appliquée aux Problèmes Industriels, Calais, France*, May 2003. [Cited on page 8]
- [60] D. Goudin, P. Hénon, F. Pellegrini, P. Ramet, J. Roman, and J.-J. Pesqué. Parallel sparse linear algebra and application to structural mechanics. *Numerical Algorithms, Baltzer Science Publisher*, 24:371–391, 2000. [Cited on page 8]
- [61] L. Grasedyck, R. Kriemann, and S. Le Borne. Parallel black box  $\mathcal{H}$ -LU preconditioning for elliptic boundary value problems. *Computing and Visualization in Science*, 11(4-6):273–291, 2008. [Cited on page 72]

- [62] Lars Grasedyck, Wolfgang Hackbusch, and Ronald Kriemann. Performance of H-LU preconditioning for sparse matrices. *Computational methods in applied mathematics*, 8(4):336–349, 2008. [Cited on page 72]
- [63] L. Grigori, J. A. Demmel, and X. S. Li. Parallel Symbolic Factorization for Sparse LU with Static Pivoting. *SIAM J. Sci. Comput.*, 29(3):1289–1314, 2007. [Cited on page 52]
- [64] Anshul Gupta. Recent progress in general sparse direct solvers. In *Lecture Notes in Computer Science*, volume 2073, pages 823–840, 2001. [Cited on page 43]
- [65] W. Hackbusch. *Hierarchical Matrices: Algorithms and Analysis*, volume 49. Springer Series in Computational Mathematics, 2015. [Cited on pages 72 and 83]
- [66] R. W. Hamming. Error Detecting and Error Correcting Codes. *Bell System Technical Journal*, 26(2):147–160, 1950. [Cited on page 70]
- [67] M. T. Heath, E. G.-Y. Ng, and B. W. Peyton. Parallel algorithms for sparse linear systems. *SIAM Review*, 33:420–460, 1991. [Cited on page 7]
- [68] B. Hendrickson and R. Leland. A multi-level algorithm for partitioning graphs. In *Supercomputing, 1995. Proceedings of the IEEE/ACM SC95 Conference*, pages 28–28, 1995. [Cited on page 53]
- [69] B. Hendrickson and E. Rothberg. Improving the run time and quality of nested dissection ordering. *SIAM Journal on Scientific Computing*, 20(2):468–489, 1998. [Cited on page 53]
- [70] Bruce Hendrickson and Tamara G. Kolda. Graph Partitioning Models for Parallel Computing. *Parallel Computing*, 26(12):1519–1534, 2000. [Cited on page 52]
- [71] Bruce Hendrickson and Robert Leland. An improved spectral graph partitioning algorithm for mapping parallel computations. *SIAM J. Sci. Comput.*, 16(2):452–469, March 1995. [Cited on page 9]
- [72] P. Hénou. *Distribution des Données et Régulation Statique des Calculs et des Communications pour la Résolution de Grands Systèmes Linéaires Creux par Méthode Directe*. PhD thesis, LaBRI, University Bordeaux 1, Talence, France, November 2001. [Cited on pages 11 and 14]
- [73] P. Hénou, P. Ramet, and J. Roman. A Mapping and Scheduling Algorithm for Parallel Sparse Fan-In Numerical Factorization. In *Proceedings of EuroPAR’99*, number 1685 in Lecture Notes in Computer Science, pages 1059–1067. Springer Verlag, September 1999. [Cited on page 14]
- [74] P. Hénou, P. Ramet, and J. Roman. PaStiX: A Parallel Sparse Direct Solver Based on a Static Scheduling for Mixed 1D/2D Block Distributions. In *Proceedings of Irregular’2000*, number 1800 in Lecture Notes in Computer Science, pages 519–525. Springer Verlag, May 2000. [Cited on pages 7, 8, 12, 14, 22, and 24]
- [75] P. Hénou, P. Ramet, and J. Roman. PaStiX: A High-Performance Parallel Direct Solver for Sparse Symmetric Definite Systems. *Parallel Computing*, 28(2):301–321, January 2002. [Cited on pages 7, 8, 9, 10, 11, 14, 22, 43, 52, and 72]
- [76] P. Hénou, P. Ramet, and J. Roman. Efficient algorithms for direct resolution of large sparse system on clusters of SMP nodes. In *SIAM Conference on Applied Linear Algebra, Williamsburg, Virginia, USA*, July 2003. [Cited on pages 8, 11, and 43]
- [77] P. Hénou, P. Ramet, and J. Roman. On finding approximate supernodes for an efficient ILU(k) factorization. *Parallel Computing*, 34:345–362, 2008. [Cited on pages 33 and 43]
- [78] P. Hénou and Y. Saad. A parallel multistage ILU factorization based on a hierarchical graph decomposition. *SIAM Journal on Scientific Computing*, 28(6):2266–2293, 2006. [Cited on page 3]
- [79] Kenneth L Ho and Lexing Ying. Hierarchical interpolative factorization for elliptic operators: differential equations. *Communications on Pure and Applied Mathematics*, 2015. [Cited on page 72]

- [80] Jonathan D. Hogg, John K. Reid, and Jennifer A. Scott. Design of a multicore sparse Cholesky factorization using dags. *SIAM Journal on Scientific Computing*, 32(6):3627–3649, 2010. [Cited on pages 4 and 29]
- [81] G. Huysmans, Stanislas Pamela, Emiel Van Der Plas, and Pierre Ramet. Non-linear MHD simulations of edge localized modes (ELMs). *Plasma Physics*, 51(12):124012, 2009. [Cited on page 5]
- [82] David Hysom and Alex Pothén. A scalable parallel algorithm for incomplete factor preconditioning. *SIAM Journal on Scientific Computing*, 22(6):2194–2215, 2001. [Cited on pages 44 and 45]
- [83] F. D. Igual, E. Chan, E. S. Quintana-Ortí, G. Quintana-Ortí, R. A. van de Geijn, and F. G. Van Zee. The FLAME approach: From dense linear algebra algorithms to high-performance multi-accelerator implementations. *J. Parallel Distrib. Comput.*, 72(9):1134–1143, 2012. [Cited on page 30]
- [84] David S. Johnson and Lyle A. Mcgeoch. *The Traveling Salesman Problem: A Case Study in Local Optimization*, pages 215–310. Chichester, UK, 1997. [Cited on page 71]
- [85] M. Joshi, G. Karypis, V. Kumar, A. Gupta, and F. Gustavson. PSPASES : Scalable Parallel Direct Solver Library for Sparse Symmetric Positive Definite Linear Systems. Technical report, University of Minnesota and IBM Thomas J. Watson Research Center, May 1999. [Cited on page 8]
- [86] G. Karypis and V. Kumar. A fast and high quality multilevel scheme for partitioning irregular graphs. *SIAM Journal on Scientific Computing*, 20(1):359–392, 1998. [Cited on page 53]
- [87] G. Karypis and V. Kumar. METIS – A Software Package for Partitioning Unstructured Graphs, Partitioning Meshes, and Computing Fill-Reducing Orderings of Sparse Matrices – Version 4.0. University of Minnesota, September 1998. [Cited on pages 8, 9, 10, and 52]
- [88] G. Karypis and V. Kumar. Multilevel k-way partitioning scheme for irregular graphs. *Journal of Parallel and Distributed Computing*, 48:96–129, 1998. [Cited on page 53]
- [89] George Karypis and Vipin Kumar. Parallel threshold-based ilu factorization. In *Proceedings of the 1997 ACM/IEEE Conference on Supercomputing*, SC ’97, pages 1–24, New York, NY, USA, 1997. ACM. [Cited on page 44]
- [90] O. Kaya and B. Uçar. Scalable sparse tensor decompositions in distributed memory systems. In *Proceedings of the International Conference for High Performance Computing, Networking, Storage and Analysis*, pages 77:1–77:11. ACM, 2015. [Cited on page 89]
- [91] O. Kaya and B. Uçar. High performance parallel algorithms for the tucker decomposition of sparse tensors. In *45th International Conference on Parallel Processing (ICPP ’16)*, pages 103–112, 2016. [Cited on page 89]
- [92] Kevin Barker and Kei Davis and Adolffy Hoisie and Darren Kerbyson and Michael Lang and Scott Pakin and José Carlos Sancho. Experiences in Scaling Scientific Applications on Current-generation Quad-core Processors. In *LSPP’08 held in conjunction with IPDPS*, Miami, Florida, USA, April 2008. [Cited on page 21]
- [93] Ronald Kriemann. H-LU factorization on many-core systems. *Computing and Visualization in Science*, 16(3):105–117, 2013. [Cited on page 72]
- [94] Jakub Kurzak, Stanimire Tomov, and Jack Dongarra. Autotuning GEMM Kernels for the Fermi GPU. *IEEE Transactions on Parallel and Distributed Systems*, 23(11):2045–2057, 2012. [Cited on page 38]
- [95] X. Lacoste. *Scheduling and memory optimizations for sparse direct solver on multi-core/multi-gpu cluster systems*. PhD thesis, Université Bordeaux, Talence, France, February 2015. [Cited on pages 5, 19, and 78]

- [96] Xavier Lacoste, Mathieu Faverge, Pierre Ramet, Samuel Thibault, and George Bosilca. Taking Advantage of Hybrid Systems for Sparse Direct Solvers via Task-Based Runtimes. In *Parallel Distributed Processing Symposium Workshops (IPDPSW), 2014 IEEE International*, pages 29–38, Phoenix, United States, May 2014. IEEE. [Cited on page 19]
- [97] B. Lathuilière. *Méthode de décomposition de domaine pour les équations du transport simplifié en neutronique*. PhD thesis, LaBRI, Bordeaux University, Talence, France, January 2010. [Cited on page 5]
- [98] X. S. Li. Evaluation of sparse LU factorization and triangular solution on multicore platforms. In J. M. Laginha M. Palma, P. Amestoy, M. J. Daydé, M. Mattoso, and J. Correia Lopes, editors, *VECPAR*, volume 5336 of *Lecture Notes in Computer Science*, pages 287–300. Springer, 2008. [Cited on page 29]
- [99] X. S. Li and J. W. Demmel. A scalable sparse direct solver using static pivoting. In *Proceedings of the Ninth SIAM Conference on Parallel Processing for Scientific Computing*, San Antonio, Texas, March 22–24, 1999. [Cited on pages 8 and 43]
- [100] R. J. Lipton, D. J. Rose, and R. E. Tarjan. Generalized nested dissection. *SIAM Journal on Numerical Analysis*, 16(2), 1979. [Cited on pages 9, 52, and 53]
- [101] R. J. Lipton and R. E. Tarjan. A separator theorem for planar graphs. *SIAM Journal on Applied Mathematics*, 36:177–189, 1979. [Cited on pages 78 and 84]
- [102] J. W.-H. Liu. Modification of the minimum-degree algorithm by multiple elimination. *ACM Trans. Math. Software*, 11(2):141–153, 1985. [Cited on page 8]
- [103] J. W.-H. Liu. The role of elimination trees in sparse factorization. *SIAM J. Matrix Anal. Appl.*, 11:134–172, 1990. [Cited on page 9]
- [104] Joseph W. H. Liu, Esmond G. Ng, and Barry W. Peyton. On finding supernodes for sparse matrix computations. *SIAM Journal on Matrix Analysis and Applications*, 14(1):242–252, 1993. [Cited on page 10]
- [105] R. F. Lucas, G. Wagenbreth, D. M. Davis, and R. Grimes. Multifrontal computations on GPUs and their multi-core hosts. In *Proceedings of the 9th international conference on High performance computing for computational science, VECPAR’10*, pages 71–82, Berlin, Heidelberg, 2011. Springer-Verlag. [Cited on page 30]
- [106] María J. Martín, Inmaculada Pardines, and Francisco F. Rivera. Scheduling of algorithms based on elimination trees on NUMA systems. In *EuroPar’99*, volume 1685 of *Lecture Notes in Computer Science*, pages 1068–1072, Toulouse, France, 1999. [Cited on page 22]
- [107] Henning Meyerhenke, Burkhard Monien, and Thomas Sauerwald. A new diffusion-based multilevel algorithm for computing graph partitions. *J. Parallel Distrib. Comput.*, 69(9):750–761, September 2009. [Cited on page 57]
- [108] G. L. Miller, S.-H. Teng, and S. A. Vavasis. A unified geometric approach to graph separators. In *Proc. 31st Annual Symposium on Foundations of Computer Science*, pages 538–547, 1991. [Cited on page 52]
- [109] G. L. Miller and S. A. Vavasis. Density graphs and separators. In *Second Annual ACM-SIAM Symposium on Discrete Algorithms*, pages 331–336, 1991. [Cited on page 52]
- [110] M. Magoulou and H.A. van der Vorst. A generalized domain decomposition paradigm for parallel incomplete lu factorization preconditionings. *Future Generation Computer Systems*, 17(8):925 – 932, 2001. High Performance Computing and Networking. [Cited on page 43]
- [111] S. Moustafa. *Massively Parallel Cartesian Discrete Ordinates Method for Neutron Transport Simulation*. PhD thesis, LaBRI, Bordeaux University, Talence, France, December 2015. [Cited on page 5]



- [112] Salli Moustafa, Ivan Dutka Malen, Laurent Plagne, Angélique Ponçot, and Pierre Ramet. Shared Memory Parallelism for 3D Cartesian Discrete Ordinates Solver. *Annals of Nuclear Energy*, pages 1–10, September 2014. [Cited on page 5]
- [113] Rajib Nath, Stanimire Tomov, and Jack Dongarra. An improved MAGMA GEMM for Fermi graphics processing units. *International Journal of High Performance Computing Applications*, 24(4):511–515, 2010. [Cited on page 38]
- [114] CUDA Nvidia. Cublas library. *NVIDIA Corporation, Santa Clara, California*, 15, 2008. [Cited on page 38]
- [115] F. Pellegrini and J. Roman. Scotch: A software package for static mapping by dual recursive bipartitioning of process and architecture graphs. In *High-Performance Computing and Networking*, volume 1067 of *Lecture Notes in Computer Science*, pages 493–498. Springer, 1996. [Cited on page 52]
- [116] F. Pellegrini and J. Roman. Sparse matrix ordering with SCOTCH. In *Proceedings of HPCN’97, Vienna, LNCS 1225*, pages 370–378, April 1997. [Cited on pages 9 and 11]
- [117] F. Pellegrini, J. Roman, and P. Amestoy. Hybridizing nested dissection and halo approximate minimum degree for efficient sparse matrix ordering. *Concurrency: Practice and Experience*, 12:69–84, 2000. Preliminary version published in *Proceedings of Irregular’99*, LNCS 1586, 986–995. [Cited on pages 9 and 11]
- [118] Francois Pellegrini. Scotch and libScotch 5.1 User’s Guide, August 2008. [Cited on pages 10 and 78]
- [119] G. Pichon, E. Darve, M. Faverge, P. Ramet, and J. Roman. Sparse supernodal solver using block low-rank compression. In *2017 IEEE International Parallel and Distributed Processing Symposium Workshops (IPDPSW)*, pages 1138–1147, May 2017. [Cited on page 67]
- [120] Gregoire Pichon, Mathieu Faverge, Pierre Ramet, and Jean Roman. Reordering strategy for blocking optimization in sparse linear solvers. *SIAM Journal on Matrix Analysis and Applications*, 38(1):226–248, 2017. [Cited on page 67]
- [121] A. Pothén and C. Sun. A mapping algorithm for parallel sparse Cholesky factorization. *SIAM J. Sci. Comput.*, 14(5):1253–1257, September 1993. [Cited on pages 7 and 15]
- [122] Hadi Pouransari, Pieter Coulier, and Eric Darve. Fast hierarchical solvers for sparse matrices using extended sparsification and low-rank approximation. *arXiv preprint arXiv:1510.07363v3*, 2015. [Cited on page 72]
- [123] G. Quintana-Ortí, E. S. Quintana-Ortí, R. A. van de Geijn, F. G. Van Zee, and E. Chan. Programming matrix algorithms-by-blocks for thread-level parallelism. *ACM Trans. Math. Softw.*, 36(3), 2009. [Cited on page 30]
- [124] Padma Raghavan, Keita Teranishi, and Esmond G. Ng. A latency tolerant hybrid sparse solver using incomplete cholesky factorization. *Numerical Linear Algebra with Applications*, 10(5-6):541–560, 2003. [Cited on page 43]
- [125] S. Rajamanickam, E.G. Boman, and M.A. Heroux. ShyLU: A hybrid-hybrid solver for multicore platforms. In *Parallel Distributed Processing Symposium (IPDPS), 2012 IEEE 26th International*, pages 631–643, May 2012. [Cited on page 53]
- [126] Donald J. Rose, R. Endre Tarjan, and George S. Lueker. Algorithmic aspects of vertex elimination on graphs. *SIAM Journal on Computing*, 5(2):266–283, 1976. [Cited on page 44]
- [127] E. Rothberg and A. Gupta. An efficient block-oriented approach to parallel sparse Cholesky factorization. *SIAM J. Sci. Comput.*, 15(6):1413–1439, November 1994. [Cited on page 7]
- [128] Y. Saad. ILUT: A dual threshold incomplete lu factorization. *Numerical Linear Algebra with Applications*, 1(4):387–402, 1994. [Cited on page 44]

- [129] Y. Saad. *Iterative Methods for Sparse Linear Systems*. Society for Industrial and Applied Mathematics, second edition, 2003. [Cited on pages 43 and 44]
- [130] O. Schenk and K. Gärtner. Solving unsymmetric sparse systems of linear equations with pardiso. *Future Gener. Comput. Syst.*, 20(3):475–487, 2004. [Cited on page 29]
- [131] W. M. Sid-Lakhdar. *Scaling the solution of large sparse linear systems using multifrontal methods on hybrid shared-distributed memory architectures*. PhD thesis, Ecole Normale Supérieure de Lyon, December 2014. [Cited on page 70]
- [132] Shaden Smith and George Karypis. Accelerating the tucker decomposition with compressed sparse tensors. In *European Conference on Parallel Processing*. Springer, 2017. [Cited on page 89]
- [133] Shaden Smith, Jongsoo Park, and George Karypis. Sparse tensor factorization on many-core processors with high-bandwidth memory. *31st IEEE International Parallel & Distributed Processing Symposium (IPDPS’17)*, 2017. [Cited on page 89]
- [134] STFC. HSL. A collection of Fortran codes for large scale scientific computation. <http://www.hsl.rl.ac.uk/>. [Cited on pages 4 and 70]
- [135] Daria A Sushnikova and Ivan V Oseledets. “Compress and eliminate” solver for symmetric positive definite sparse matrices. *arXiv preprint arXiv:1603.09133v3*, 2016. [Cited on page 72]
- [136] Guangming Tan, Linchuan Li, Sean Triechele, Everett Phillips, Yungang Bao, and Ninghui Sun. Fast implementation of dgemv on fermi gpu. In *Proceedings of 2011 International Conference for High Performance Computing, Networking, Storage and Analysis*, SC ’11, pages 35:1–35:11, New York, NY, USA, 2011. ACM. [Cited on page 38]
- [137] Rajeev Thakur and William Gropp. Test suite for evaluating performance of MPI implementations that support MPI\_THREAD\_MULTIPLE. In *EuroPVM/MPI*, volume 4757 of *Lecture Notes in Computer Science*, pages 46–55, 2007. [Cited on page 23]
- [138] Francois Trahay, Alexandre Denis, Olivier Aumage, and Raymond Namyst. Improving reactivity and communication overlap in MPI using a generic I/O manager. In *EuroPVM/MPI*, volume 4757 of *Lecture Notes in Computer Science*, pages 170–177, 2007. [Cited on page 22]
- [139] Field G Van Zee, Ernie Chan, Robert A Van de Geijn, Enrique S Quintana-Orti, and Gregorio Quintana-Orti. The LibFlame library for dense matrix computations. *Computing in science & engineering*, 11(6):56–63, 2009. [Cited on page 30]
- [140] Vasily Volkov and James W. Demmel. Benchmarking GPUs to tune dense linear algebra. In *Proceedings of the 2008 ACM/IEEE conference on Supercomputing*, SC ’08, pages 31:1–31:11, Piscataway, NJ, USA, 2008. IEEE Press. [Cited on pages 33 and 38]
- [141] Shen Wang, Xiaoye S. Li, François-Henry Rouet, Jianlin Xia, and Maarten V. De Hoop. A Parallel Geometric Multifrontal Solver Using Hierarchically Semiseparable Structure. *ACM Trans. Math. Softw.*, 42(3):21:1–21:21, May 2016. [Cited on page 72]
- [142] James W. Watts III. A conjugate gradient-truncated direct method for the iterative solution of the reservoir simulation pressure equation. June 1981. [Cited on page 44]
- [143] Jianlin Xia, Shivkumar Chandrasekaran, Ming Gu, and Xiaoye S. Li. Superfast multifrontal method for large structured linear systems of equations. *SIAM Journal on Matrix Analysis and Applications*, 31(3):1382–1411, 2010. [Cited on page 72]
- [144] Ichitaro Yamazaki and Xiaoye S. Li. On techniques to improve robustness and scalability of a parallel hybrid linear solver. In *High Performance Computing for Computational Science – VECPAR 2010*, volume 6449 of *Lecture Notes in Computer Science*, pages 421–434. Springer, 2011. [Cited on page 53]
- [145] Ichitaro Yamazaki, Stanimire Tomov, and Jack Dongarra. One-sided Dense Matrix Factorizations on a Multicore with Multiple GPU Accelerators. *Procedia Computer Science*, 9(Complete):37–46, 2012. [Cited on page 37]

- [146] Kai Yang, Hadi Pouransari, and Eric Darve. Sparse hierarchical solvers with guaranteed convergence. *arXiv preprint arXiv:1611.03189*, 2016. [Cited on page 72]
- [147] A. YarKhan. *Dynamic Task Execution on Shared and Distributed Memory Architectures*. PhD thesis, Innovative Computing Laboratory, University of Tennessee, dec 2012. [Cited on page 30]
- [148] C D Yu, W Wang, and D Pierce. A CPU-GPU Hybrid Approach for the Unsymmetric Multifrontal Method. *Parallel Computing*, 37(12):759–770, October 2011. [Cited on page 30]